



LAWRENCE
LIVERMORE
NATIONAL
LABORATORY

FY05 HPCRM Annual Report: High-Performance
Corrosion-Resistant Iron-Based Amorphous Metal
Coatings Evaluation of Corrosion Resistance FY05
HPCRM Annual Report # Rev. 1DOE-DARPA
Co-Sponsored Advanced Materials Program

J. C. Farmer, J. J. Haslam, S. D. Day

September 20, 2007

This document was prepared as an account of work sponsored by an agency of the United States Government. Neither the United States Government nor the University of California nor any of their employees, makes any warranty, express or implied, or assumes any legal liability or responsibility for the accuracy, completeness, or usefulness of any information, apparatus, product, or process disclosed, or represents that its use would not infringe privately owned rights. Reference herein to any specific commercial product, process, or service by trade name, trademark, manufacturer, or otherwise, does not necessarily constitute or imply its endorsement, recommendation, or favoring by the United States Government or the University of California. The views and opinions of authors expressed herein do not necessarily state or reflect those of the United States Government or the University of California, and shall not be used for advertising or product endorsement purposes.

This work was performed under the auspices of the U.S. Department of Energy by University of California, Lawrence Livermore National Laboratory under Contract W-7405-Eng-48.

UCRL-TR-234799

FY05 HPCRM ANNUAL REPORT:

**HIGH-PERFORMANCE CORROSION-RESISTANT
IRON-BASED AMORPHOUS METAL COATINGS**

EVALUATION OF CORROSION RESISTANCE

*FY05 HPCRM Annual Report – Rev. 1
DOE-DARPA Co-Sponsored Advanced Materials
Program*

**Joseph C. Farmer, Jeffrey J. Haslam & S. Daniel Day
Lawrence Livermore National Laboratory
Livermore, California**



TABLE OF CONTENTS

Title Page UCRL-SR-21844.....	i
Table of Contents.....	ii
Abstract.....	1
Nomenclature.....	2
introduction.....	3
Materials Design and Synthesis.....	4
Full Density Corrosion-Resistant Compositions.....	5
Melt Spinning Process.....	5
Arc Melting with Drop Casting.....	6
Thermal Properties.....	7
Electrochemical Corrosion Testing.....	7
Range of Environments.....	7
Determining Critical Potential with Cyclic Polarization.....	7
Alloy Screening with Cyclic Polarization.....	9
Determining Corrosion Rate with Linear Polarization.....	10
Validation with Salt Fog Testing.....	12
Threshold for Passive Film Breakdown with Potential-Step Method.....	12
Thresholds for Passive Film Breakdown in Seawater.....	13
Thresholds for Passive Film Breakdown in Hot Calcium Chloride.....	17
Effect of Devitrification on Corrosion Resistance.....	18
Long-Term Corrosion Testing.....	19
Geometries of Coated Samples.....	19
Open Circuit Corrosion Potential During Long-Term Exposure.....	20
Corrosion Rates with Linear Polarization During Long-Term Exposure.....	20
Complex Impedance During Long-Term Exposure.....	20
Summary.....	21
Acknowledgments.....	22
References.....	22
Tables.....	26
Figures.....	29

FY05 HPCRM ANNUAL REPORT: HIGH-PERFORMANCE CORROSION-RESISTANT IRON-BASED AMORPHOUS METAL COATINGS – EVALUATION OF CORROSION RESISTANCE

*Joseph C. Farmer, Jeffrey H. Haslam and S. Daniel Day
Lawrence Livermore National Laboratory
Livermore, California 94550*

ABSTRACT

New corrosion-resistant, iron-based amorphous metals have been identified from published data or developed through combinatorial synthesis, and tested to determine their relative corrosion resistance. Many of these materials can be applied as coatings with advanced thermal spray technology. Two compositions have corrosion resistance superior to wrought nickel-based Alloy C-22 (UNS # N06022) in some very aggressive environments, including concentrated calcium-chloride brines at elevated temperature.

Two Fe-based amorphous metal formulations have been found that appear to have corrosion resistance comparable to, or better than that of Ni-based Alloy C-22, based on breakdown potential and corrosion rate. Both Cr and Mo provide corrosion resistance, B enables glass formation, and Y lowers critical cooling rate (CCR). SAM1651 has yttrium added, and has a nominal critical cooling rate of only 80 Kelvin per second, while SAM2X7 (similar to SAM2X5) has no yttrium, and a relatively high critical cooling rate of 610 Kelvin per second.

Both amorphous metal formulations have strengths and weaknesses. SAM1651 (yttrium added) has a low critical cooling rate (CCR), which enables it to be rendered as a completely amorphous thermal spray coating. Unfortunately, it is relatively difficult to atomize, with powders being irregular in shape. This causes the powder to be difficult to pneumatically convey during thermal spray deposition. Gas atomized SAM1651 powder has required cryogenic milling to eliminate irregularities that make flow difficult. SAM2X5 (no yttrium) has a high critical cooling rate, which has caused problems associated with devitrification. SAM2X5 can be gas atomized to produce spherical powders of SAM2X5, which enable more facile thermal spray deposition.

The reference material, nickel-based Alloy C-22, is an outstanding corrosion-resistant engineering material. Even so, crevice corrosion has been observed with C-22 in hot sodium chloride environments without buffer or inhibitor. Comparable metallic alloys such as SAM2X5 and SAM1651 may also experience crevice corrosion under sufficiently harsh conditions. Accelerated crevice corrosion tests are now being conducted to intentionally induce crevice corrosion, and to determine those environmental conditions where such localized attack occurs.

HPCRM FY05 Annual Report – UCRL-TR-234799
DOE-DARPA Co-Sponsored Advanced Materials Program

Such materials are extremely hard, and provide enhanced resistance to abrasion and gouges (stress risers) from backfill operations, and possibly even tunnel boring. The hardness of Type 316L Stainless Steel is approximately 150 VHN, that of Alloy C-22 is approximately 250 VHN, and that of HVOF SAM2X5 ranges from 1100-1300 VHN.

These new materials provide a viable coating option for repository engineers. SAM2X5 and SAM1651 coatings can be applied with thermal spray processes without any significant loss of corrosion resistance. Both Alloy C-22 and Type 316L stainless lose their resistance to corrosion during thermal spraying. Containers for the transportation, storage and disposal of spent nuclear fuel (SNF) and high-level radioactive waste (HLW) with corrosion resistant coatings are envisioned. For example, an enhanced multi-purpose container (MPC) could be made with such coatings, leveraging existing experience in the fabrication of such containers. These coating materials could be used to protect the final closure weld on SNF/HLW disposal containers, eliminate need for stress mitigation. Integral drip shield could be produced by directly spraying it onto the disposal container, thereby eliminating the need for an expensive titanium drip shield. In specific areas where crevice corrosion is anticipated, such as the contact point between the disposal container and pallet, HVOF coatings could be used to buildup thickness, thereby selectively adding corrosion life where it is needed.

Both SAM2X5 & SAM1651 have high boron content which enable them to absorb neutrons and therefore be used for criticality control in baskets. Alloy C-22 and 316L have no neutron absorber, and cannot be used for such functions. Borated stainless steel and Gd-doped Ni-Cr-Mo alloys are being shown to have relatively poor corrosion performance.

NOMENCLATURE

Multi-Purpose Container	MPC
Critical Cooling Rate	CCR
Cyclic Polarization:	CP
Corrosion Rate	CR
Defense Advanced Projects Agency	DARPA
Defense Sciences Office	DSO
Department of Energy	DOE
Electrochemical Impedance Spectroscopy	EIS
Equivalent Weight	EW
Conversion Factor	K
Melt-Spun Ribbon	MSR
High Level Waste	HLW
Hardness Rockwell C	HRC
High-Velocity Oxy-Fuel Process:	HVOF
Multi-Purpose Container	MPC
Office of Civilian Radioactive Waste Management	OCRWM
Office of Science & Technology International	OSTI
Potential-Step Test	PST
Structural Amorphous Metal	SAM
Spent Nuclear Fuel	SNF

HPCRM FY05 Annual Report – UCRL-TR-234799
DOE-DARPA Co-Sponsored Advanced Materials Program

Vickers Hardness Number	VHN
Modulation Frequency	f
Corrosion Current Density	i_{corr}
Electrode Area	A
Tafel Parameter	B
Critical Potential:	$E_{critical}$
Open Circuit Corrosion Potential:	E_{corr}
Reversal Potential:	E_{rev}
Potential of Anodic Oxidation Peak:	E_{peak}
Repassivation Potential:	E_{rp}
Faraday's Constant	F
Corrosion Current	I_{corr}
Universal Gas Constant	R
Polarization Resistance	R_p
Temperature	T
Complex Impedance	Z
Real Part of the Complex Impedance	Z_{real} (also Z')
Imaginary Part of the Complex Impedance	Z_{imag} (also Z'')
Amplitude of Complex Impedance	$ Z $
Anodic Tafel Slope	β_a
Cathodic Tafel Slope	β_c
Impedance Phase Angle	ϕ
Density	ρ

INTRODUCTION

Corrosion costs the Department of Defense billions of dollars every year, with an immense quantity of material in various structures undergoing corrosion. For example, in addition to fluid and seawater piping, ballast tanks, and propulsions systems, approximately 345 million square feet of structure aboard naval ships and crafts require costly corrosion control measures. The use of advanced corrosion-resistant materials to prevent the continuous degradation of this massive surface area would be extremely beneficial. The Fe-based corrosion-resistant, amorphous-metal coatings under development may prove of importance for applications on ships. The possible advantages of amorphous metals has been recognized for some time [Latanison 1985].

Two Fe-based amorphous metal formulations have been found that appear to have corrosion resistance comparable to, or better than that of Ni-based Alloy C-22, based on breakdown potential and corrosion rate. Both Cr and Mo provide corrosion resistance, B enables glass formation, and Y lowers critical cooling rate (CCR). SAM1651 has yttrium added, and has a nominal critical cooling rate of only 80 Kelvin per second, while SAM2X7 (similar to SAM2X5) has no yttrium, and a relatively high critical cooling rate of 610 Kelvin per second.

Both amorphous metal formulations have strengths and weaknesses. SAM1651 (yttrium added) has a low critical cooling rate (CCR), which enables it to be rendered as a completely amorphous thermal spray coating. Unfortunately, it is relatively difficult to atomize, with powders being

irregular in shape. This causes the powder to be difficult to pneumatically convey during thermal spray deposition. Gas atomized SAM1651 powder has required cryogenic milling to eliminate irregularities that make flow difficult. SAM2X5 (no yttrium) has a high critical cooling rate, which has caused problems associated with devitrification. SAM2X5 can be gas atomized to produce spherical powders of SAM2X5, which enable more facile thermal spray deposition.

These new materials provide a viable coating option for repository engineers. SAM2X5 and SAM1651 coatings can be applied with thermal spray processes without any significant loss of corrosion resistance. Both Alloy C-22 and Type 316L stainless lose their resistance to corrosion during thermal spraying. Containers for the transportation, storage and disposal of spent nuclear fuel (SNF) and high-level radioactive waste (HLW) with corrosion resistant coatings are envisioned. For example, an enhanced multi-purpose container (MPC) could be made with such coatings, leveraging existing experience in the fabrication of such containers. These coating materials could be used to protect the final closure weld on SNF/HLW disposal containers, eliminate need for stress mitigation. Integral drip shield could be produced by directly spraying it onto the disposal container, thereby eliminating the need for an expensive titanium drip shield. In specific areas where crevice corrosion is anticipated, such as the contact point between the disposal container and pallet, HVOF coatings could be used to buildup thickness, thereby selectively adding corrosion life where it is needed. Such materials are extremely hard, and provide enhanced resistance to abrasion and gouges (stress risers) from backfill operations, and possibly even tunnel boring. The hardness of Type 316L Stainless Steel is approximately 150 VHN, that of Alloy C-22 is approximately 250 VHN, and that of HVOF SAM2X5 ranges from 1100-1300 VHN. Both SAM2X5 & SAM1651 have high boron content which enable them to absorb neutrons and therefore be used for criticality control in baskets, while C-22 and 316L have no neutron absorber, and cannot be used for such functions. Borated stainless steel and Gd-doped Ni-Cr-Mo alloys are being shown to have relatively poor corrosion performance.

MATERIALS DESIGN AND SYNTHESIS

This project has three primary long-term goals, all directed towards development of advanced amorphous-metal thermal-spray coatings with corrosion resistance superior to: (1) Type 316L stainless steel [UNS # S31603], (2) nickel-based Alloy C-22 [UNS # N06022], and (3) Ti Grade 7 (UNS # R52400). Computational materials science has been used to help guide the design these new materials [Kaufman 2004; Farmer et al. 2004].

Several thermal spray processes have been developed by industry and include: flame spray, wire-arc; plasma spray; water-stabilized plasma spray; high-velocity oxy-fuel; and the detonation gun. Any of these can be used for the deposition of Fe-based amorphous metals, with varying degrees of residual porosity and crystalline structure. The coatings discussed here were made with the high-velocity oxy-fuel (HVOF) process, which involves a combustion flame, and is characterized by gas and particle velocities that are three to four times the speed of sound (mach 3 to 4). This process is ideal for depositing metal and cermet coatings. These coatings have typical bond strengths of about 8,600 pounds per square inch, porosities of less than one percent (<1%), and micro-hardness of 68 HRC.

Full Density Corrosion-Resistant Compositions

The development of an appropriate powder composition for the production of a corrosion-resistant thermal-spray coating requires that the alloy first be tested in a form with no porosity, and with little or no crystalline phases present. Testing of such materials enables determination of the best possible corrosion performance for a given composition. Melt spinning and arc-melting with drop casting have been used as methods to synthesize completely amorphous, Fe-based, corrosion-resistant alloys with near theoretical density, thereby enabling the effects of coating morphology on corrosion resistance to be separated from the effects of elemental composition.

Melt Spinning Process.

Cooling rates as great as one billion Kelvin per second (10^9 K/s) have been achieved with melt spinning. In contrast, the cooling rate in a typical thermal spray process such as HVOF are on the order of ten thousand Kelvin per second (10^4 K/s). The melt-spun ribbons produced with this equipment are several meters long, several millimeters wide, and approximately 150 microns thick.

The melt spinning involves the ejection of a liquid melt onto a rapidly moving copper wheel with a pressure-controlled gas. The liquid melt solidifies onto the wheel, with subsequent separation from the wheel by thermal contraction and centrifugal force, and collection in a chamber. By changing the tangential velocity of the wheel, as well as other processing parameters, the cooling rate can be controlled over a very broad range. The specific processing parameters for the melt-spinning process can be selected to establish cooling rates that are representative of a given thermal spray process. If a specific cooling rate produces an amorphous, glassy metal during melt spinning, it should also produce a glassy structure during thermal spray. It is therefore possible to use melt spinning to simulate the type of microstructure that can be achievable with thermal spraying, such as the high-velocity oxy-fuel process. Furthermore, an entire series of developmental materials, with different compositions, heat capacities, and thermal conductivity, can be made with the exact same cooling rate, thereby enabling materials scientists and engineers to determine the relative ease of processing.

Several alloy compositions of Fe-based amorphous metals have been produced, characterized, and tested [Farmer et al. 2005]. In principle, all were intended to be compositional modifications of the SAM40 parent material, obeying the following the general formula: $[(\text{SAM40})_{100-x} + \text{Y}_x]$ where Y is the added element, and x is the amount of the addition in atomic percent. Additives investigated included nickel, chromium, molybdenum, tungsten, yttrium, titanium and zirconium. The nickel and molybdenum additions are known to greatly influence the electrochemical properties of conventional stainless steel alloys [Asphahani 1980]. The yttrium, titanium, and zirconium additions, while not normally added to steels are known to form very stable oxides and are expected to increase the stability and passivity of the oxide film in a variety of environments. The SAM1651 formulation has the same nominal elemental composition as the P-containing Fe-based amorphous metal formulation discussed in the literature by Pang et al. [2002]. These materials have been selected with particular emphasis on glass forming ability,

thermal stability, hardness, and corrosion resistance, all under conditions of interest [Farmer et al. 2004].

The melt-spinning process was used to perform a systematic study of various elemental compositions, each based on the Fe-based SAM40 composition, with 1, 3, 5, and 7 atomic percent additions of specific elements believed to be beneficial to glass formation or corrosion resistance (Table 1). Elemental additions investigated included nickel, molybdenum, yttrium, titanium, zirconium, and chromium. The densities of the amorphous metals prepared with melt spinning were determined, and all were less dense than nickel-based N06022 (Alloy C-22), and therefore offer a weight advantage over such classical corrosion-resistant alloys. The first re-crystallization peak for each of melt-spun ribbons was determined with DTA, and was similar to that of the parent material (SAM40). The formula with the yttrium additions showed re-crystallization peaks at higher temperatures than achieved with other formulae, showing that yttrium additions do indeed promote thermal stability and glass formability. Some formulae exhibited a second re-crystallization process at a higher temperature than the first, with titanium and zirconium based formulations showing these processes at the highest temperatures. All of the “as-cast” amorphous metal formulae produced by the HPCRM Team exhibited hardness far superior to many of the conventional materials of interest, such as Type 316L stainless steel, and nickel-based N06022 (Alloy C-22). Thus, coatings of these materials would also be expected to be less prone to erosion, wear and gouging than conventional engineering alloys. Partially devitrified samples of the HPCRM materials exhibited dramatic increases in hardness. Thus, carefully controlled heat treatment of these materials can be used to achieve dramatic improvements in resistance to erosion, wear and penetration.

Arc Melting with Drop Casting

In addition to the melt-spinning process, arc-melted drop-cast ingots were synthesized for corrosion testing. These ingots were cast into cylindrical molds, thus forming long rods with a nominal diameter of 2-3 millimeters. By exploring the findings of Poon et al. [2004], it has been learned that additions of 2-3 atomic percent yttrium or zirconium can enhance the glass-forming ability (GFA), and substantially lower the required critical cooling rate (CCR). Such formulations are relatively easily cast as large-diameter (several millimeter) rods. X-ray diffraction (XRD) patterns for a SAM2X5 melt-spun ribbon, and a SAM1651 drop-cast ingot, were determined at various temperatures [Yang et al. 2004]. The data at 150, 300 and 500°C indicate very little crystalline structure, with the broad peaks suggesting the presence of dispersed crystalline phases in an amorphous matrix. These data also show the onset of devitrification of SAM1651 and SAM40 (parent material) at 800°C and above. From the electron backscatter images, the advantages of rare earth additions are evident. The exact composition of this material, which has also been produced as melt-spun ribbon, is published elsewhere [Farmer et al. 2004].

Optimization of the thermal spray process through careful selection of powder size and process temperature, has now yielded coatings of SAM40 (non-optimized elemental coating) that are virtually pore-free, and for all practical purposes, fully dense. These new coating architectures have also been shown, through detailed examination with XRD and SEM, to be amorphous. An optimized thermal spray process is now being used to render SAM2X5 and SAM1651

amorphous metal formulations as high-performance corrosion-resistant coatings, with nearly full density, no significant porosity, and good bond strength.

THERMAL PROPERTIES

In addition to having enhanced corrosion resistance, these new Fe-based amorphous metals have substantially improved thermal characteristics, which will improve processing ability, and performance in targeted applications, as shown by the University of Wisconsin at Madison [Perepezko et al. 2004; Farmer et al. 2004]. While there was some sample-to-sample variability, results were generally consistent. For example, SAM2X5 has a glass transition temperature of $\sim 579^{\circ}\text{C}$, a recrystallization temperature of $\sim 628^{\circ}\text{C}$, a melting point of $\sim 1133^{\circ}\text{C}$, and a reduced glass transition temperature of ~ 0.57 (with a value of 0.6 being ideal). SAM2X7, an alloy in the same family as SAM2X5, has a glass transition temperature of $\sim 573^{\circ}\text{C}$, a recrystallization temperature of $\sim 630^{\circ}\text{C}$, a melting point of $\sim 1137^{\circ}\text{C}$, and a reduced glass transition temperature of 0.57. Similarly, SAM1651 has a glass transition temperature of $\sim 584^{\circ}\text{C}$, a recrystallization temperature of $\sim 653^{\circ}\text{C}$, a melting point of $\sim 1121^{\circ}\text{C}$, and a reduced glass transition temperature of ~ 0.55 . The critical cooling rates for SAM2X7 and SAM1651, have been determined to be ~ 610 and ≤ 80 K per second, respectively. Clearly, the yttrium additions in SAM1651 enhance glass-forming ability, as reported by Guo and Poon [2003]. A summary of thermal analyses (DTA or DSC) of the Fe-based amorphous metals of interest to HPCRM are shown in Table 2.

ELECTROCHEMICAL CORROSION TESTING

Range of Environments

Actual Yucca Mountain brines are categorized with the trilateral diagram shown in Figure 1. The boundary between the sulfate-chloride ((SO_4^{-2})) and calcium chloride ((Ca^{+2})) regions is idealized. Many of the water compositions that fall in the idealized calcium chloride ((Ca^{+2})) region may actually evolve to sulfate-chloride ((SO_4^{-2})) or bicarbonate ((HCO_3^{-})) type brines due to the presence of fluoride. The matrix of test solutions now being used at LLNL for the evaluation of iron-based amorphous metals is given in Table 3, and represents extremes of composition that could evolve from the evaporative concentration of natural ground waters and dust deliquescence.

Determining Critical Potential with Cyclic Polarization

Spontaneous breakdown of the passive film and localized corrosion require that the open-circuit corrosion potential exceed the critical potential:

$$E_{corr} \geq E_{critical}$$

The resistance to localized corrosion is quantified through measurement of the open-circuit corrosion potential (E_{corr}), the breakdown potential ($E_{critical}$) and the repassivation potential (E_{rp}). The greater the difference between the open-circuit corrosion potential and the repassivation potential (ΔE), the more resistant a material is to modes of localized corrosion such as pitting and crevice corrosion.

Cyclic polarization (CP) is used as a means of measuring the critical potential ($E_{critical}$) of corrosion resistant materials, relative to their open-circuit corrosion potential (E_{corr}). In the published scientific literature, different bases exist for determining the critical potential from electrochemical measurements. Some have defined the critical potential for crevice corrosion of Alloy 22 as the point where the current density increases to 1 to 10 $\mu\text{A}/\text{cm}^2$ (10^{-6} to 10^{-5} A/cm^2) during the forward (anodic) scan, whereas others define the repassivation potential as the point where the current density drops to 0.1 to 1 $\mu\text{A}/\text{cm}^2$ (10^{-6} to 10^{-7} A/cm^2), and use the repassivation potential as a conservative estimate of the critical value [Farmer et al. 2000a].

Cyclic polarization measurements have been based on a procedure similar to ASTM G-5, with slight modification [American Society for Testing and Materials]. For example, ASTM G-5 calls for an electrolyte of 1N H_2SO_4 , whereas natural seawater, synthetic bicarbonate brines, synthetic sulfate-chloride brines, 4M NaCl solutions, and 5M CaCl_2 solutions with various levels of nitrate were used in this study. The compositions of the synthetic brines are given in the literature [Farmer et al. 2000]. Furthermore, ASTM G-5 calls for the use of de-aerated solutions, whereas aerated and de-aerated solutions were used here. After a 24-hour hold period, during which the open circuit corrosion potential is determined, the potential is scanned in the positive (anodic) direction from a level slightly more negative than the corrosion potential (cathodic limit), to a reversal potential (E_{rev}) near that required for oxygen evolution (anodic level). During the positive scan, anodic oxidation peaks may be observed (centered at E_{peak}) that have been correlated with the oxidation of molybdenum at the alloy surface (passive film), as well as current excursions that are usually associated with breakdown of the passive film. During the negative (cathodic) scan, a hysteresis loop will be observed in cases where passivity has been lost. As the scan continues, the current density may eventually decrease to a level equivalent to that experienced during the positive scan, and indicative of reformation of the passive film. The potential at which this occurs is known as the repassivation potential (E_{rp}).

Temperature-controlled borosilicate glass (Pyrex) electrochemical cells like the one shown in Figure 2 were used for cyclic polarization and other similar electrochemical measurements. This cell has three electrodes, a working electrode (test specimen), the reference electrode, and the counter electrode. A standard silver silver-chloride electrode, filled with near-saturation potassium chloride solution, is used as the reference, and communicates with the test solution via a Luggin probe placed in close proximity to the working electrode, thereby minimizing Ohmic losses. Numerical corrections for the reference electrode junction potential have been estimated, and have been found to be insignificant (Farmer et al. 2000). The electrochemical cell is equipped with a water-cooled junction to maintain reference electrode at ambient temperature, thereby maintaining integrity of the potential measurement, and a water-cooled condenser to prevent the loss of volatile species from the electrolyte.

There competing methodologies (Methods A, B and C) for the determination of the threshold potential for localized corrosion from cyclic polarization curves are shown in Figure 3, which is an actual cyclic polarization curve for Alloy C-22 in 5M CaCl_2 at 105°C. Method A is the point during the anodic potential scan when the passive oxide film breaks down, thereby allowing anodic dissolution of the underlying metal, with a relatively high anodic current density. The current density corresponding to a complete loss of passivity is assumed to be either 20 or 200

$\mu\text{A}/\text{cm}^2$. When it can be accurately measured, this is the true “critical potential.” Alternatively, the repassivation potential can be determined with either Methods B or C. The repassivation potential is determined during the reverse scan, and is the point following passive film breakdown where the current density decreases to a level known to correspond to the passive current density (the current density that can be sustained by an intact oxide film). The passive current density can either be assumed, shown as Method B, or it can be established from the intersection of the forward and reverse potential scans, shown as Method C. Method C is considered to be the most rigorous approach for determining the repassivation potential, since the intersection point occurs at the actual (not assumed) passive current density.

- Method A – Initial Breakdown of Passive Film
 - Critical Potential ($E_{critical}$) = Breakdown Potential (E_{20} or E_{200})
 - Based Threshold Current Density of 20 or 200 $\mu\text{A}/\text{cm}^2$
- Method B – Repassivation of Surface
 - Critical Potential ($E_{critical}$) = Repassivation Potential (E_{R1} or E_{R2})
 - Based Threshold Current Density of 1 or 2 $\mu\text{A}/\text{cm}^2$
- Method C – Repassivation of Surface
 - Critical Potential ($E_{critical}$) = Repassivation Potential (E_{RP})
 - Intersection of Forward Scan with Hysteresis Loop (Cross-Over Point)

As illustrated by Figure 4, the repassivation potential, determined by Method C in most cases, has been used as a quantitative metric for screening elemental compositions of competing iron-based amorphous metals, thereby determining the specific composition (of those tested) with the best resistance to passive film breakdown in the test solution. A wide variety of alloy compositions, which are shown in Table 1, were explored using cyclic polarization as a screening method. However, as will be evident in the discussion of subsequent potential-step test data, superior and more credible methods exist for the determination of the critical potential. The potential step-methods are used after the initial screening, and provide better results.

Alloy Screening with Cyclic Polarization

As shown in Figure 5, cyclic polarization was used as a means of evaluating the relative passive film stability of a drop-cast ingot of SAM1651, a disk of wrought nickel-based Alloy C-22 (reference material), and a thermal spray (high-velocity oxy-fuel or HVOF) coating of Alloy C-22. The test was conducted in Half Moon Bay seawater at 30°C, and the potential was measured relative to a standard silver / silver chloride reference electrode. The scan rate was 0.1667 volts per second. The current density for the ‘as-sprayed’ Alloy C-22 HVOF coating is based upon apparent electrode area, and was not corrected for surface roughness. In the case of the SAM1651, no passive film breakdown was observed, which is evident from the lack of hysteresis, even after scanning the voltage to a level close to oxygen evolution. Passive film breakdown was observed with wrought Alloy C-22, with a repassivation potential by Method C easily identified. Surprisingly, the Alloy C-22 coating loses has very poor corrosion resistance in comparison to both the SAM1651 ingot and the wrought Alloy C-22, which is reflected in a low repassivation potential.

As shown in Figure 6, cyclic polarization was used to compare the performance of a drop-cast ingot of SAM1651 against that of wrought Alloy C-22 in 5M calcium chloride at 105°C, which is an extremely aggressive environment. In the case of the drop-cast ingot of SAM1651, no significant passive film breakdown was observed at 0.9 to 1.0 volts. There was no positive hysteresis loop observed with this iron-based amorphous metal. There was hysteresis, but with the observed current density during the reverse less than that observed during the forward scan (indicative of even lower reactivity). In sharp contrast, there is an obvious breakdown of the nickel-based Alloy C-22 passive film at only 0.2 volts, showing a clear vulnerability in this aggressive environment. The repassivation potential is easily identified from the intersection of the hysteresis loop with the forward scan.

Cyclic polarization of melt spun ribbons was used to compare the relative corrosion resistance of a large number candidate alloy compositions in 5M CaCl₂ at 105°C, with the results summarized in Figure 7. The alloy compositions are defined in Table 1. As previously discussed, the quantifiable metric used as a basis of comparison was the difference between the open circuit corrosion potential (E_{corr}) and the repassivation potential (E_{rp}). Several of the candidate alloy compositions had a larger metric value ($E_{\text{rp}} - E_{\text{corr}}$) than the reference material, which has been established as nickel-based Alloy C-22, due to its own outstanding corrosion performance. Note that DARPA Milestone 1 corresponds to the metric value for Type 316L stainless steel and DARPA Milestone 2 corresponds to the metric value for nickel-based Alloy C-22. It is therefore concluded that several types of iron-based amorphous metals exist which all have passive film stabilities that are comparable to that of the reference material.

Cyclic polarization of melt spun ribbons was also used to compare the relative corrosion resistance of a large number candidate alloy compositions in near-ambient Half Moon Bay seawater at 30°C, with the results summarized in Figure 8. The alloy compositions are defined in Table 1. DARPA Milestone 1 corresponds to the metric value for Type 316L stainless steel and DARPA Milestone 2 corresponds to the metric value for nickel-based Alloy C-22. It is therefore concluded that several types of iron-based amorphous metals exist which all have passive film stabilities in seawater at 30°C that are comparable to that of the reference material.

Cyclic polarization of melt spun ribbons was further used to compare the relative corrosion resistance of a large number candidate alloy compositions in near-boiling Half Moon Bay seawater at 90°C, with the results summarized in Figure 9. The alloy compositions are defined in Table 1. DARPA Milestone 1 corresponds to the metric value for Type 316L stainless steel and DARPA Milestone 2 corresponds to the metric value for nickel-based Alloy C-22. It is therefore concluded that several types of iron-based amorphous metals exist which all have passive film stabilities in seawater at 90°C that are comparable to that of the reference material.

Determining Corrosion Rate with Linear Polarization

The linear polarization method has been used as a method for determining the corrosion rates of the various amorphous metal coatings, including SAM2X5 and SAM1651. This method is based upon experimental determination of electrokinetic parameters in the classic Tafel equation with a potentiostat. The classic Butler-Volmer expression collapses into the well-known anodic Tafel equation at high anodic potential, where the contribution of the electrochemical reduction

HPCRM FY05 Annual Report – UCRL-TR-234799
DOE-DARPA Co-Sponsored Advanced Materials Program

(cathodic) reaction to the overall current at the electrode surface becomes insignificant (defined as < 1%). At high cathodic potential, where the contribution of the electrochemical oxidation (anodic metal dissolution) reaction to the net electrode current is insignificant, the Butler-Volmer expression becomes the cathodic Tafel equation.

The procedure used for linear polarization testing consists of the following steps:

- Hold the sample for ten (10) seconds at the open circuit potential (OCP).
- Beginning at a potential 20 mV below the OCP (OCP-20 mV), increase the potential linearly at a constant rate of 0.1667 mV per second, to a potential 20 mV above the OCP (OCP+20 mV).
- Record the current being passed from the counter electrode to the working electrode by the potentiostat, as a function of potential relative to the standard/silver silver-chloride (Ag/AgCl) reference electrode.
- Determine the parameters in the cathodic Tafel line by performing linear regression on the voltage-current data from 10 mV below the OCP (OCP-10 mV) to 10 mV above the OCP (OCP+10 mV). The slope of this line is the polarization resistance, R_p .

The polarization resistance (R_p) is defined as:

$$R_p = \left(\frac{\partial E}{\partial I} \right)_{E_{corr}}$$

A parameter (B) is defined in terms of the slopes of the anodic and cathodic branches of the Tafel line:

$$B = \frac{\beta_a \beta_c}{2.303(\beta_a - \beta_c)}$$

The corrosion current (I_{corr}) is then defined as;

$$I_{corr} = \frac{R}{R_p}$$

The corrosion rate (CR) is then calculated as:

$$CR = K \frac{I_{corr}}{A \times \rho} (EW) \text{ (mmpy)}$$

The parameter K is a conversion factor used to express the corrosion rate (CR) in the units of millimeters per year (mmpy) and has a value of 3.27×10^{-3} (mm·g)/(μ A·cm·yr); I_{corr} is the corrosion current in microamps (μ A); A is the surface area of the sample in square centimeters (cm^2); and ρ is the density of the sample in grams per cubic centimeter (g/cm^3).

Linear polarization was used to determine the approximate corrosion rates of the thermal spray coatings of two amorphous metals of interest (HVOF SAM1651 and SAM2X5 coatings) and the reference material (wrought nickel-based Alloy C-22) in three relevant environments, Half Moon Bay seawater at two temperature levels, and in hot concentrated calcium chloride (5M CaCl₂ at 105°C). This data is summarized in Figure 10. In seawater at both 30 and 90°C, the corrosion rates of HVOF SAM2X5 and SAM1651 coatings exhibited slightly lower corrosion rates than either wrought sample of Alloy C-22. The corrosion rates of all materials increased with temperature, as expected. In calcium chloride at 105°C, the corrosion rates of HVOF SAM2X5 and SAM1651 coatings were comparable to, or slightly lower than that of wrought Alloy C-22. In general, the corrosion rates observed in the hot calcium chloride (105°C) were higher than those observed in the heated seawater (90°C), which was also expected.

Validation with Salt Fog Testing

The corrosion resistance of the amorphous metal coatings was verified during salt fog testing. As previously discussed [Farmer et al. 2004], the salt fog test was used to compare various wrought and thermal-spray alloys, melt-spun ribbons, arc-melted drop-cast ingots, and thermal-spray coatings for their susceptibility to corrosion by salt sprays, like those that might be encountered aboard naval ships (this test is also known as the ‘salt spray’ test). The most recent tests have focused on refined, state-of-the-art Fe-based amorphous-metal formulations, in the form of arc-melted drop-cast ingots, melt-spun ribbons, and high-velocity oxy-fuel coatings with no significant porosity and near theoretical density. In contrast, the first tests focused on early thermal-spray coatings, which had residual porosity and crystalline structure, and lower resistance to corrosion.

Both salt fog tests were conducted according to ASTM B117 “Standard Test Method of Salt Spray (Fog) Testing.” A General Motors (GM) test cycle, GM9540P, was used in both tests. The performance of the test developmental amorphous metal samples was evaluated by qualitative comparison to baseline or reference samples. Four types of reference samples were included to establish baseline performance. These references include: Type 316L stainless steel, nickel-based Alloy C-22 (N06022), Ti Grade 7, and the 50:50 nickel-chromium binary.

Salt fog testing was conducted on several thermal spray coatings, including HVOF coatings of Alloy C-22, Type 316L stainless steel, SAM40 (also referred to as DAR4)), SAM2X5 (also referred to as LDAR2X5) and SAM1651 (also referred to as CBCTL1651 or LDAR7) by Aprigliano et al. [Aprigliano et al. 2005]. After 13 cycles in the ASTM Standard B-117 Salt Fog Test, the HVOF coatings of Type 316L stainless steel and SAM40 showed substantial corrosion (Figure 11). Very slight rust spots were observed on the C-22 coating. In contrast, the newer SAM2X5 and SAM1651 formulations showed no corrosion at 30 cycles. The salt fog testing of SAM2X5 and SAM1651 were continued to almost 60 cycles with no evidence of corrosion.

Threshold for Passive Film Breakdown with Potential-Step Method

Potentiostatic step tests have been used to determine the potential at which the passive film breaks down on the reference material, Alloy C-22, and on the two amorphous metals of primary interest, SAM2X5 and SAM1651. During prolonged periods of potentiostatic polarization, which

are typically 24 hours in duration, the current is monitored as a function of time. In cases where passivity is lost, the current increases, and the test sample is aggressively attacked. In cases where passivity is maintained, the current decays to a relatively constant asymptotic level, consistent with the known passive current density. In these tests, periods of polarization are preceded by one hour at the open circuit corrosion potential.

Thresholds for Passive Film Breakdown in Seawater

See Figure 12. Potential-step testing has been performed on wrought Alloy C-22 (reference material); fully dense and completely amorphous melt spun ribbons of SAM2X5; optimized HVOF coatings produced with -53/+30 micron powders of SAM2X5; and optimized HVOF coatings produced with -30/+15 micron powders of SAM2X5. All were tested in Half Moon Bay seawater heated to 90°C. To eliminate the need for surface roughness corrections in the conversion of measured current and electrode area to current density, the SAM2X5 and SAM1651 coatings were polished to a 600-grit finish prior to testing. The curves represent the asymptotic current density reached after 24 hours at the corresponding potential (each data point represents a 24 hour test). The constant potential was applied after 1 hour at the open circuit corrosion potential (OCP). From previous work presented in the FY04 Annual Report (given in references), it has been found that coatings produced with SAM2X5 powders below a critical size are fully dense and are completely amorphous. The coatings produced with finer powders are therefore expected to have lower porosity and less residual crystalline phases present than those produced with larger particles. These data enable a clear and unambiguous determination of the threshold potentials for passive film breakdown in a non-creviced condition. First, it is clear that the passive film on wrought Alloy C-22 commences breakdown at a potential of approximately 200 mV relative to a standard Ag/AgCl reference electrode (approximately 600 mV above the open circuit corrosion potential), and has the least corrosion resistance of any sample evaluated during this test. Passive film breakdown on the SAM2X5 melt-spun ribbon did not occur until a potential in excess of 1200 mV vs. Ag/AgCl (1400 mV above OCP) was applied. Furthermore, the observed passive current density observed with this sample was extremely low. Both HVOF coatings of SAM2X5 (large and small powder sizes) also exhibited outstanding passive film stability, superior to that of the reference material. The passive film on the coating produced with -30/+15 micron powder remained intact until application of 1000 mV vs. Ag/AgCl (1200 mV above OCP), with a current density well within the passive range of several microamps per square centimeter. Similar observations were made with the coating produced with -53/+30 micron powders. Any differences in morphology did not have significant impact on corrosion resistance

See Figure 13. Transients in current density at a constant applied potential of 1000 mV vs. OCP for wrought Alloy C-22 (reference material), a fully dense and completely amorphous melt spun ribbon (MSR) of SAM2X5, HVOF coatings produced with -53/+30 micron powders of SAM2X5, and HVOF coatings produced with -30/+15 micron powders of SAM2X5, all in Half Moon Bay seawater heated to 90°C, are compared. The constant potential was applied after 1 hour at the open circuit corrosion potential (OCP). The passive film on the melt spun ribbon and HVOF coatings of SAM2X5 is more stable than that on wrought nickel-based Alloy C-22 under these conditions, leading to the conclusion that this iron-based amorphous metal has superior corrosion resistance. These coatings were produced with TNC powder by UCD and Plasmatech.

See Figure 14. Transients in current density at various levels of constant applied potential ranging from 100 to 1400 mV vs. OCP for Alloy C-22 in Half Moon Bay seawater at 90°C. This reference material was polished to a 600-grit finish. The constant potential was applied after 1 hour at the open circuit corrosion potential (OCP). Passive film stability is lost above 700 mV vs. OCP. These coatings were produced with TNC powder by UCD and Plasmatech.

See Figure 15. Transients in current density at various levels of constant applied potential ranging from 100 to 1600 mV vs. OCP for a melt-spun ribbon of SAM2X5 in Half Moon Bay seawater at 90°C are indicative of good passive film stability. The constant potential was applied after 1 hour at the open circuit corrosion potential (OCP). The passive film stability of this SAM2X5 sample is maintained at potentials up to 1500 mV vs. OCP, which is approximately 800 mV higher than the critical potential observed with Alloy-C22. At an applied potential of 1600 mV vs. OCP, passivity is lost after several hours. These coatings were produced with TNC powder by UCD and Plasmatech.

See Figure 16. Transients in current density at various levels of constant applied potential ranging from 100 to 1500 mV vs. OCP for a recently optimized SAM2X5 HVOF coating (-30/+15 micron powder) in Half Moon Bay seawater at 90°C are indicative of good passive film stability. The constant potential was applied after 1 hour at the open circuit corrosion potential (OCP). To eliminate the need for surface roughness corrections in the conversion of measured current and electrode area to current density, the SAM2X5 coating was polished to a 600-grit finish prior to testing. The curves represent the asymptotic current density reached after 24 hours at the corresponding potential (each data point represents a 24 hour test). The specified fixed potential was applied after 1 hour at the open circuit corrosion potential (OCP). The passive film stability of this SAM2X5 sample is maintained at potentials up to 1400 mV vs. OCP, which is approximately 700 mV higher than the critical potential observed with Alloy-C22. At an applied potential of 1500 mV vs. OCP, passivity is lost after several hours. These coatings were produced with TNC powder by UCD and Plasmatech.

See Figure 17. Transients in current density at various levels of constant applied potential ranging from 100 to 1500 mV vs. OCP for a recently optimized SAM2X5 HVOF coating (-53/+30 micron powder) in Half Moon Bay seawater at 90°C are indicative of exceptional passive film stability. To eliminate the need for surface roughness corrections in the conversion of measured current and electrode area to current density, the SAM2X5 coatings were polished to a 600-grit finish prior to testing. The constant potential was applied after 1 hour at the open circuit corrosion potential (OCP). The passive film stability of this SAM2X5 sample is maintained at potentials up to 1400 mV vs. OCP, which is approximately 700 mV higher than the critical potential observed with Alloy-C22. At an applied potential of 1500 mV vs. OCP, passivity is lost after several hours. These coatings were produced with TNC powder by UCD and Plasmatech.

See Figure 18. Potential-step testing has been performed on HVOF coatings of SAM1651 in deaerated Half Moon Bay seawater heated to 90°C. Tests were also performed on the reference material, Alloy C-22, in both wrought and thermally sprayed condition. To eliminate the need for surface roughness corrections in the conversion of measured current and electrode area to current density, the SAM1651 coating was polished to a 600-grit finish prior to testing. The Alloy C-22

thermal spray coating was tested in the as-sprayed condition, so a roughness factor must be applied to convert the apparent current density into actual current density. The curves represent the asymptotic current density reached after 24 hours at the corresponding potential. In this series of experiments, the passive film on wrought Alloy C-22 also commences breakdown at a potential of approximately 600 mV above the open circuit corrosion potential. Passive film breakdown on the HVOF coating of SM1651 occurred at an applied potential between 500 and 600 mV, where breakdown occurred at approximately 400 mV for the Alloy C-22 HVOF coating. In near-boiling seawater, the passive film stability of SAM1651 is comparable to that of Alloy C-22, but inferior to that of SAM2X5.

See Figure 19. Transients in current density at various levels of constant applied potential ranging from 100 to 800 mV vs. OCP for a HVOF coating of SAM1651 in Half Moon Bay seawater at 90°C are indicative of good passive film stability, comparable to that of wrought Alloy C-22. To eliminate the need for surface roughness corrections in the conversion of measured current and electrode area to current density, the SAM2X5 coatings were polished to a 600-grit finish prior to testing. To eliminate the need for surface roughness corrections in the conversion of measured current and electrode area to current density, the SAM1651 coating was polished to a 600-grit finish prior to testing. Passive film breakdown on the HVOF coating of SM1651 occurred at an applied potential between 500 and 600 mV vs. OCP, with a clear loss of passivity at 700 mV. These coatings were produced by TNC and INL before fabrication of the optimized UCD-Plasmatech coatings previously discussed.

See Figure 20. Transients in current density at various levels of constant applied potential ranging from 100 to 800 mV vs. OCP for a polished HVOF coating of SAM1651 on a Type 316L stainless steel substrate (S/N No. E316L409) in Half Moon Bay seawater at 90°C are indicative of good passive film stability, comparable to that of wrought Alloy C-22. To eliminate the need for surface roughness corrections in the conversion of measured current and electrode area to current density, the SAM2X5 coatings were polished to a 600-grit finish prior to testing. To eliminate the need for surface roughness corrections in the conversion of measured current and electrode area to current density, the SAM1651 coating was polished to a 600-grit finish prior to testing. Passive film breakdown on the HVOF coating of SM1651 occurred at an applied potential between 500 and 600 mV vs. OCP, with a clear loss of passivity at 700 mV. The coating represented by this figure is one of the first known thermal spray coatings with the SAM1651 composition, and was produced by TNC and their subcontractor before fabrication of the optimized UCD/Plasmatech coatings, which are represented by the preceding figures.

See Figure 21. Transients in current density at various levels of constant applied potential ranging from 100 to 500 mV vs. OCP for an unpolished (as sprayed) HVOF coating of nickel-based Alloy C-22 on a Type 316L stainless steel substrate (S/N No. E316L255) in Half Moon Bay seawater at 90°C show a clear and unambiguous loss of passivity at the highest potential level. Since this Alloy C-22 coating was tested in the as-sprayed condition, a roughness factor must be applied to convert the ‘apparent’ current density into the ‘actual’ current density. The coating represented by this figure was produced by TNC and their subcontractor before fabrication of the optimized UCD/Plasmatech coatings, which are represented by the preceding figures.

See Figure 22. Transients in current density at various levels of constant applied potential ranging from 100 to 736 mV vs. OCP for an unpolished (as sprayed) HVOF coating of SAM1651 on a Type 316L stainless steel substrate (S/N No. E316L410) in Half Moon Bay seawater at 90°C are indicative of good passive film stability, comparable to that of wrought Alloy C-22. Since this as-sprayed SAM1651 coating was tested in the as-sprayed condition, a roughness factor (which is expected to range from a minimum of $\times 2$ to more than $\times 10$) must be applied to convert the ‘apparent’ current density into the ‘actual’ current density. While passivity at 158 mV vs. OCP is clear, polished samples with minimal roughness, or unambiguous knowledge of the roughness factor is required to interpret measured ‘apparent’ current densities at higher applied potential in terms of passivity, or the loss of passivity. From visual inspection, it was evident that passivity was maintained at higher potentials. The ambiguity associated with early electrochemical test data such as this has lead the investigators to use polished samples with 600-grit finish for clear determinations of critical potentials. The coating represented by this figure is one of the first known thermal spray coatings with the SAM1651 composition, and was produced by TNC and their subcontractor before fabrication of the optimized UCD/Plasmatech coatings, which are represented by the preceding figures.

See Figure 23. Transients in current density at various levels of constant applied potential ranging from 100 to 615 mV vs. OCP for an early unpolished (as sprayed) HVOF coating of SAM2X5 on a Type 316L stainless steel substrate (S/N No. E316L445) in Half Moon Bay seawater at 90°C are indicative of good passive film stability, comparable to that of wrought Alloy C-22. Since this as-sprayed SAM2X5 coating was tested in the as-sprayed condition, a roughness factor (which is expected to range from a minimum of $\times 2$ to more than $\times 10$) must be applied to convert the ‘apparent’ current density into the ‘actual’ current density. While passivity at 315 mV vs. OCP is clear, current transients are observed at 415 mV on this as-sprayed surface that may be indicative of the onset of passive film breakdown. Such breakdown is clearly evident at a slightly higher potential of 515 mV vs. OCP. While this data shows very good corrosion resistance, more recent optimization has resulted in far better performance with this formulation. The coating represented by this figure is one of the first known thermal spray coatings with the SAM2X5 composition, and was produced by TNC and their subcontractor before fabrication of the new optimized UCD/Plasmatech coatings, which are represented by the preceding figures. The importance of supplier standardization and qualification is illustrated by the enhanced performance that has evolved as we have continued to work with these materials.

See Figure 24. Transients in current density at various levels of constant applied potential ranging from 100 to 460 mV vs. OCP for an early unpolished (as sprayed) HVOF coating of SAM40XV on a Type 316L stainless steel substrate (S/N No. E316L325) in Half Moon Bay seawater at 90°C are indicative of good passive film stability, comparable to that of wrought Alloy C-22. SAM40XV was an early version of SAM2X5 that TNC prepared for HPCRM with slightly less molybdenum added, and a corresponding lower critical potential. Since this as-sprayed SAMXV coating was tested in the as-sprayed condition, a roughness factor (which is expected to range from a minimum of $\times 2$ to more than $\times 10$) must be applied to convert the ‘apparent’ current density into the ‘actual’ current density. While passivity at 100 to 244 mV vs. OCP is clear, current transients observed at 460 and 560 mV are clearly indicative of passive film breakdown. Such high apparent current densities occur at higher potential in the case of SAM2X5. The coating represented by this figure is one of the first known thermal spray coatings

with the SAM40XV composition, and was produced by TNC and their subcontractor before fabrication of the new optimized UCD/Plasmatech coatings, which are represented by the preceding figures. The importance of supplier standardization and qualification is illustrated by the enhanced performance that has evolved as we have continued to work with these materials.

Thresholds for Passive Film Breakdown in Hot Calcium Chloride

See Figure 25. Potential-step testing has been performed on HVOF coatings of SAM1651 on a Type 316L stainless steel substrate (S/N No. E316L475) in extremely aggressive 5M CaCl₂ heated to 105°C. Tests were also performed on the reference material, Alloy C-22, in both wrought and thermally sprayed condition (S/N Nos. CC-22 4008 and E316L256, respectively). To eliminate the need for surface roughness corrections in the conversion of measured current and electrode area to current density, the SAM1651 coating was polished to a 600-grit finish prior to testing. The Alloy C-22 thermal spray coating was tested in the as-sprayed condition, so a roughness factor must be applied to convert the apparent current density into actual current density. The curves represent the asymptotic current density reached after 24 hours at the corresponding potential. In this series of experiments, the passive film on wrought Alloy C-22 also commences breakdown at a potential of only 240 mV above the open circuit corrosion potential, with evidence of repassivation at potentials above 400 mV. Even with the repassivation at higher potential, the window of vulnerability between 240 to 400 mV is problematic for the reference material (Alloy C-22). Passive film breakdown on the HVOF coating of SAM1651 occurred at a significantly higher applied potential, between 360 and 400 mV, where breakdown of the passive film on thermally sprayed Alloy C-22 was virtually spontaneous. The new SAM1651 coating provides clear advantages for operation in corrosive hot chloride brines with divalent cations, such as calcium.

See Figure 26. Transients in current density at various levels of constant applied potential ranging from 100 to 450 mV vs. OCP for a polished HVOF coating of SAM1651 on a Type 316L stainless steel substrate (S/N No. E316L475) in 5M CaCl₂ at 105°C are indicative of good passive film stability, which is superior to that of wrought Alloy C-22 in this environment this very aggressive environment. To eliminate the need for surface roughness corrections in the conversion of measured current and electrode area to current density, the SAM1651 coating was polished to a 600-grit finish prior to testing. Passive film breakdown on the HVOF coating of SAM1651 occurred at an applied potential between 360 and 400 mV vs. OCP, with a clear loss of passivity at 450 mV. The coating represented by this figure is one of the first known thermal spray coatings with the SAM1651 composition, and was produced by TNC and their subcontractor before fabrication of the optimized UCD/Plasmatech coatings, which are represented by the preceding figures. The performance of this SAM1651 coating was very impressive.

See Figure 27. Transients in current density at various levels of constant applied potential ranging from 100 to 550 mV vs. OCP for wrought Alloy C-22 (S/N No. CC-22 4008) in 5M CaCl₂ at 105°C, and shows complete breakdown of the passive film in two potential regimes, one regime located between 300-400 mV vs. OCP (350 mV), and the second located above 500 mV vs. OCP (550 mV). Like the polished SAM1651 coating, this reference was also polished to a 600-grit finish.

See Figure 28. Transients in current density at various levels of constant applied potential ranging from 100 to 350 mV vs. OCP for an unpolished (as-sprayed) HVOF coating of Alloy C-22 on a Type 316L stainless steel substrate (S/N No. E316L256) in 5M CaCl₂ at 105°C appears to be passive at 100-150 mV vs. OCP, but has a clear loss of passivity at potentials above 200 mV vs. OCP (250-350 mV). Since this as-sprayed Alloy C-22 coating was tested in the as-sprayed condition, a roughness factor (which is expected to range from a minimum of ×2 to more than ×10) must be applied to convert the ‘apparent’ current density into the ‘actual’ current density. The coating represented by this figure was produced by TNC and their subcontractor before fabrication of the optimized UCD/Plasmatech coatings, which are represented by preceding figures.

Effect of Devitrification on Corrosion Resistance

See Figure 29. To assess the sensitivity of these iron-based amorphous metals to devitrification, which can occur at very elevated temperature, melt-spun ribbon of SAM40 (also referred to as DAR40) were intentionally devitrified by heat treating them at various temperatures for one hour. After heat treatment, the samples were evaluated in low temperature seawater (30°C), to determine the impact of the heat treatment on passive film stability and corrosion resistance. The temperatures used for the heat treatment were: 150, 300, 800 and 1000°C. Untreated (as received) ribbons were also tested, and provide insight into the baseline performance. These samples showed no significant hysteresis and change in repassivation potential at heat treatments of 150-300°C, but showed a dramatic loss of corrosion resistance when heat treatments were performed at 800-1000°C, which are above the known recrystallization temperature of approximately 600-650°C (623°C) given in Table 2 (Perepezko et al. 2004). Both ribbons treated at elevated temperature show large hysteresis loops, which are indicative of passive film breakdown, with a clearly defined repassivation potential near -600 mV vs. Ag/AgCl (about 100 mV above the OCP). The operational limit for these materials, when being used for corrosion resistance, appears to be bounded by the recrystallization temperature.

See Figure 30. Melt spun ribbons of SAM40 (DAR40) were also intentionally devitrified by heat treating at 800°C for one hour and then subjected to cyclic polarization in 5M CaCl₂ at 105°C. In comparison to the as-received sample, the sample heat-treated at 800C showed a dramatic loss of corrosion resistance. As discussed in regard to the preceding figure, this heat-treatment temperature was known to be above the recrystallization temperature of approximately 600-650°C (623°C) given in Table 2 (Perepezko et al. 2004). The heat-treated ribbon showed a large hysteresis loop in the hot concentrated calcium chloride solution, which is indicative of passive film breakdown, with a clearly defined repassivation potential near the OCP. The post heat-treatment microstructural characterization with electron microscopy and X-ray diffraction by Yang et al. verify the existence of a completely amorphous material below the recrystallization temperature, and the development of crystalline precipitates during heat treatment above this limit. These electron microscopy images may also indicate that the corrosive attack of the precipitated crystalline phases occur to a depth of approximately 10 microns. When being used for corrosion resistance in hot geothermal brines such as calcium chloride, the operational limit also appears to be bounded by the recrystallization temperature.

See Figure 31. Melt spun ribbons of SAM2X5 were also intentionally devitrified by heat treating at 800°C for one hour and then subjected to cyclic polarization in 5M CaCl₂ at 105°C. In comparison to the as-received sample, the sample heat-treated at 800C showed a dramatic loss of corrosion resistance. As discussed in regard to the preceding figure, this heat-treatment temperature was known to be above the recrystallization temperature of approximately 600-650°C (623°C) given in Table 2 (Perepezko et al. 2004). The heat-treated ribbon showed a large hysteresis loop in the hot concentrated calcium chloride solution, which is indicative of passive film breakdown, with a clearly defined repassivation potential near the OCP. The post heat-treatment microstructural characterization with electron microscopy and X-ray diffraction by Yang et al. verify the existence of a completely amorphous material below the recrystallization temperature, and the development of crystalline precipitates during heat treatment above this limit. These electron microscopy images may also indicate that the corrosive attack of the precipitated crystalline phases occur to a depth of approximately 10 microns. When being used for corrosion resistance in hot geothermal brines such as calcium chloride, the operational limit also appears to be bounded by the recrystallization temperature.

LONG-TERM CORROSION TESTING

See Figure 32. Temperature controlled baths for long-term corrosion testing of weight loss and crevice corrosion samples, with simultaneous monitoring of the open-circuit corrosion potential, corrosion rate via linear polarization, and passive film stability with electrochemical impedance spectroscopy (EIS). Water cooled condensers are used to prevent the loss of water and other volatiles from the baths, and a water-cooled reference electrode junction is used to enable the Ag/AgCl reference electrodes to be operated at standard temperature, thereby providing a sound thermodynamic reference. The upper photograph show LLNL technicians attending to the test equipment.

Geometries of Coated Samples

See Figure 33. Weight loss and crevice samples for the long term test are 4-inch × 4-inch × ¼-inch Alloy C-22 substrates with a 40-mil thermal spray coating of amorphous metal (SAM2X5, SAM1651, etc.). The crevice samples have a hole in the center to accommodate a crevice former, and are not shown. The long-term measurements of open-circuit corrosion potential, corrosion rate via linear polarization, and electrochemical impedance spectra are done with a ¾-inch diameter Alloy C-22 rod with a hemispherical end, and with a 40-mil thermal spray coating of amorphous metal (SAM2X5, SAM1651, etc.). Small disks are used for quick screening tests with cyclic polarization, but are not considered truly representative coatings due to their small size and differences in cooling rate experienced by the disks and larger substrates with greater thermal mass and cooling capacity. The granularity of these disks is not representative can be easily seen. While small circular disk samples are relatively inexpensive and easy to produce, and can be employed in standard corrosion test cells with relative ease, they may not provide the best source of data.

Open Circuit Corrosion Potential During Long-Term Exposure

See Figure 34. The long-term corrosion test for the SAM2X5 has been initiated, and the initial open circuit corrosion potentials for this material has been measured in several fully aerated environments, and will be monitored as a function of time for the next year. These environments include Half Moon Bay seawater, 3.5 m NaCl, 3.5 m NaCl with 0.5 m KNO₃, 6.0 m NaCl and 6.0 m NaCl with 0.9 m KNO₃. For each solution composition, tests are being done at two temperature levels, 30 and 90°C.

Corrosion Rates with Linear Polarization During Long-Term Exposure

See Figure 35. In addition to monitoring the open circuit corrosion potential in these fully aerated solutions, linear polarization is also being used periodically to measure the corrosion current, which is normalized by the apparent area of the electrode, and used to estimate the general corrosion rate. The roughness factor for these unpolished (as sprayed) SAM2X5 HVOF samples must be used to convert the apparent current density to the corrosion rate. In this figure, the first series of bars (blue) represent the estimated corrosion rate with no roughness correction, and the second series of bars (magenta) represent the estimated corrosion rate with the minimum estimated roughness factor of 2. The actual roughness may be significantly higher, and is in the process of being quantified. Even without the roughness factor correction, the measured corrosion rates are very low. It is somewhat surprising that in this case, the presence of nitrate appears to accelerate the general corrosion rate, both at 3.5 and 6.0 NaCl concentrations.

Complex Impedance During Long-Term Exposure

See Figure 36. In addition to obtaining corrosion rates with linear polarization during the long term test, electrochemical impedance spectroscopy is used to periodically measure the complex impedance as a function of frequency. Such measurements are made for each environment. The data is presented in the form of a standard Bode plot, with the impedance amplitude as a function of frequency shown here. Interpretation of these data in terms of a simple linear circuit model is enabling the resistance and capacitance of the thermally sprayed samples, along with the electrolyte resistance to be determined as a function of time, temperature and environment. As the nature of the passive film changes, it will be detected through these impedance measurements. The corresponding phase angle of the complex impedance is given in the following figure.

See Figure 37. The phase angle as a function of frequency is shown here for the complex impedance data being gathered during the long-term test, and corresponds to the impedance amplitude in the previous figure.

See Figure 38. This figure shows the gamma pit at LLNL. Actual spent fuel containers will be subjected to relatively high fluxes of gamma radiation, which will cause radiolytic reactions in the aqueous environment, including the production of hydrogen peroxide and other species. Work has begun on making electrochemical corrosion measurements inside the gamma pit, so that the impact of radiation on the amorphous metal coatings, and on the Alloy C-22 reference material can be assessed.

SUMMARY

The current Fe-based amorphous metals include specific elements known to impart corrosion and oxidation resistance, such as Cr, Mo, W. Additions of Y and Zr improve glass formability, while forming protective oxide scales at high temperature. In the future, the addition of titanium may also lead improved passive film stability at higher temperatures, and is being explored.

Ingots and melt-spun ribbons of the Y- and Mo-containing Fe-based amorphous metals have no grain boundaries, and therefore have more corrosion resistance than nickel-based Alloy C-22. While the passive film on nickel-based C-22 undergoes breakdown in 5M CaCl₂ at 105°C at low potential, the passive film on the new Fe-based amorphous metal remains stable at a potential above that required for oxygen evolution.

Electrochemical tests have proven that corrosion performance superior to wrought and thermally sprayed coatings of nickel-based Alloy C-22 can be achieved with the new iron-based amorphous metals. For example, the passive film on wrought Alloy C-22 undergoes breakdown at 100 to 200 mV vs. Ag/AgCl in 5M CaCl₂ at 105°C, whereas SAM1651 maintains stable passivity, even as the potential is increased to levels approaching that required for oxygen evolution. These materials are far superior to thermal-spray coatings of Alloy C-22 in seawater. While it has not been possible to render Alloy C-22 as a corrosion resistant, thermal spray coating, such possibilities do exist with the amorphous metal formulations.

These novel materials can be produced as either bulk alloys or coatings. For example, melt spinning and arc melting with drop casting can be used to render these materials as fully dense pore-free bulk alloys. Coatings can be produced with advanced thermal spray processes, or by physical vapor deposition processes such as magnetron sputtering or electron-beam evaporation. The materials can also be rendered as bulk alloys by using HVOF to form large plates on a flat mandrel. Near theoretical density is achieved through precise control of powder size with atomization and classification.

Early HVOF coatings of SAM35, SAM40, SAM40X3 had non-optimal elemental compositions, and were produced with non-optimal thermal spray parameters (powder size, gun pressure, and particle velocity), and exhibited light rusting after 13 cycles in the classic salt fog test. However, additional work with optimized elemental compositions of these Fe-based amorphous metals, and samples in the form of fully dense pore-free materials, have shown no corrosion after 24 cycles in this aggressive test. The most promising formulations at the present time are believed to be SAM2X5 and SAM1651. Salt-fog testing of HVOF coatings of these materials showed no corrosion after more than 30 cycles (and up to 54 cycles) in the salt fog test. Such performance cannot be achieved with thermally sprayed Type 316L stainless steel, as this material loses most of its desirable corrosion-resistance during the thermal spray process. To a lesser extent, similar difficulties are encountered during the thermal spraying of Alloy C-22.

The reference material, nickel-based Alloy C-22, is an outstanding corrosion-resistant engineering material. Even so, crevice corrosion has been observed with C-22 in hot sodium chloride environments without buffer or inhibitor. Comparable metallic alloys such as SAM2X5

and SAM1651 may also experience crevice corrosion under sufficiently harsh conditions. Accelerated crevice corrosion tests are now being conducted to intentionally induce crevice corrosion, and to determine those environmental conditions where such localized attack occurs.

Such materials could also be used to coat the entire outer surface of containers for the transportation and long-term storage of spent nuclear fuel, to protect welds and heat affected zones, thereby preventing exposure to environments that might cause stress corrosion cracking, and as a means of criticality control inside containers [Farmer et al. 2000a & 2000b]. In the future, it may be possible to substitute such high-performance iron-based materials for more-expensive nickel-based alloys, thereby enabling cost savings in a wide variety of industrial applications.

ACKNOWLEDGMENTS

Work was sponsored by the Defense Advanced Research Projects Agency (DARPA) Defense Science Office (DSO), and the United States Department of Energy (DOE) Office of Civilian and Radioactive Waste Management (OCRWM). This work was done under the auspices of the U.S. DOE by Lawrence Livermore National Laboratory (LLNL) under Contract No. W-7405-Eng-48.

The HPCRM Team expresses their gratitude to sponsors for financial support, and supportive colleagues for making this work possible. A special thanks to Jeffrey Walker (DOE OSTI), Leo Christodoulou (DARPA DSO), and Joe Payer (Case Western Reserve University) for sharing their considerable knowledge and insight in field of mining and repository operations, engineering and materials science, and for their innovative solutions to many of the technical problems that have been addressed.

Several specific collaborations are gratefully acknowledged: Nancy Yang et al. at Sandia National for collaboration on the effects of heating on devitrification and corrosion resistance; Lou Aprigliano who is retired from NSWC for his collaboration on the salt fog testing of materials; Daniel Branagan et al. at TNC for the synthesis of melt-spun ribbons, SAM2X5 and SAM1651 powder, and SAM2X5 and SAM1651 coatings; and Craig Blue et al. at ORNL for the synthesis of drop-cast ingots and SAM1651 powder; Brad Beardsley for the production of industrial caliber coatings for evaluation; and the remainder of the HPCRM Team for their valuable insight and technical guidance in the successful execution of the project.

Execution of this multi-institutional materials development program would not have been possible without the outstanding administrative support and communication skills of Lesa Christman, and the exceptional resource management expertise of Sharice Tippens. The programmatic support of LLNL's Program Leader for Nuclear Energy, David McCallen has enabled this project to transition to a higher level than would have otherwise been possible.

REFERENCES

- ASTM 1989. Designation G 5-87, Annual Book of ASTM Standards, Section 3, Vol. 3.02, pp. 79–85 (1989).

HPCRM FY05 Annual Report – UCRL-TR-234799
DOE-DARPA Co-Sponsored Advanced Materials Program

- A. I. Asphahani, *Materials Performance*, Vol. 19, No. 12, pp. 33–43 (1980).
- A. J. Bard, L. R. Faulkner, *Kinetics of Electrode Reactions*, Chapter 3, pp. 86-118; *Techniques Based on Concepts of Impedance*, Chapter 9, pp. 316-369: *Electrochemical Methods, Fundamentals and Applications*, John Wiley & Sons, New York, New York (1980).
- D. J. Branagan, M. C. Marshall, B. E. Meacham, E. J. Buffa, *High-Performance Iron-Based HVOF Amorphous Coatings*, Submission to Lawrence Livermore National Laboratory for HPCRM Annual Report, NanoSteel Company, Idaho Falls, Idaho, 46 pages, September 17 (2004).
- D. J. Branagan, M. C. Marshall, B. E. Meacham, L. F. Aprigliano, R. Bayles, E. J. Lemieux, T. M. Wolejsza, F. J. Martin, J. C. Farmer, J. J. Haslam, S. D. Day, *Wear and Corrosion Resistant Amorphous / Nanostructured Steel Coatings for Replacement of Electrolytic Hard Chromium*, UCRL Report, Lawrence Livermore National Laboratory, Livermore, California. 7 pages (2005); *Proceedings of the International Thermal Spray Conference and Exposition*, American Society of Materials International, Seattle, Washington, May 15-18, 2006 (in press).
- D. Chidambaram, C. R. Clayton, M. R. Dorfman, *Evaluation of the Electrochemical Behavior of HVOF-Sprayed Alloy Coatings*, *Surface and Coatings Technology*, Vol. 176, pp. 307-317 (2004).
- J. C. Farmer, G. E. Gdowski, R. D. McCright, H. S. Ahluwalia, *Corrosion Models for Performance Assessment of High-Level Radioactive Waste Containers*, *Nuclear Engineering Design*, Vol. 129, pp. 57-88 (1991).
- J. C. Farmer et al., *Protective Ceramic Coatings for High-Level Radioactive Waste Containers*, UCRL-MI-131293, Presented to Ceramic Peer Review Panel, SRI International, Palo Alto, CA, August 17 (1998a).
- J. C. Farmer, K. R. Wilfinger, *Process Level Model for Ceramic Coating*, UCRL-ID-131899 Rev. 2, November 14 (1998b).
- J. C. Farmer, R. D. McCright, *Crevice Corrosion and Pitting of High-Level Waste Containers: Integration of Deterministic and Probabilistic Models*, Paper No. 98160, Symposium 98-T-2A, Annual Meeting of the National Association of Corrosion Engineers (NACE), Corrosion 98, San Diego, CA March 22-27 (1998c).
- J. C. Farmer, R. D. McCright, J. C. Estill, S. R. Gordon, *Development of Integrated Mechanistically-Based Degradation-Mode Models for Performance Assessment of High-Level Containers*, *Proceedings of the Symposium on the Scientific Basis for Nuclear Waste Management XXII*, D. J. Wronkiewicz, J. H. Lee, Eds., Materials Research Society Symposium Series, Warrendale, PA, Vol. 556, pp. 855-862 (1999).
- J. Farmer, S. Lu, T. Summers, D. McCright, A. Lingenfelter, F. Wang, J. Estill, L. Hackel, H-L. Chen, G. Gordon, V. Pasupathi, P. Andresen, S. Tang, M. Herrera, *Modeling and Mitigation of Stress Corrosion Cracking in Closure Welds of High-Level Waste Containers for Yucca Mountain*, *Proceedings of the Annual Meeting of the American Society of Mechanical Engineers, Pressure Vessels and Piping*, 11 pages, Seattle, Washington, July (2000a).
- J. Farmer, S. Lu, D. McCright, G. Gdowski, F. Wang, T. Summers, P. Bedrossian, J. Horn, T. Lian, J. Estill, A. Lingenfelter, W. Halsey, *General and Localized Corrosion of High-Level Waste Container in Yucca Mountain*, *Proceedings of the Annual Meeting of the American Society of Mechanical Engineers, Pressure Vessels and Piping*, 11 pages, Seattle, Washington, July (2000b).

HPCRM FY05 Annual Report – UCRL-TR-234799
DOE-DARPA Co-Sponsored Advanced Materials Program

- J. C. Farmer et al., High-Performance Corrosion-Resistant Amorphous Metals, Proc. Global 2003, New Orleans, Louisiana, American Nuclear Society (2003).
- J. C. Farmer, J. J. Haslam, S. D. Day, D. J. Branagan, C. A. Blue, J. D. K. Rivard, L. F. Aprigliano, N. Yang, J. H. Perepezko, M. B. Beardsley, Corrosion Characterization of Iron-Based High-Performance Amorphous-Metal Thermal-Spray Coatings, PVP2005-71664, Proceedings of ASME PVP: Pressure Vessels & Piping Division Conference, Grand Hyatt, Denver, Colorado, July 17-21, 2005, American Society of Mechanical Engineers, Three Park Avenue, New York, New York, 7 pages (2005).
- J. C. Farmer, J. J. Haslam, S. D. Day, D. J. Branagan, M. C. Marshall, B. E. Mecham, E. J. Buffa, C. A. Blue, J. D. K. Rivard, D. C. Harper, M. B. Beardsley, D. T. Weaver, L. F. Aprigliano, L. Kohler, R. Bayles, E. J. Lemieux, T. M. Wolejsza, N. Yang, G. Lucadamo, J. H. Perepezko, K. Hildal, L. Kaufman, A. H. Heuere, F. Ernst, G. M. Michal, H. Kahn, E. J. Lavernia, High-Performance Corrosion-Resistant Materials: Iron-Based Amorphous-Metal Thermal-Spray Coatings, High-Performance Corrosion-Resistant Materials (HPCRM) Annual Report, UCRL-TR-206717, Lawrence Livermore National Laboratory, Livermore, California, 178 pages, September 28 (2004).
- D. V. Fix, J. C. Estill, R. B. Rebak, Effect of Small Variation in Composition of Plates and Weld Filler Wires on the General Corrosion Rate of Ni-Cr-Mo Alloys, PVP2005-71173, Proceedings of ASME PVP: Pressure Vessels & Piping Division Conference, Denver, Colorado, July 17-21, 2005, American Society of Mechanical Engineers, 9 pages (2005).
- F. Guo, S. J. Poon, G. J. Shiflet, Metallic Glass Ingots Based on Yttrium, Applied Physics Letters, Vol. 83, No. 13, pp. 2575-2577 (2003).
- J. C. Hamilton, J. C. Farmer, R. J. Anderson, In Situ Raman Spectroscopy of Anodic Films Formed on Copper and Silver in Sodium Hydroxide Solution, J. Electrochem. Soc., Vol. 85, No. 4, pp. 739-745 (1986).
- J. J. Haslam, J. C. Farmer, R. W. Hopper, K. R. Wilfinger, Ceramic Coatings for Corrosion Resistant Nuclear Waste Container Evaluated in Simulated Ground Water at 90C, UCRL-JRNL-206107, Lawrence Livermore National Laboratory, Livermore, California, August 17, 2004 (34 p.); Metallurgical and Materials Transactions A, Volume 36A, May 2005, p. 1085-1095 (2004).
- G. O. Ilvebare, T. Lian, J. C. Farmer, Environmental Considerations in the Studies of Corrosion Resistant Alloys for High-Level Radioactive Waste Containers, Paper No. 02539, NACE Corrosion 2002, Denver, Colorado, April 7-11 (2002).
- K. Kishitake, H. Era, F. Otsubo, Characterization of Plasma Sprayed Fe-10Cr-10Mo-(C,B) Amorphous Coatings, Vol. 5, No. 2, pp. 145-153 (1996).
- W. T. Kim, K. Clay, C. Small, B. Cantor, Heat Treatment of a Melt Spun Fe70Cr18Mo2B10 Alloy, Journal of Non-Crystalline Solids, Vol. 127, pp. 273-286 (1991).
- K. J. King, J. C. Estill, R. B. Rebak, Anodic Behavior of Specimens Prepared from a Full-Diameter Alloy 22 Fabricated Container for Nuclear Waste, PVP2005-71176, Proceedings of ASME PVP: Pressure Vessels & Piping Division Conference, Denver, Colorado, July 17-21, 2005, American Society of Mechanical Engineers, 9 pages (2005).
- R. M. Latanison, Corrosion Resistance of Metastable Alloys Processed by Rapid Solidification, Workshop on Amorphous Metals and Semiconductors, Electric Power Research Institute (EPRI), May 12-18, 1985.
- L. Kaufman, Calculation of Coating Compositions for Use in Various Corrosive Environments with Pourbaix and Thermal Stability Diagrams, Massachusetts Institute of

HPCRM FY05 Annual Report – UCRL-TR-234799
DOE-DARPA Co-Sponsored Advanced Materials Program

Technology, Submission to Lawrence Livermore National Laboratory for HPCRM Annual Report, Cambridge, Massachusetts, 38 pages, September 8 (2004).

- Z. P. Lu, C. T. Liu, W. D. Porter, Role of Yttrium in Glass Formation of Fe-Based Bulk Metallic Glasses, Vol. 83, No. 13, Applied Physics Letters, pp. 2581-2583.
- J. S. Newman, Electrode Kinetics, Chapter 8, pp. 186-211, Electrochemical Systems, 2nd Edition, Prentice Hall International Series in the Physical and Chemical Engineering Sciences, Prentice Hall, Englewood Cliffs, New Jersey (1973).
- S. J. Pang, T. Zhang, K. Asami, A. Inoue, Acta Materialia 50, 489-497 (2002).
- S. Pang, T. Zhang, K. Asami, A. Inoue, Materials Transactions, Effects of Chromium on the Glass Formation and Corrosion Behavior of Bulk Glassy Fe-Cr-Mo-C-B Alloys, Vol. 43, No. 8, pp. 2137-2142 (2002a).
- S. J. Pang, T. Zhang, K. Asami, A. Inoue, Synthesis of Fe-Cr-Mo-C-B-P Bulk Metallic Glasses with High Corrosion Resistance, Acta Materialia, Vol. 50, pp. 489-497 (2002b).
- J. H. Perepezko, K. Hildal, Thermal and Kinetic Analysis of Amorphous Fe-Based Alloys for Use in Thermal Spray Processing, Submission to Lawrence Livermore National Laboratory for HPCRM Annual Report, University of Wisconsin, Madison, Wisconsin, 74 pages, September 9 (2004).
- D. E. Polk, B. C. Giessen, Overview of Principles and Applications, Chapter 1, pp. 2-35, Metallic Glasses, J. J. Gilman, H. J. Leamy, Eds., American Society of Metals, Metals Park, Ohio, 348 p. (1978).
- H. Shinimiya, A. Nakazawa, Z. Kato, A. A. El Moneium, Y. Niizeki, K. Asami, K. Hashimoto, Corrosion Resistant Bulk Amorphous Ni-Cr-Ta-Mo-Nb-5P Alloys in Concentrated Hydrochloric Acids, Paper 319, Session on Corrosion and Electrochemistry of Advanced Materials in Honor of Koji Hashimoto, 208th Meeting of the Electrochemical Society, Westing Bonaventure Hotel, Los Angeles, California, October 16-21, 2005, Electrochemical Society, Pennington, New Jersey (2005).
- M. Telford, The Case for Bulk Metallic Glass, Materials Today, March 2004, Elsevier Ltd., pp. 36-43 (2004).
- K. R. Wilfinger, J. C. Farmer, R. W. Hopper, T. E. Shell, Corrosion Protection of Metallic Waste Packages Using Thermal Sprayed Ceramic Coatings, Proceedings of the Symposium on the Scientific Basis for Nuclear Waste Management XXII, D. J. Wronkiewicz, J. H. Lee, Eds., Materials Research Society Symposium Series, Warrendale, PA, Vol. 556, pp. 927-934 (1999).
- N. Yang, J. Farmer, G. Lucadamo, J. Haslam, Microstructural Factors and Their Implication to Corrosion and Damage Tolerance of Fe-Cr-Mo Based SAM40 and SAM1651, Submission to Lawrence Livermore National Laboratory for HPCRM Annual Report, Sandia National Laboratory, Livermore, California, August 30, 2004, 43 pages.
- A. Yilmaz, P. Pasupathi, R. Rebak, Stifling of Crevice Corrosion in Alloy 22 During Constant Potential Tests, PVP2005-71174, Proceedings of ASME PVP: Pressure Vessels & Piping Division Conference, Denver, Colorado, July 17-21, 2005, American Society of Mechanical Engineers, 10 pages (2005).

HPCRM FY05 Annual Report – UCRL-TR-234799
DOE-DARPA Co-Sponsored Advanced Materials Program

TABLES

Table 1 – The melt-spinning process was used to perform a systematic study of various elemental compositions, each based on the Fe-based DAR40 composition, with 1, 3, 5, and 7 atomic percent additions of specific elements believed to be beneficial to glass formation or corrosion resistance. Elemental additions investigated included nickel, molybdenum, yttrium, titanium, zirconium, and chromium.

Original Data	Formula	Fe	Cr	Mn	Mo	W	B	C	Si	Y	Zr	Ti	Ni	P	Other
DAR27	$(\text{Fe}_{0.8}\text{Cr}_{0.2})_{73}\text{Mo}_2\text{W}_2\text{B}_{16}\text{C}_4\text{Si}_1\text{Mn}_2$	58.4	14.6	2.0	2.0	2.0	16.0	4.0	1.0						
DAR35	$\text{Fe}_{54.5}\text{Mn}_2\text{Cr}_{15}\text{Mo}_2\text{W}_{1.5}\text{B}_{16}\text{C}_4\text{Si}_5$	54.2	15.0	2.0	2.0	1.5	16.0	4.0	5.0						0.3
DAR40	$\text{Fe}_{52.3}\text{Mn}_2\text{Cr}_{19}\text{Mo}_{2.5}\text{W}_{1.7}\text{B}_{16}\text{C}_4\text{Si}_{2.5}$	52.3	19.0	2.0	2.5	1.7	16.0	4.0	2.5						
DAR40X3	$\text{Fe}_{50.7}\text{Mn}_{1.9}\text{Cr}_{18.4}\text{Mo}_{5.4}\text{W}_{1.6}\text{B}_{15.5}\text{C}_{3.9}\text{Si}_{2.4}$	50.7	18.4	1.9	5.4	1.6	15.5	3.9	2.4						0.2
LDAR1	$(\text{DAR40})_{100-x} + \text{Ni}_x$														
LDAR1X1	$(\text{DAR40})_{99} + \text{Ni}_1$	51.8	18.8	2.0	2.5	1.7	15.8	4.0	2.5				1.0		
LDAR1X3	$(\text{DAR40})_{97} + \text{Ni}_3$	50.7	18.4	1.9	2.4	1.6	15.5	3.9	2.4				3.0		
LDAR1X5	$(\text{DAR40})_{95} + \text{Ni}_5$	49.7	18.1	1.9	2.4	1.6	15.2	3.8	2.4				5.0		
LDAR1X7	$(\text{DAR40})_{93} + \text{Ni}_7$	48.6	17.7	1.9	2.3	1.6	14.9	3.7	2.3				7.0		
LDAR2X1	$(\text{DAR40})_{99} + \text{Mo}_1$	51.8	18.8	2.0	3.5	1.7	15.8	4.0	2.5						
LDAR2X3	$(\text{DAR40})_{97} + \text{Mo}_3$	50.7	18.4	1.9	5.4	1.6	15.5	3.9	2.4						
LDAR2X5	$(\text{DAR40})_{95} + \text{Mo}_5$	49.7	18.1	1.9	7.4	1.6	15.2	3.8	2.4						
LDAR2X7	$(\text{DAR40})_{93} + \text{Mo}_7$	48.6	17.7	1.9	9.3	1.6	14.9	3.7	2.3						
LDAR3X1	$(\text{DAR40})_{99} + \text{Y}_1$	51.8	18.8	2.0	2.5	1.7	15.8	4.0	2.5	1.0					
LDAR3X3	$(\text{DAR40})_{97} + \text{Y}_3$	50.7	18.4	1.9	2.4	1.6	15.5	3.9	2.4	3.0					
LDAR3X5	$(\text{DAR40})_{95} + \text{Y}_5$	49.7	18.1	1.9	2.4	1.6	15.2	3.8	2.4	5.0					
LDAR3X7	$(\text{DAR40})_{93} + \text{Y}_7$	48.6	17.7	1.9	2.3	1.6	14.9	3.7	2.3	7.0					
LDAR4X1	$(\text{DAR40})_{99} + \text{Ti}_1$	51.8	18.8	2.0	2.5	1.7	15.8	4.0	2.5			1.0			
LDAR4X3	$(\text{DAR40})_{97} + \text{Ti}_3$	50.7	18.4	1.9	2.4	1.6	15.5	3.9	2.4			3.0			
LDAR4X5	$(\text{DAR40})_{95} + \text{Ti}_5$	49.7	18.1	1.9	2.4	1.6	15.2	3.8	2.4			5.0			
LDAR4X7	$(\text{DAR40})_{93} + \text{Ti}_7$	48.6	17.7	1.9	2.3	1.6	14.9	3.7	2.3			7.0			
LDAR5X1	$(\text{DAR40})_{99} + \text{Zr}_1$	51.8	18.8	2.0	2.5	1.7	15.8	4.0	2.5		1.0				
LDAR5X3	$(\text{DAR40})_{97} + \text{Zr}_3$	50.7	18.4	1.9	2.4	1.6	15.5	3.9	2.4		3.0				
LDAR5X5	$(\text{DAR40})_{95} + \text{Zr}_5$	49.7	18.1	1.9	2.4	1.6	15.2	3.8	2.4		5.0				
LDAR5X7	$(\text{DAR40})_{93} + \text{Zr}_7$	48.6	17.7	1.9	2.3	1.6	14.9	3.7	2.3		7.0				
LDAR6	$\text{Fe}_{42}\text{Cr}_{16}\text{Mo}_{16}\text{B}_5\text{C}_{10}\text{P}_{10}$	43.0	16.0		16.0		5.0	10.0							10.0
LDAR7	$\text{CBCTL1651} = \text{Fe}_{48}\text{Mo}_{14}\text{Cr}_{15}\text{Y}_2\text{C}_{15}\text{B}_6$	48.0	15.0		14.0		6.0	15.0		2.0					
LDAR8	$(\text{CBCTL161})_{97} + \text{W}_3$	46.6	14.6		13.6	3.0	5.8	14.6		1.9					
LDAR9	$(\text{DAR40})_{90} + \text{Mo}_7 + \text{Y}_3$	47.1	17.1	1.8	9.3	1.5	14.4	3.6	2.3	3.0					
LDAR10	$\text{Fe}_{57.3}\text{Cr}_{21.4}\text{Mo}_{2.6}\text{W}_{1.8}\text{B}_{16.9}$	57.3	21.4		2.6	1.8	16.9								

HPCRM FY05 Annual Report – UCRL-TR-234799
DOE-DARPA Co-Sponsored Advanced Materials Program

Table 2 – Summary of thermal analysis (DTA or DSC) on Fe-based glass forming alloys suitable for spray deposition.

Alloy	T _g (°C)	T _x (°C)	T _m (°C)	T _L (°C)	T _{rg} (°C)
DAR35	545-565	613	1074	1350	0.51
DAR40	568-574	623	1110	1338	0.53
DAR40X3	561-567	630	1130	1260	0.55
LDAR1X1	not clear	612	1121	min. 1270	N.A.
LDAR1X3	560	589	1119	min. 1300	0.53
LDAR1X5	540	572	1115	min. 1300	0.52
LDAR1X7	510	545	1112	min. 1300	0.50
LDAR2X1	575	620	1124	1190-1210	0.57
LDAR2X3	578	626	1131	1190-1210	0.57
LDAR2X5	579	628	1133	1190-1210	0.57
LDAR2X7	573	630	1137	1190-1210	0.57
LDAR3X1	560	614	1108	min. 1320	0.52
LDAR3X3	573	659	1138	min. 1380	0.51
LDAR3X5	590	677	1143	min. 1400	0.52
LDAR3X7	not clear	697	1164	min. 1420	
LDAR4X1	573	621	1135	min. 1300	0.54
LDAR4X3	568	623	1146	min. 1320	0.53
LDAR4X5	580	623	1194	1290	0.55
LDAR4X7	558	616	1198	1255	0.54
LDAR5X1	570	622	1134	min. 1360	0.52
LDAR5X3	575	641	1147	min. 1410	0.50
LDAR5X5	596	659	1193	min. 1420	0.51
LDAR6	580	623 ²⁾	995	1238-1250	0.56
LDAR7	584	653 ²⁾	1121	1290	0.55
LDAR8	565	637 ²⁾	1137	1350-1370	0.52
LDAR9	572	677 ²⁾	1146	1223	0.56
LDAR10	535	568 ¹⁾	1210	1350-1370	0.50
LDAR11	535	572 ¹⁾	1202	1365-1395	0.49

HPCRM FY05 Annual Report – UCRL-TR-234799
DOE-DARPA Co-Sponsored Advanced Materials Program

Table 3 – Current Test Matrix at Lawrence Livermore National Laboratory

Test Matrix at Lawrence Livermore National Laboratory						
Test Solution Type	NaCl	KNO ₃	T	CaCl ₂	Ca(NO ₃) ₂	T
	M or m	M or m	°C	M or m	M or m	°C
Half Moon Bay SW			30, 90			
Half Moon Bay SW			30, 90			
Chloride-Nitrate	1 M	None	30, 90			
Chloride-Nitrate	3.5 m	None	30, 90			
Chloride-Nitrate	3.5 m	0.175 m	30, 90			
Chloride-Nitrate	3.5 m	0.525 m	30, 90			
Chloride-Nitrate	6.0 m	None	30, 90			
Chloride-Nitrate	6.0 m	0.300 m	30, 90			
Chloride-Nitrate	6.0 m	0.900 m	30, 90			
Calcium Chloride				5 M	None	105
Calcium Chloride				12 m	None	130
Calcium Chloride				12 m	6 m	130

Published References: PVP 2005-71173; 71174; 71175; 71176.

FIGURES

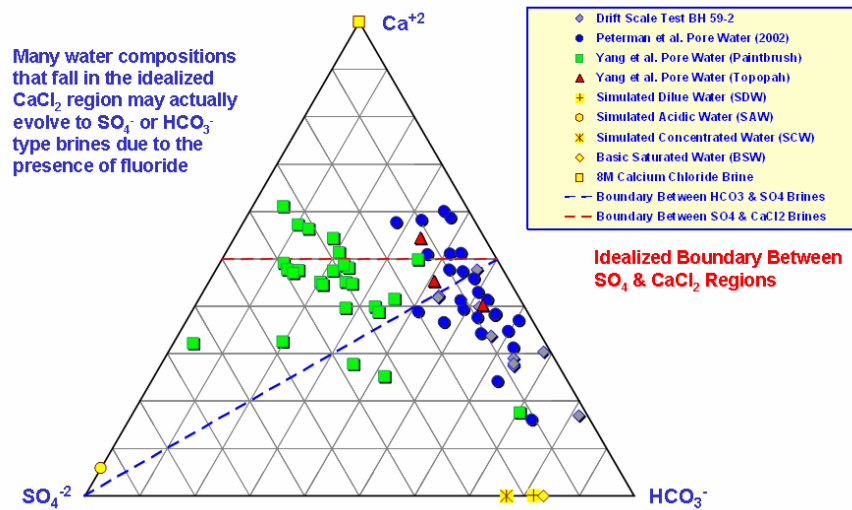


Figure 1. The classification of actual Yucca Mountain brines is shown in this pseudo ternary (trilateral) diagram. The boundary between the sulfate-chloride (SO_4^{-2}) and calcium chloride (Ca^{+2}) regions is idealized. Many of the water compositions that fall in the idealized calcium chloride (Ca^{+2}) region may actually evolve to sulfate-chloride (SO_4^{-2}) or bicarbonate (HCO_3^-) type brines due to the presence of fluoride.



Figure 2. Electrochemical corrosion measurements at LLNL are made in special temperature controlled electrochemical cells which enable testing at elevated temperature for prolonged periods of time (years if necessary). Water cooled condensers are included to prevent the loss of volatiles from the electrochemical cell, while a water cooled junction enables the reference electrode to be maintained at standard temperature during testing, thereby minimizing error.

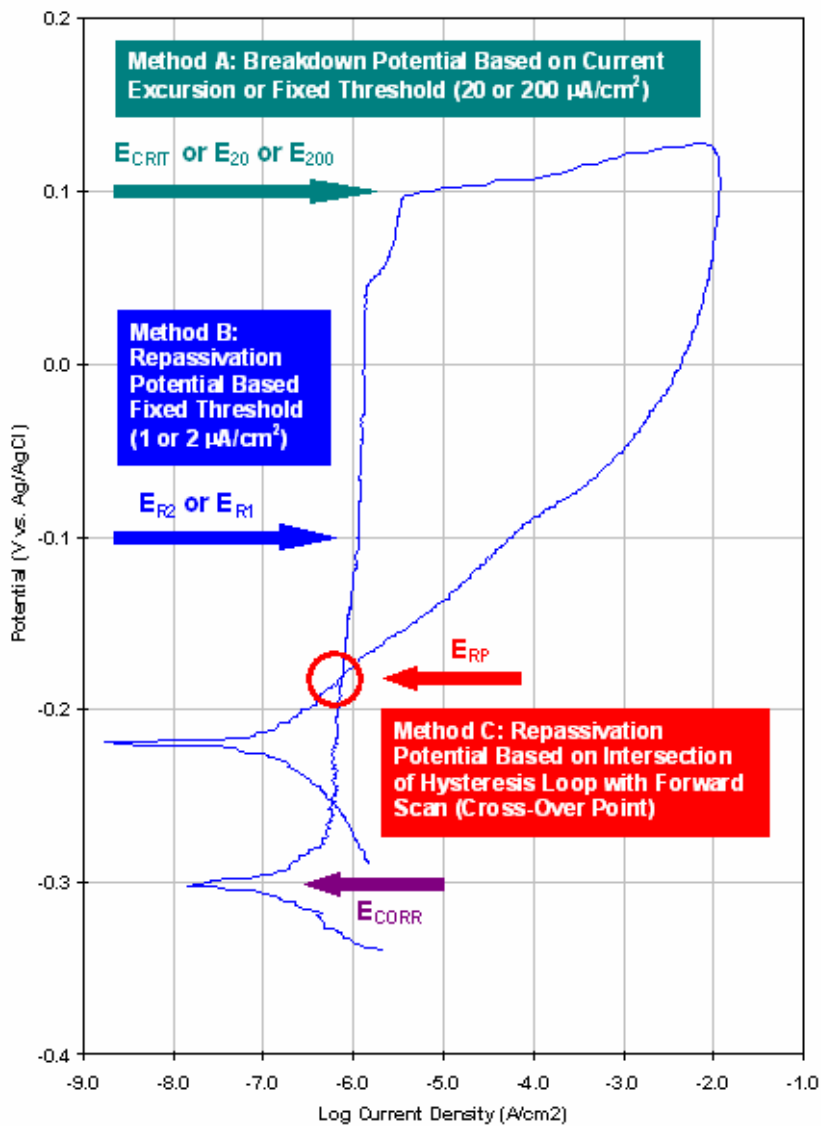


Figure 3. Three competing methodologies (Methods A, B and C) are shown for determination of the threshold potential for localized corrosion from cyclic polarization curves, such as the one shown here for nickel-based Alloy C-22 in 5M CaCl₂ at 105 °C. Method A is the point during the anodic potential scan when the passive oxide film breaks down, thereby allowing anodic dissolution of the underlying metal, with a relatively high anodic current density. When it can be accurately measured, this is the true “critical potential.” Alternatively, the repassivation potential can be determined with either Methods B or C. The repassivation potential is determined during the reverse scan, and is the point following passive film breakdown where the current density decreases to a level known to correspond to the passive current density (the current density that can be sustained by an intact oxide film). The passive current density can either be assumed, shown as Method B, or it can be established from the intersection of the forward and reverse potential scans, shown as Method C. Method C is considered to be the most rigorous approach for determining the repassivation potential, since the intersection point occurs at the actual (not assumed) passive current density.

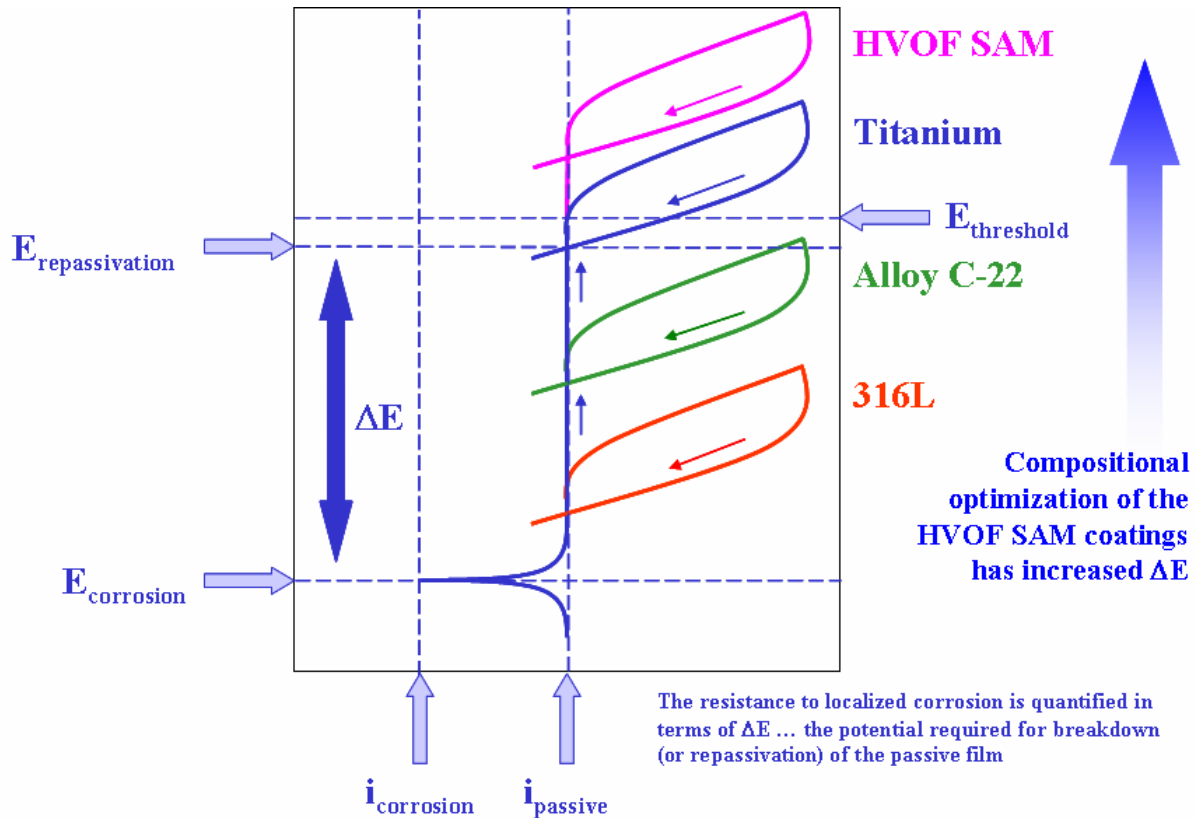


Figure 4. The repassivation potential, determined by Method C in most cases, has been used as a quantitative metric for screening elemental compositions of competing iron-based amorphous metals, thereby determining the specific composition (of those tested) with the best resistance to passive film breakdown in the test solution. A wide variety of alloy compositions, which are shown in Table 1, were explored using cyclic polarization as a screening method. However, as will be evident in the discussion of subsequent potential-step test data, superior and more credible methods exist for the determination of the critical potential. The potential step-methods are used after the initial screening, and provide better results.

Cyclic Polarization of HPCRM Fe-Based SAM in
Sea Water at 30°C (Navy Mission)

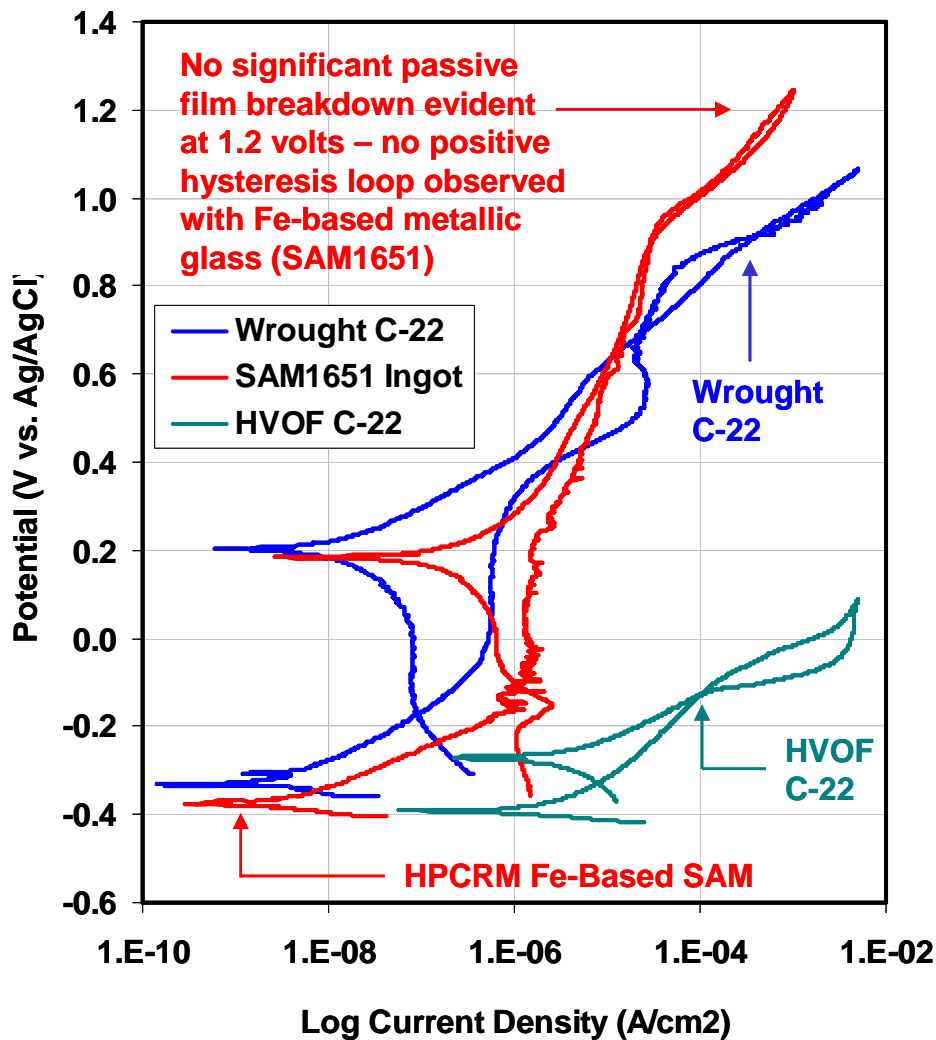


Figure 5. Cyclic polarization was used as a means of evaluating the relative passive film stability of a drop-cast ingot of SAM1651, a disk of wrought nickel-based Alloy C-22 (reference material), and a thermal spray (high-velocity oxy-fuel or HVOF) coating of Alloy C-22. The test was conducted in Half Moon Bay seawater at 30C, and the potential was measured relative to a standard silver / silver chloride reference electrode. The scan rate was 0.1667 volts per second. The current density for the ‘as-sprayed’ Alloy C-22 HVOF coating is based upon apparent electrode area, and was not corrected for surface roughness. In the case of the SAM1651, no passive film breakdown was observed, which is evident from the lack of hysteresis, even after scanning the voltage to a level close to oxygen evolution. Passive film breakdown was observed with wrought Alloy C-22, with a repassivation potential by Method C easily identified. Surprisingly, the Alloy C-22 coating loses has very poor corrosion resistance in comparison to both the SAM1651 ingot and the wrought Alloy C-22, which is reflected in a low repassivation potential.

Cyclic Polarization of Alloy C-22 and HPCRM
Fe-Based SAM in 5M CaCl₂ at 105°C (DOE Mission)

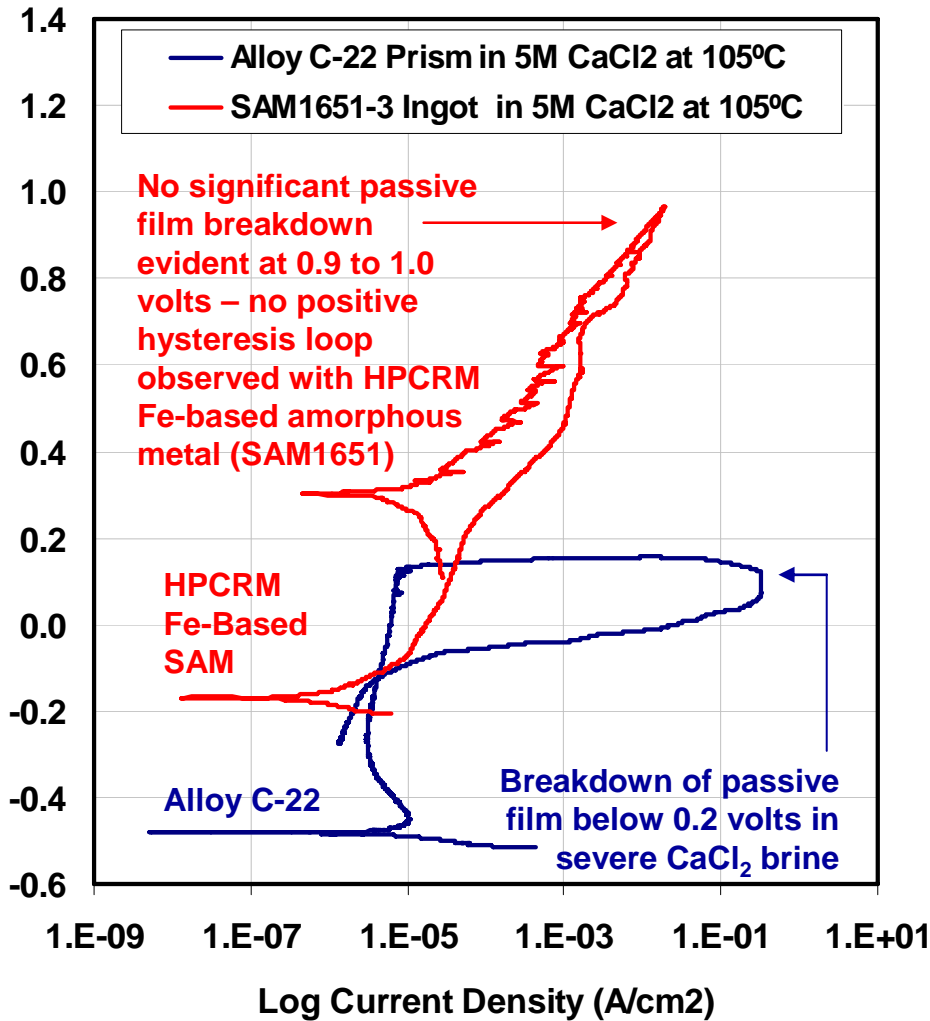


Figure 6. Cyclic polarization was used to compare the performance of a drop-cast ingot of SAM1651 against that of wrought Alloy C-22 in 5M calcium chloride at 105 °C, which is an extremely aggressive environment. In the case of the drop-cast ingot of SAM1651, no significant passive film breakdown was observed at 0.9 to 1.0 volts. There was no positive hysteresis loop observed with this iron-based amorphous metal. There was hysteresis, but with the observed current density during the reverse less than that observed during the forward scan (indicative of even lower reactivity). In sharp contrast, there is an obvious breakdown of the nickel-based Alloy C-22 passive film at only 0.2 volts, showing a clear vulnerability in this aggressive environment. The repassivation potential is easily identified from the intersection of the hysteresis loop with the forward scan.

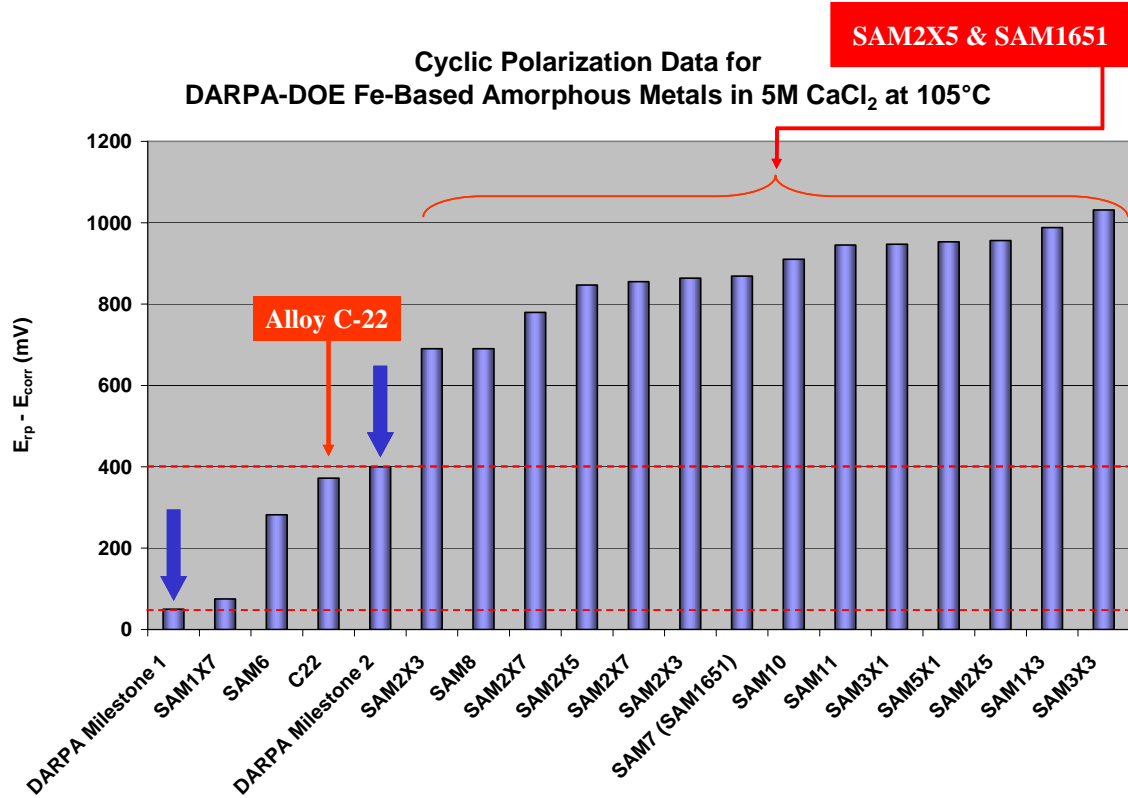


Figure 7. Cyclic polarization of melt spun ribbons was used to compare the relative corrosion resistance of a large number candidate alloy compositions in 5M CaCl₂ at 105 °C. The alloy compositions are defined in Table 1. As previously discussed, the quantifiable metric used as a basis of comparison was the difference between the open circuit corrosion potential (E_{corr}) and the repassivation potential (E_{rp}). Several of the candidate alloy compositions had a larger metric value ($E_{rp} - E_{corr}$) than the reference material, which has been established as nickel-based Alloy C-22, due to its own outstanding corrosion performance. Note that DARPA Milestone 1 corresponds to the metric value for Type 316L stainless steel and DARPA Milestone 2 corresponds to the metric value for nickel-based Alloy C-22. It is therefore concluded that several types of iron-based amorphous metals exist which all have passive film stabilities that are comparable to that of the reference material.

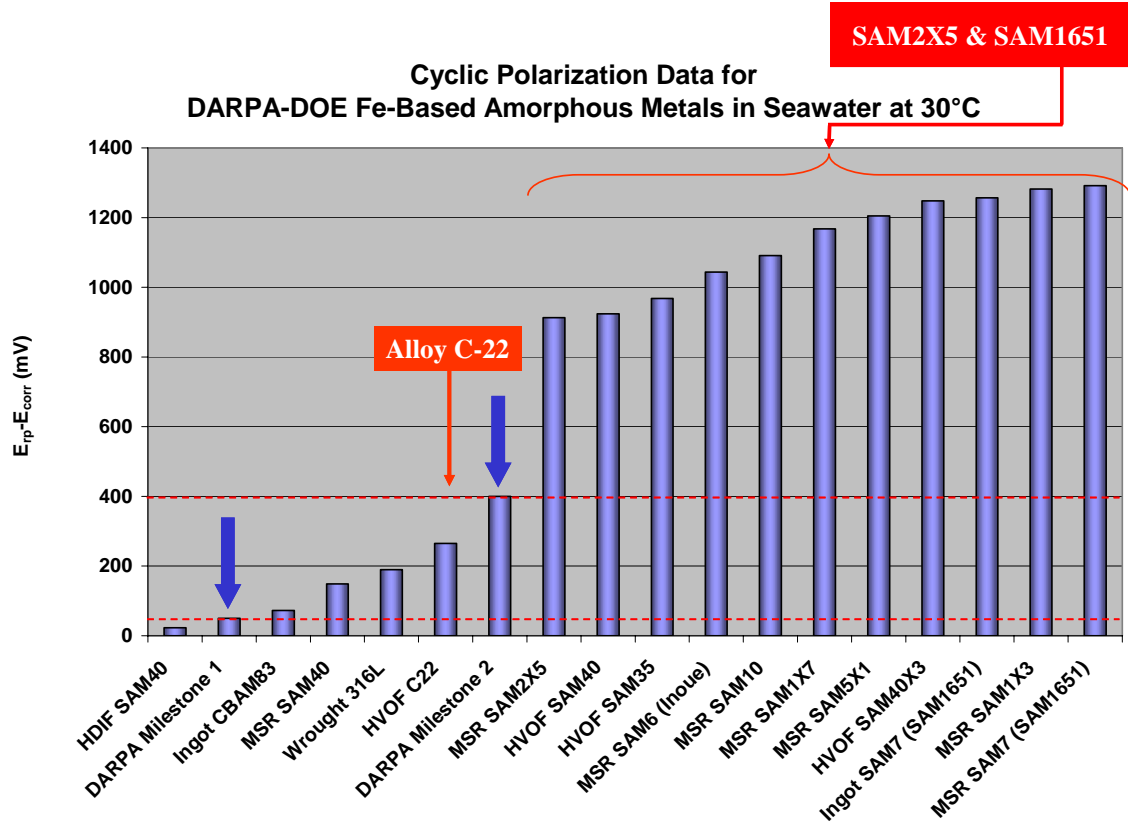


Figure 8. Cyclic polarization of melt spun ribbons was used to compare the relative corrosion resistance of a large number candidate alloy compositions in near-ambient Half Moon Bay seawater at 30 °C. The alloy compositions are defined in Table 1. DARPA Milestone 1 corresponds to the metric value for Type 316L stainless steel and DARPA Milestone 2 corresponds to the metric value for nickel-based Alloy C-22. It is therefore concluded that several types of iron-based amorphous metals exist which all have passive film stabilities in seawater at 30 °C that are comparable to that of the reference material.

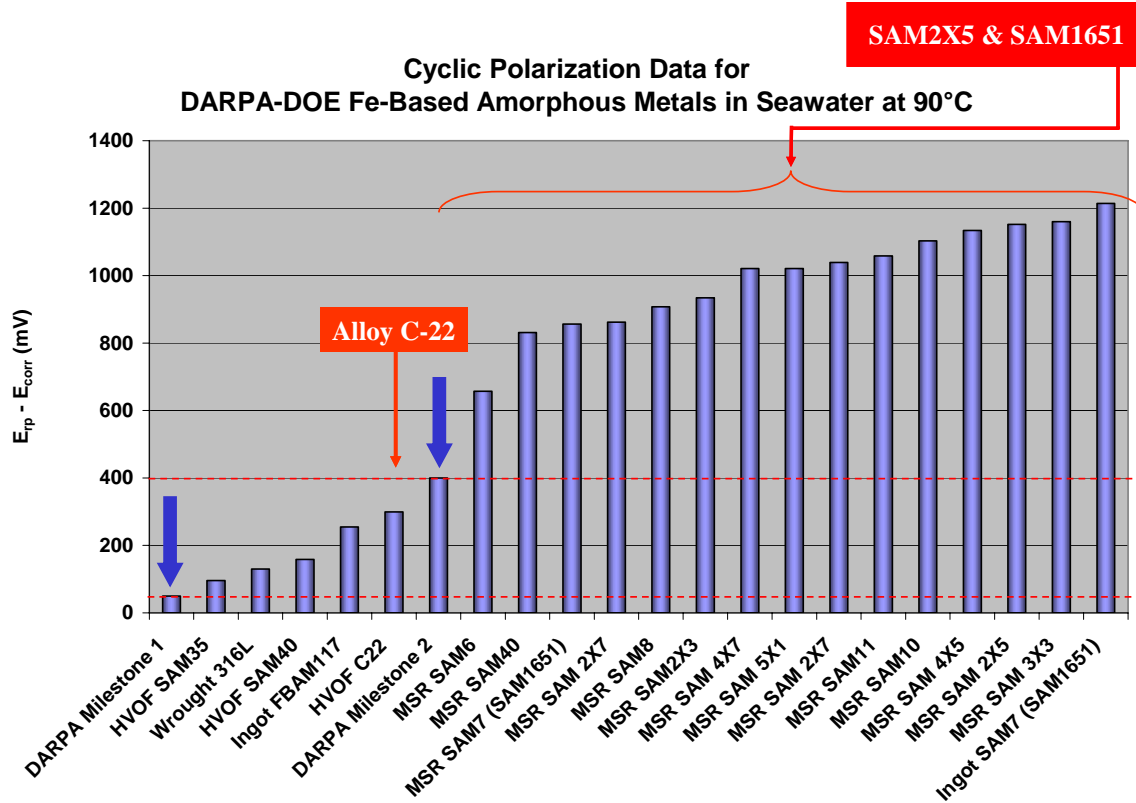


Figure 9. Cyclic polarization of melt spun ribbons was used to compare the relative corrosion resistance of a large number candidate alloy compositions in near-boiling Half Moon Bay seawater at 90 °C. The alloy compositions are defined in Table 1. DARPA Milestone 1 corresponds to the metric value for Type 316L stainless steel and DARPA Milestone 2 corresponds to the metric value for nickel-based Alloy C-22. It is therefore concluded that several types of iron-based amorphous metals exist which all have passive film stabilities in seawater at 90 °C that are comparable to that of the reference material.

HPCRM FY05 Annual Report – UCRL-TR-234799
DOE-DARPA Co-Sponsored Advanced Materials Program

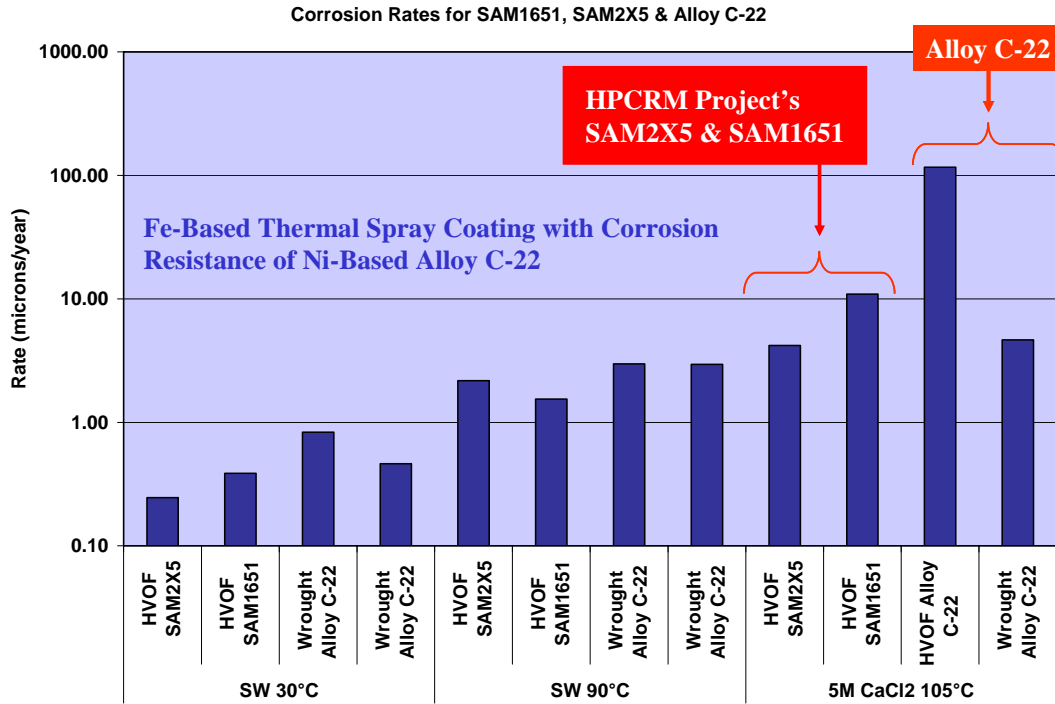


Figure 10. Linear polarization was used to determine the approximate corrosion rates of the thermal spray coatings of two amorphous metals of interest (HVOF SAM1651 and SAM2X5 coatings) and the reference material (wrought nickel-based Alloy C-22) in three relevant environments, Half Moon Bay seawater at two temperature levels, and in hot concentrated calcium chloride (5M CaCl₂ at 105 °C). In seawater at both 30 and 90 °C, the corrosion rates of HVOF SAM2X5 and SAM1651 coatings exhibited slightly lower corrosion rates than either wrought sample of Alloy C-22. The corrosion rates of all materials increased with temperature, as expected. In calcium chloride at 105 °C, the corrosion rates of HVOF SAM2X5 and SAM1651 coatings were comparable to, or slightly lower than that of wrought Alloy C-22. In general, the corrosion rates observed in the hot calcium chloride (105 °C) were higher than those observed in the heated seawater (90 °C), which was also expected.

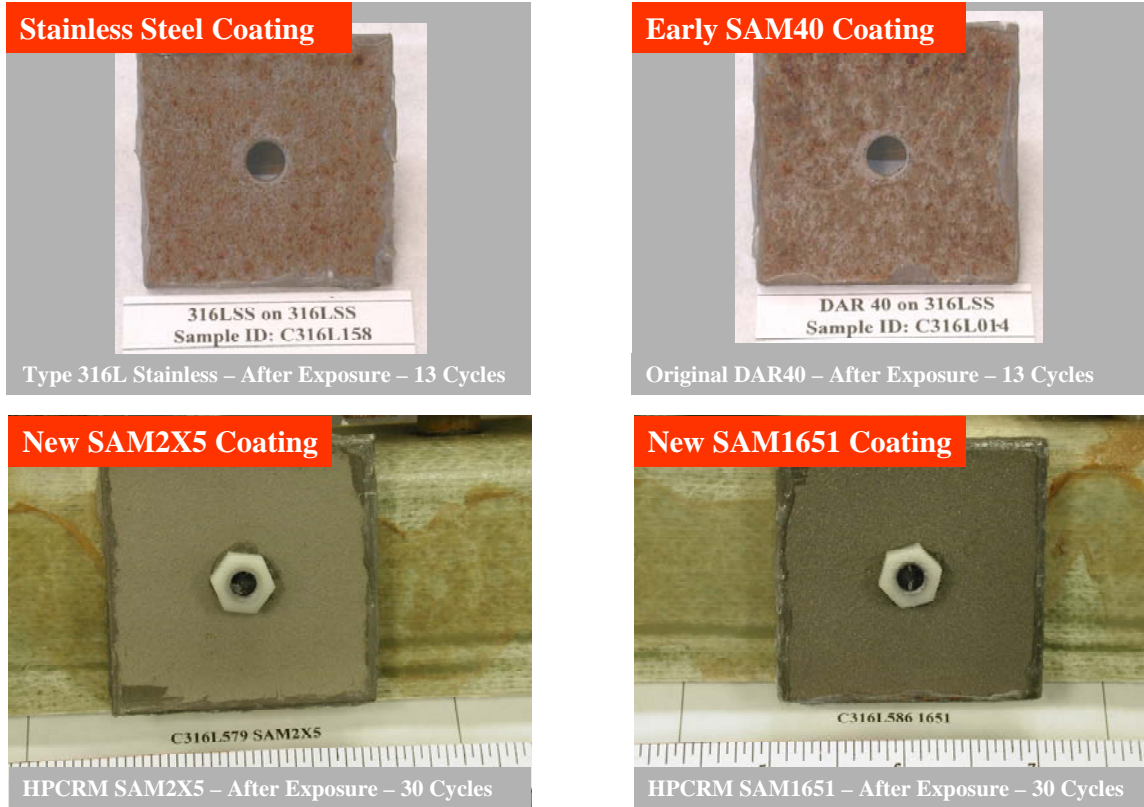


Figure 11. Salt fog testing was conducted on several thermal spray coatings, including HVOF coatings of Alloy C-22, Type 316L stainless steel, SAM40 (also referred to as DAR4)), SAM2X5 (also referred to as LDAR2X5) and SAM1651 (also referred to as CBCTL1651 or LDAR7). After 30 cycles in the ASTM Standard B-117 Salt Fog Test, the HVOF coating of Alloy C-22 showed slight rusting (not shown), while the HVOF coatings of Type 316L stainless steel and SAM40 showed substantial corrosion. In contrast, the newer SAM2X5 and SAM1651 formulations showed no corrosion at 30 cycles. The salt fog testing of SAM2X5 and SAM1651 were continued to almost 60 cycles with no evidence of corrosion.

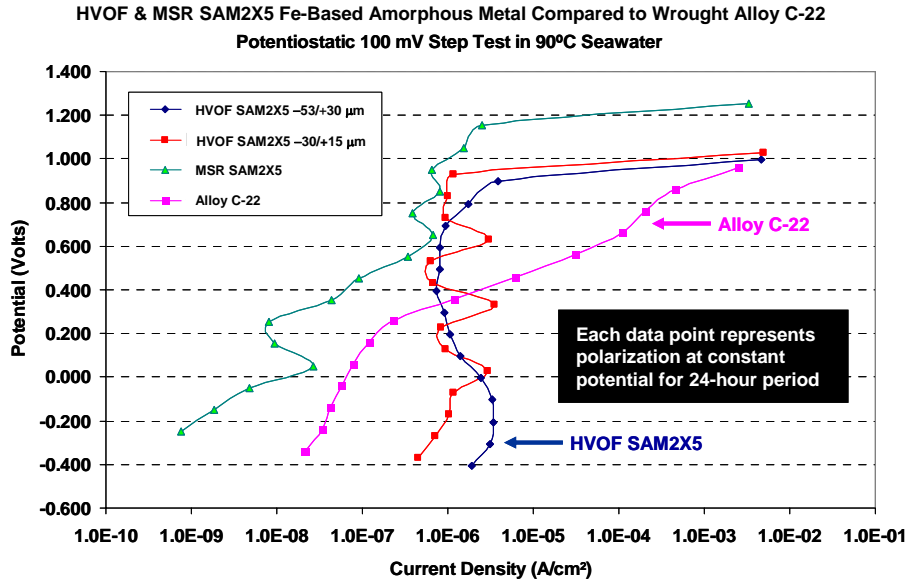


Figure 12. Potential-step testing has been performed on wrought Alloy C-22 (reference material); fully dense and completely amorphous melt spun ribbons of SAM2X5; optimized HVOF coatings produced with -53/+30 micron powders of SAM2X5; and optimized HVOF coatings produced with -30/+15 micron powders of SAM2X5. All were tested in Half Moon Bay seawater heated to 90 °C. To eliminate the need for surface roughness corrections in the conversion of measured current and electrode area to current density, the SAM2X5 and SAMI651 coatings were polished to a 600-grit finish prior to testing. The curves represent the asymptotic current density reached after 24 hours at the corresponding potential (each data point represents a 24 hour test). The constant potential was applied after 1 hour at the open circuit corrosion potential (OCP). From previous work presented in the FY04 Annual Report (given in references), it has been found that coatings produced with SAM2X5 powders below a critical size are fully dense and are completely amorphous. The coatings produced with finer powders are therefore expected to have lower porosity and less residual crystalline phases present than those produced with larger particles. These data enable a clear and unambiguous determination of the threshold potentials for passive film breakdown in a non-creviced condition. First, it is clear that the passive film on wrought Alloy C-22 commences breakdown at a potential of approximately 200 mV relative to a standard Ag/AgCl reference electrode (approximately 600 mV above the open circuit corrosion potential), and has the least corrosion resistance of any sample evaluated during this test. Passive film breakdown on the SAM2X5 melt-spun ribbon did not occur until a potential in excess of 1200 mV vs. Ag/AgCl (1400 mV above OCP) was applied. Furthermore, the observed passive current density observed with this sample was extremely low. Both HVOF coatings of SAM2X5 (large and small powder sizes) also exhibited outstanding passive film stability, superior to that of the reference material. The passive film on the coating produced with -30/+15 micron powder remained intact until application of 1000 mV vs. Ag/AgCl (1200 mV above OCP), with a current density well within the passive range of several microamps per square centimeter. Similar observations were made with the coating produced with -53/+30 micron powders. Any differences in morphology did not have significant impact on corrosion resistance.

HPCRM FY05 Annual Report – UCRL-TR-234799
DOE-DARPA Co-Sponsored Advanced Materials Program

Potentiostatic Polarization for 24 Hours at OCP + 1000 mV in Seawater at 90C

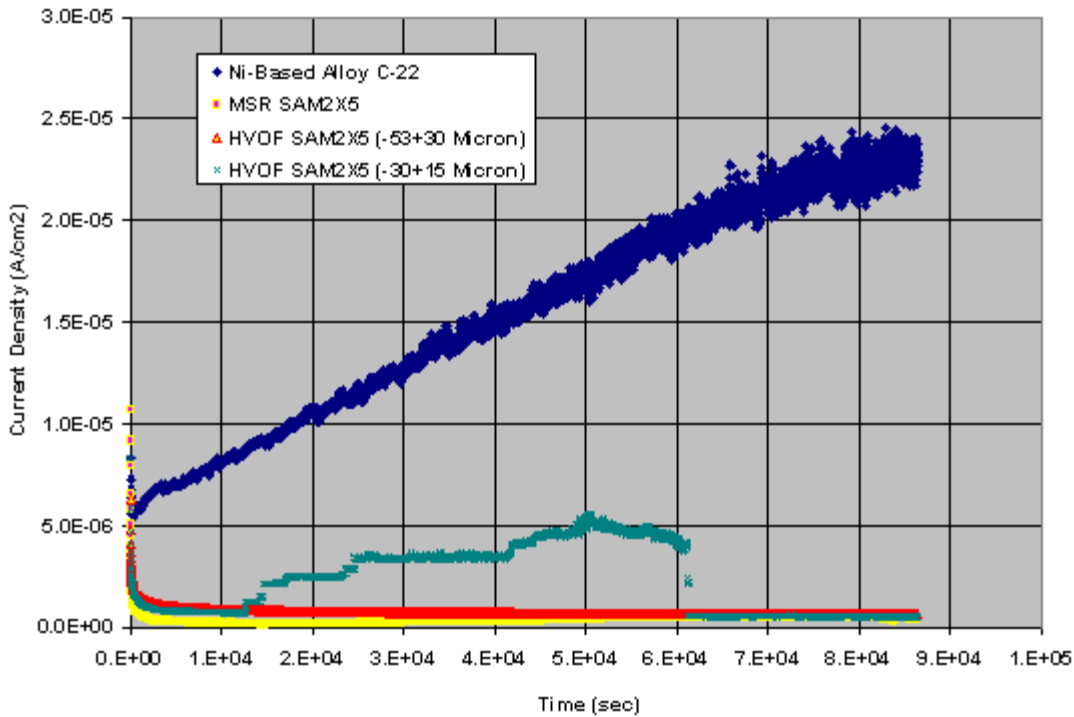


Figure 13. Transients in current density at a constant applied potential of 1000 mV vs. OCP for wrought Alloy C-22 (reference material), a fully dense and completely amorphous melt spun ribbon (MSR) of SAM2X5, HVOF coatings produced with -53/+30 micron powders of SAM2X5, and HVOF coatings produced with -30/+15 micron powders of SAM2X5, all in Half Moon Bay seawater heated to 90 °C, are compared. The constant potential was applied after 1 hour at the open circuit corrosion potential (OCP). The passive film on the melt spun ribbon and HVOF coatings of SAM2X5 is more stable than that on wrought nickel-based Alloy C-22 under these conditions, leading to the conclusion that this iron-based amorphous metal has superior corrosion resistance. These coatings were produced with TNC powder by UCD and Plasmatech.

*HPCRM FY05 Annual Report – UCRL-TR-234799
DOE-DARPA Co-Sponsored Advanced Materials Program*

Potentiostatic Polarization of Alloy C-22 for 24 Hours (Each Step) in Seawater at 90C

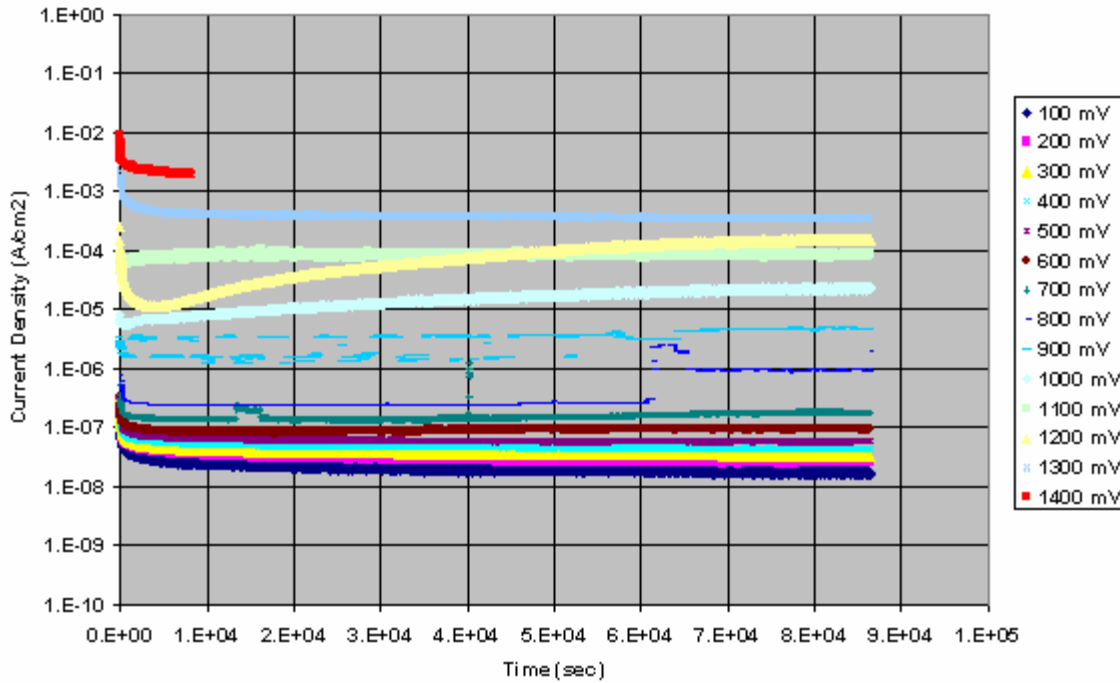


Figure 14. Transients in current density at various levels of constant applied potential ranging from 100 to 1400 mV vs. OCP for Alloy C-22 in Half Moon Bay seawater at 90 °C. This reference material was polished to a 600-grit finish. The constant potential was applied after 1 hour at the open circuit corrosion potential (OCP). Passive film stability is lost above 700 mV vs. OCP. These coatings were produced with TNC powder by UCD and Plasmatech.

*HPCRM FY05 Annual Report – UCRL-TR-234799
DOE-DARPA Co-Sponsored Advanced Materials Program*

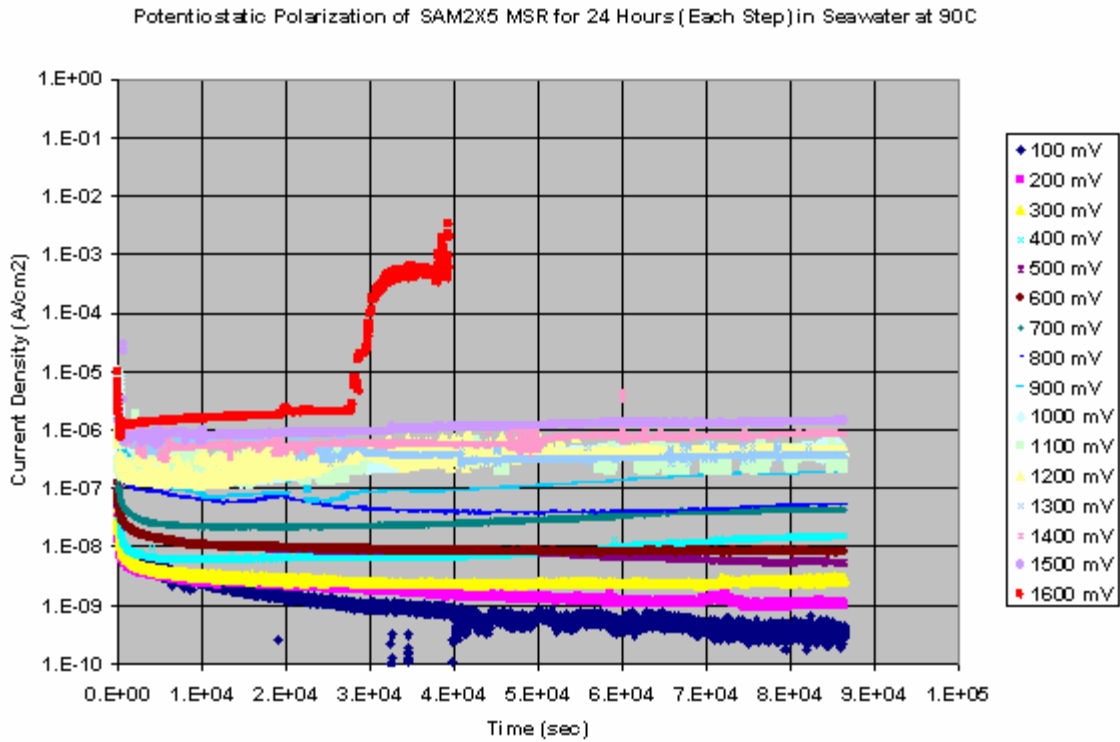


Figure 15. Transients in current density at various levels of constant applied potential ranging from 100 to 1600 mV vs. OCP for a melt-spun ribbon of SAM2X5 in Half Moon Bay seawater at 90 °C are indicative of good passive film stability. The constant potential was applied after 1 hour at the open circuit corrosion potential (OCP). The passive film stability of this SAM2X5 sample is maintained at potentials up to 1500 mV vs. OCP, which is approximately 800 mV higher than the critical potential observed with Alloy-C22. At an applied potential of 1600 mV vs. OCP, passivity is lost after several hours. These coatings were produced with TNC powder by UCD and Plasmatech.

HPCRM FY05 Annual Report – UCRL-TR-234799
DOE-DARPA Co-Sponsored Advanced Materials Program

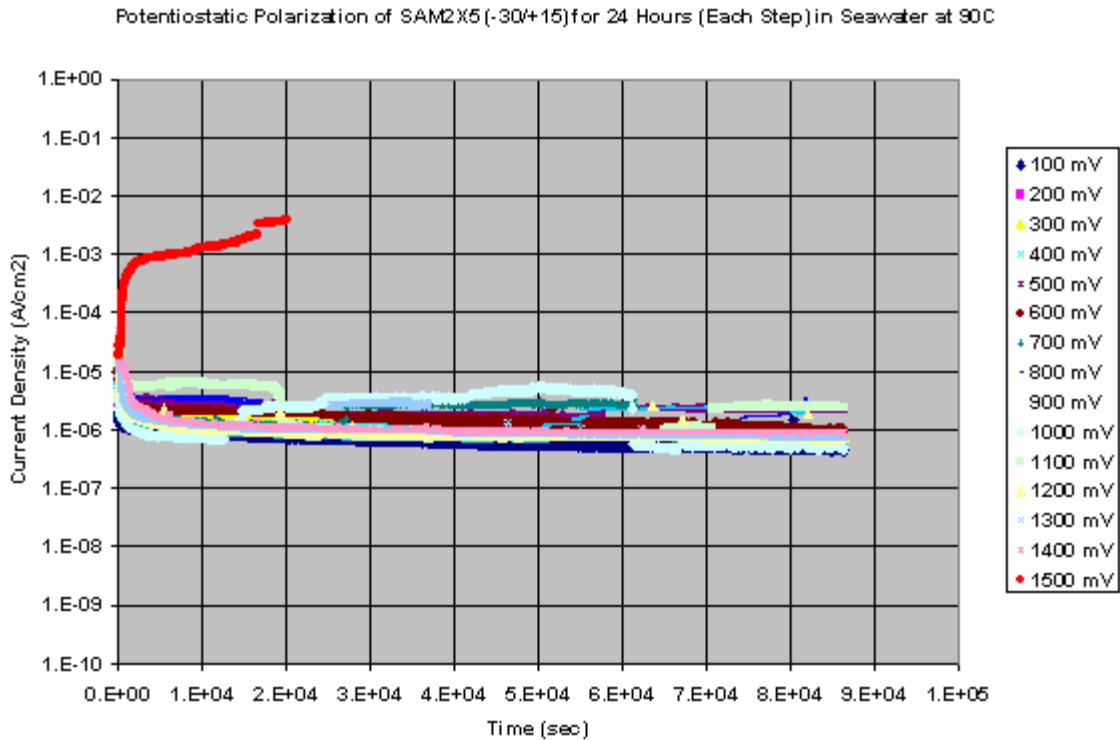


Figure 16. Transients in current density at various levels of constant applied potential ranging from 100 to 1500 mV vs. OCP for a recently optimized SAM2X5 HVOF coating (-30/+15 micron powder) in deaerated Half Moon Bay seawater at 90 °C are indicative of good passive film stability. The constant potential was applied after 1 hour at the open circuit corrosion potential (OCP). To eliminate the need for surface roughness corrections in the conversion of measured current and electrode area to current density, the SAM2X5 coating was polished to a 600-grit finish prior to testing. The curves represent the asymptotic current density reached after 24 hours at the corresponding potential (each data point represents a 24 hour test). The specified fixed potential was applied after 1 hour at the open circuit corrosion potential (OCP). The passive film stability of this SAM2X5 sample is maintained at potentials up to 1400 mV vs. OCP, which is approximately 700 mV higher than the critical potential observed with Alloy-C22. At an applied potential of 1500 mV vs. OCP, passivity is lost after several hours. These coatings were produced with TNC powder by UCD and Plasmatech.

HPCRM FY05 Annual Report – UCRL-TR-234799
DOE-DARPA Co-Sponsored Advanced Materials Program

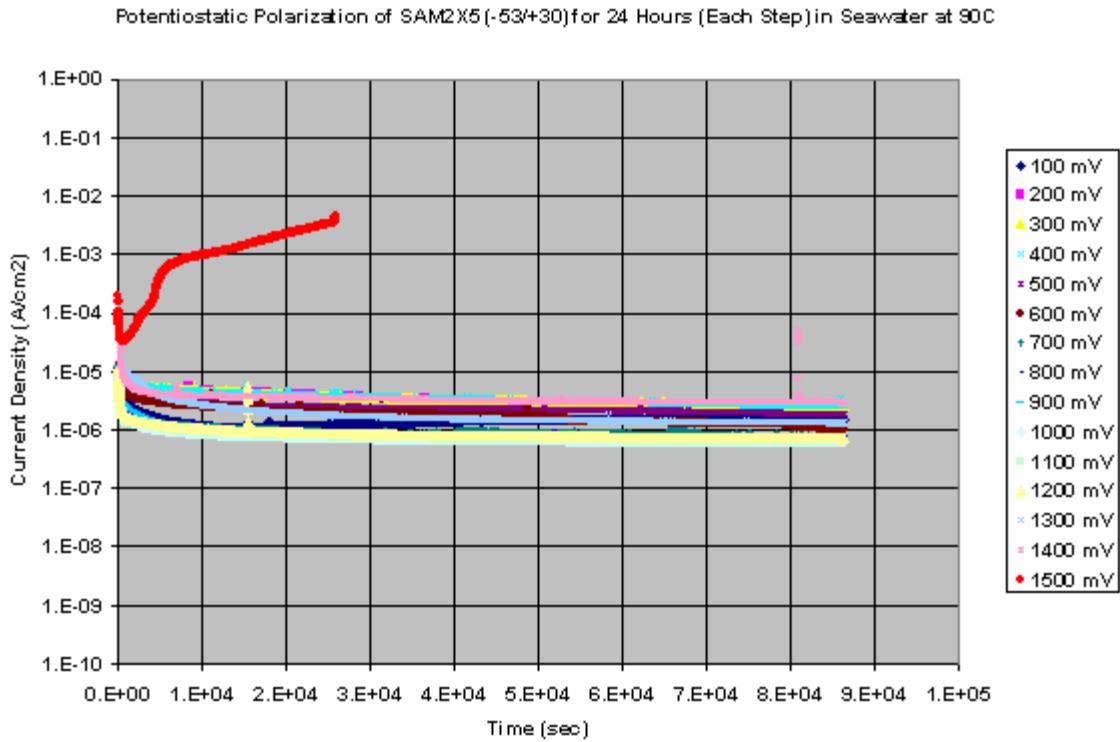


Figure 17. Transients in current density at various levels of constant applied potential ranging from 100 to 1500 mV vs. OCP for a recently optimized SAM2X5 HVOF coating (-53/+30 micron powder) in Half Moon Bay seawater at 90 °C are indicative of exceptional passive film stability. To eliminate the need for surface roughness corrections in the conversion of measured current and electrode area to current density, the SAM2X5 coatings were polished to a 600-grit finish prior to testing. The constant potential was applied after 1 hour at the open circuit corrosion potential (OCP). The passive film stability of this SAM2X5 sample is maintained at potentials up to 1400 mV vs. OCP, which is approximately 700 mV higher than the critical potential observed with Alloy-C22. At an applied potential of 1500 mV vs. OCP, passivity is lost after several hours. These coatings were produced with TNC powder by UCD and Plasmatech.

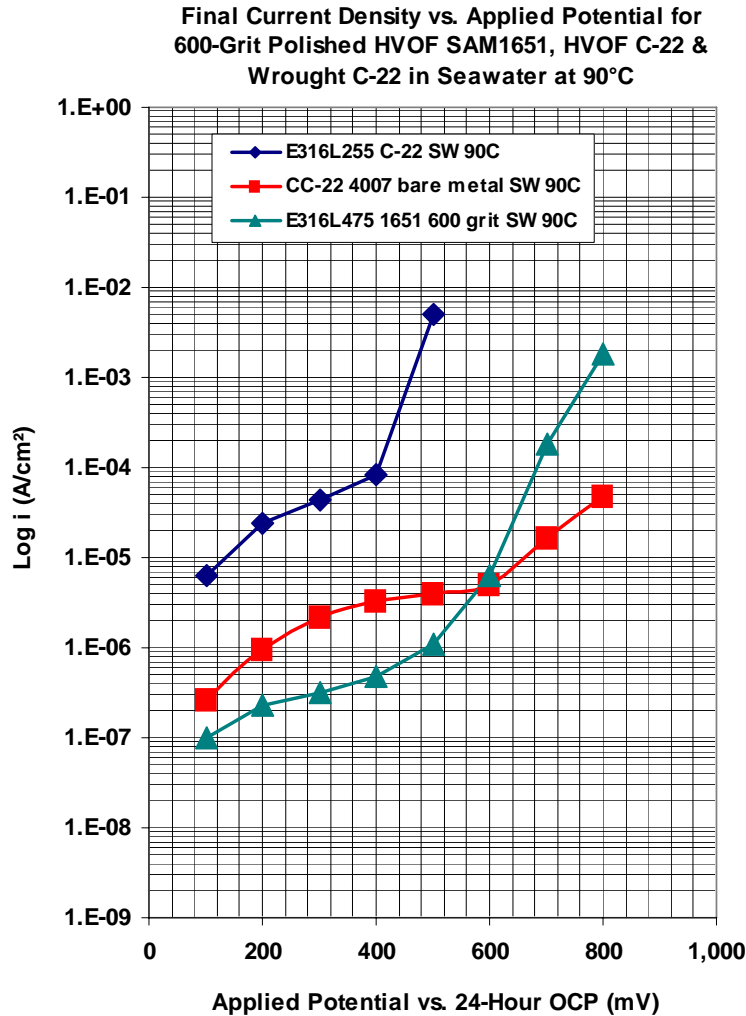


Figure 18. Potential-step testing has been performed on HVOF coatings of SAM1651 in deaerated Half Moon Bay seawater heated to 90 °C. Tests were also performed on the reference material, Alloy C-22, in both wrought and thermally sprayed condition. To eliminate the need for surface roughness corrections in the conversion of measured current and electrode area to current density, the SAM1651 coating was polished to a 600-grit finish prior to testing. The Alloy C-22 thermal spray coating was tested in the as-sprayed condition, so a roughness factor must be applied to convert the apparent current density into actual current density. The curves represent the asymptotic current density reached after 24 hours at the corresponding potential. In this series of experiments, the passive film on wrought Alloy C-22 also commences breakdown at a potential of approximately 600 mV above the open circuit corrosion potential. Passive film breakdown on the HVOF coating of SM1651 occurred at an applied potential between 500 and 600 mV, where breakdown occurred at approximately 400 mV for the Alloy C-22 HVOF coating. In near-boiling seawater, the passive film stability of SAM1651 is comparable to that of Alloy C-22, but inferior to that of SAM2X5.

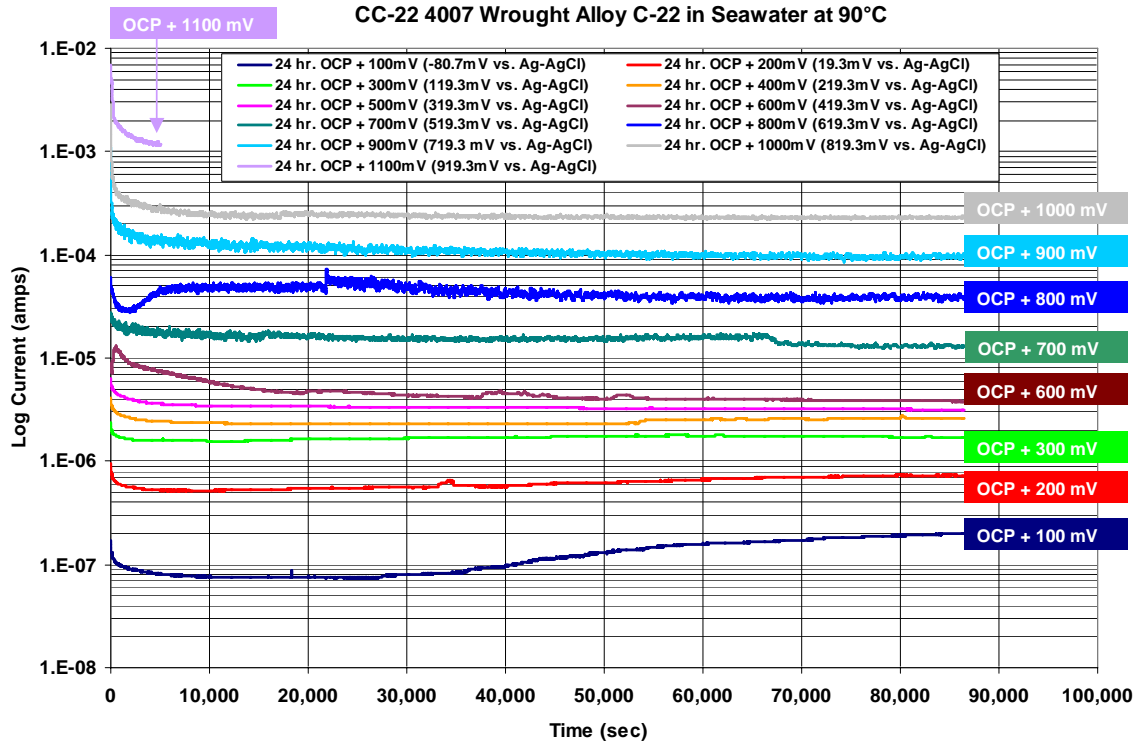


Figure 19. Transients in current density at various levels of constant applied potential ranging from 100 to 800 mV vs. OCP for a HVOF coating of SAM1651 in deaerated Half Moon Bay seawater at 90 °C are indicative of good passive film stability, comparable to that of wrought Alloy C-22. To eliminate the need for surface roughness corrections in the conversion of measured current and electrode area to current density, the SAM2X5 coatings were polished to a 600-grit finish prior to testing. To eliminate the need for surface roughness corrections in the conversion of measured current and electrode area to current density, the SAM1651 coating was polished to a 600-grit finish prior to testing. Passive film breakdown on the HVOF coating of SMI651 occurred at an applied potential between 500 and 600 mV vs. OCP, with a clear loss of passivity at 700 mV. These coatings were produced by TNC and INL before fabrication of the optimized UCD-Plasmatech coatings previously discussed.

HPCRM FY05 Annual Report – UCRL-TR-234799
DOE-DARPA Co-Sponsored Advanced Materials Program

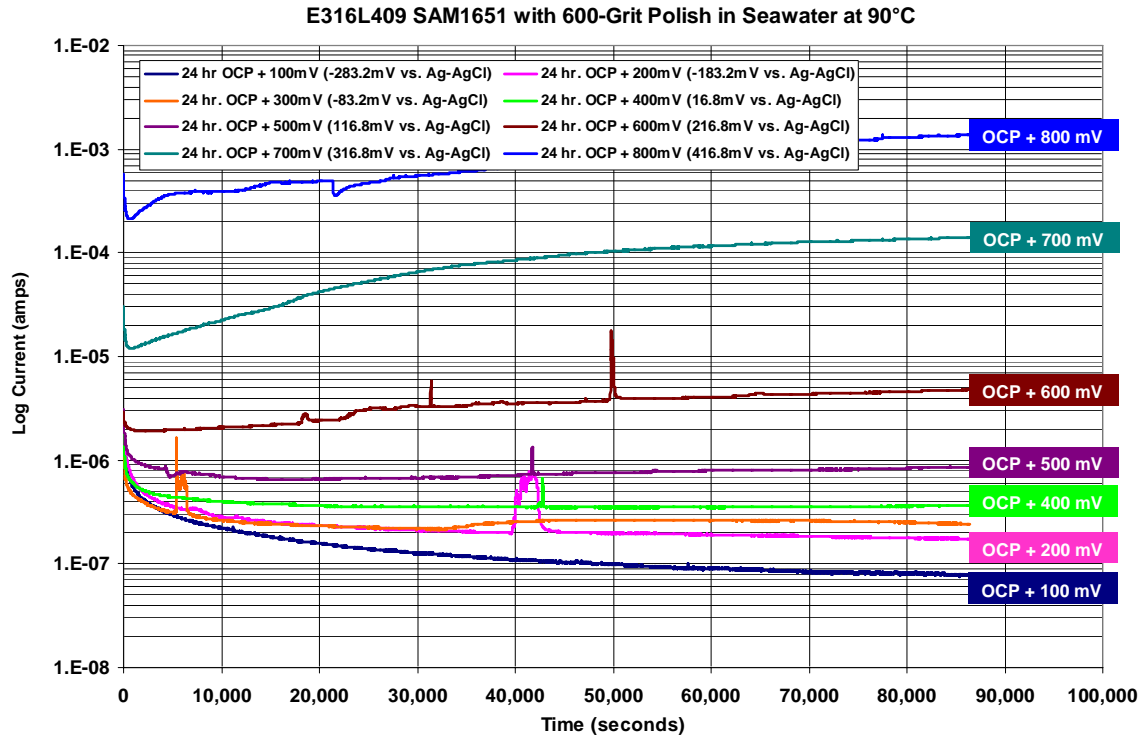


Figure 20. Transients in current density at various levels of constant applied potential ranging from 100 to 800 mV vs. OCP for a polished HVOF coating of SAM1651 on a Type 316L stainless steel substrate (S/N No. E316L409) in Half Moon Bay seawater at 90 °C are indicative of good passive film stability, comparable to that of wrought Alloy C-22. To eliminate the need for surface roughness corrections in the conversion of measured current and electrode area to current density, the SAM2X5 coatings were polished to a 600-grit finish prior to testing. To eliminate the need for surface roughness corrections in the conversion of measured current and electrode area to current density, the SAM1651 coating was polished to a 600-grit finish prior to testing. Passive film breakdown on the HVOF coating of SM1651 occurred at an applied potential between 500 and 600 mV vs. OCP, with a clear loss of passivity at 700 mV. The coating represented by this figure is one of the first known thermal spray coatings with the SAM1651 composition, and was produced by TNC and their subcontractor before fabrication of the optimized UCD/Plasmatech coatings, which are represented by the preceding figures.

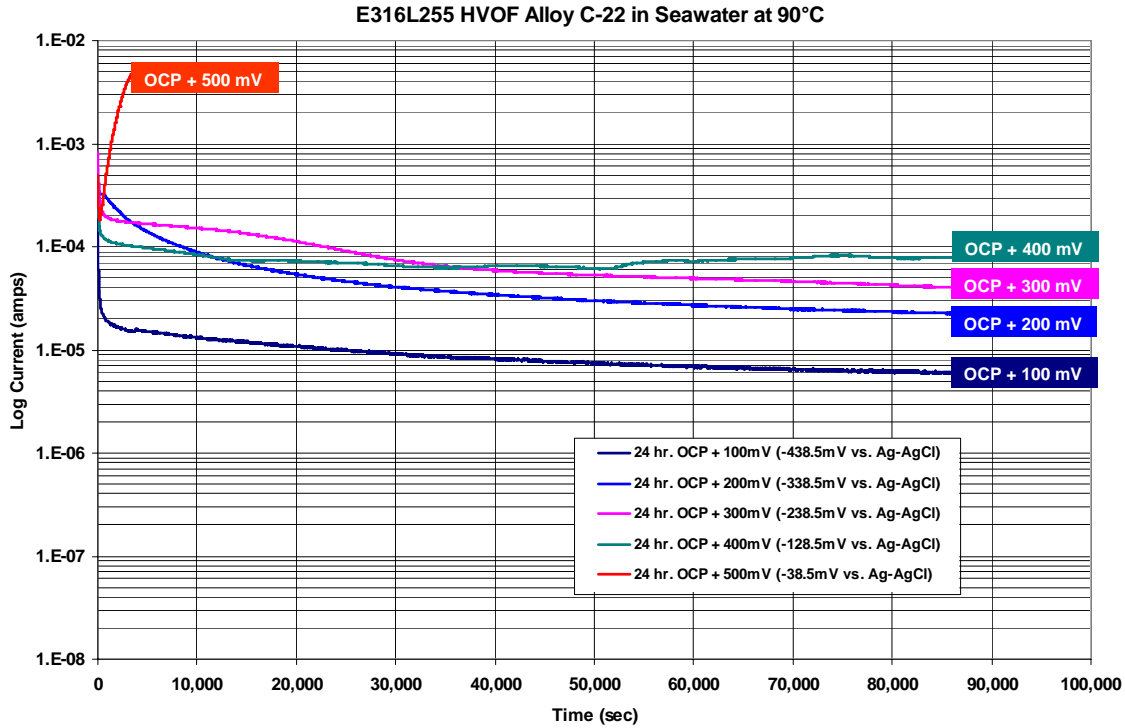


Figure 21. Transients in current density at various levels of constant applied potential ranging from 100 to 500 mV vs. OCP for an unpolished (as sprayed) HVOF coating of nickel-based Alloy C-22 on a Type 316L stainless steel substrate (S/N No. E316L255) in Half Moon Bay seawater at 90 °C show a clear and unambiguous loss of passivity at the highest potential level. Since this Alloy C-22 coating was tested in the as-sprayed condition, a roughness factor must be applied to convert the ‘apparent’ current density into the ‘actual’ current density. The coating represented by this figure was produced by TNC and their subcontractor before fabrication of the optimized UCD/Plasmatech coatings, which are represented by the preceding figures.

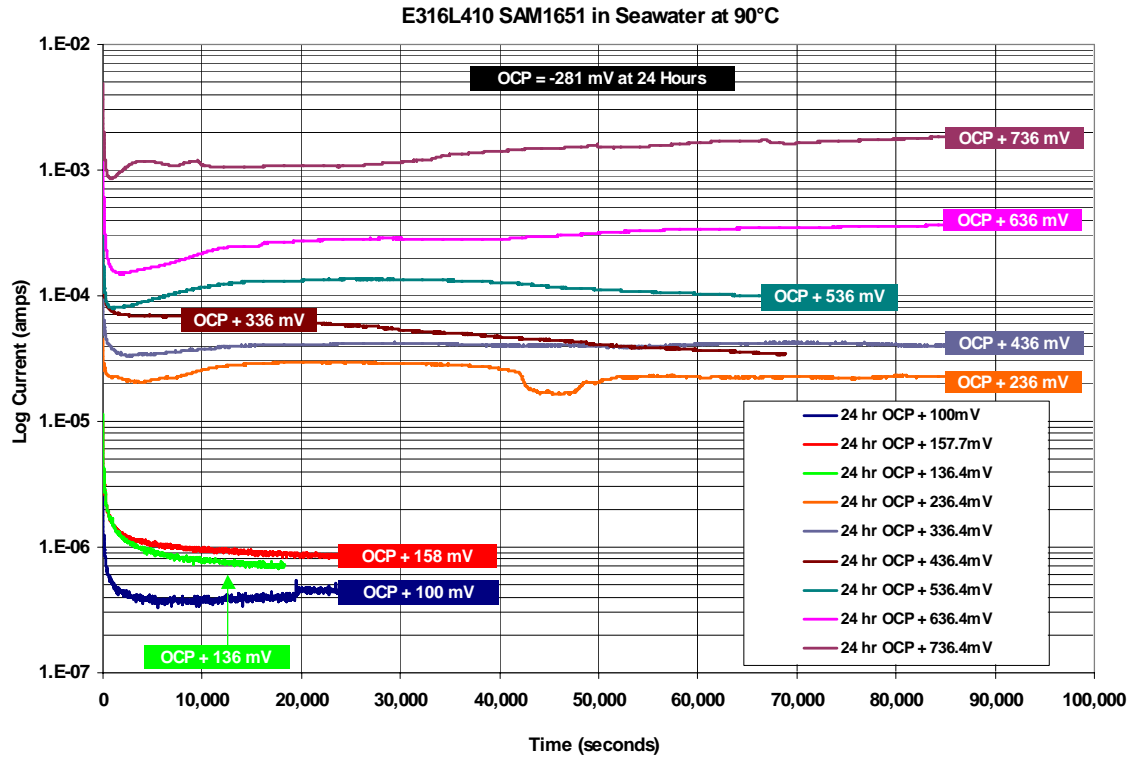


Figure 22. Transients in current density at various levels of constant applied potential ranging from 100 to 736 mV vs. OCP for an unpolished (as sprayed) HVOF coating of SAM1651 on a Type 316L stainless steel substrate (S/N No. E316L410) in Half Moon Bay seawater at 90 °C are indicative of good passive film stability, comparable to that of wrought Alloy C-22. Since this as-sprayed SAM1651 coating was tested in the as-sprayed condition, a roughness factor (which is expected to range from a minimum of $\times 2$ to more than $\times 10$) must be applied to convert the ‘apparent’ current density into the ‘actual’ current density. While passivity at 158 mV vs. OCP is clear, polished samples with minimal roughness, or unambiguous knowledge of the roughness factor is required to interpret measured ‘apparent’ current densities at higher applied potential in terms of passivity, or the loss of passivity. From visual inspection, it was evident that passivity was maintained at higher potentials. The ambiguity associated with early electrochemical test data such as this has lead the investigators to use polished samples with 600-grit finish for clear determinations of critical potentials. The coating represented by this figure is one of the first known thermal spray coatings with the SAM1651 composition, and was produced by TNC and their subcontractor before fabrication of the optimized UCD/Plasmatech coatings, which are represented by the preceding figures.

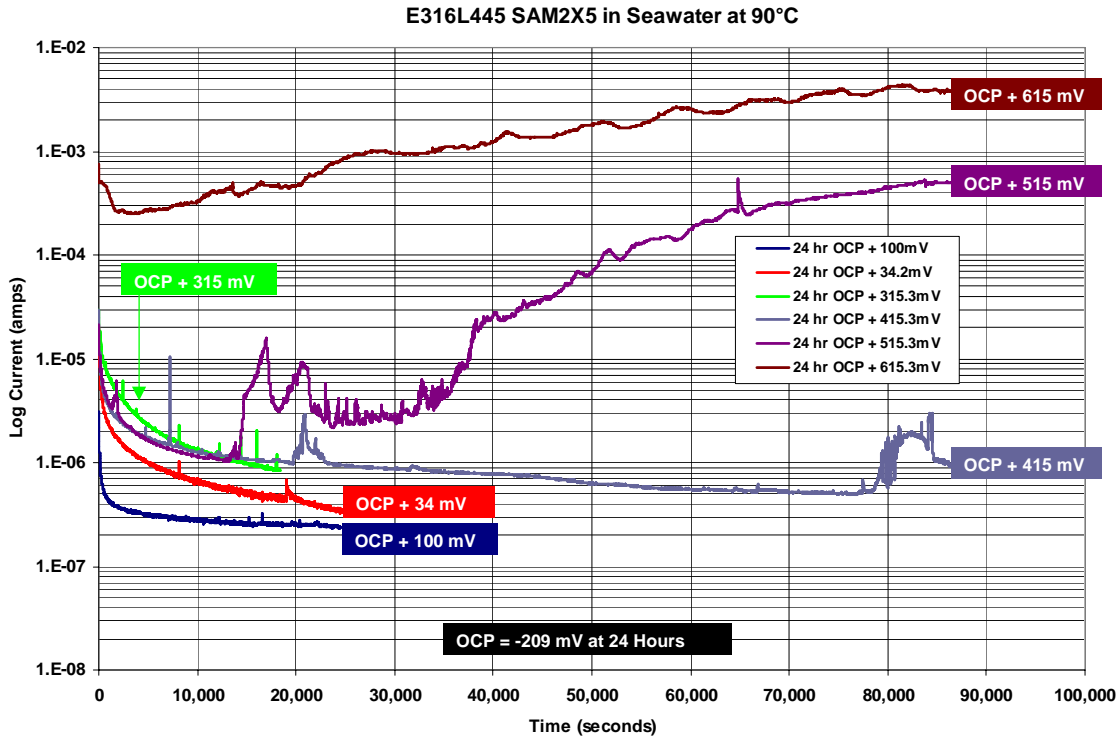


Figure 23. Transients in current density at various levels of constant applied potential ranging from 100 to 615 mV vs. OCP for an early unpolished (as sprayed) HVOF coating of SAM2X5 on a Type 316L stainless steel substrate (S/N No. E316L445) in Half Moon Bay seawater at 90 °C are indicative of good passive film stability, comparable to that of wrought Alloy C-22. Since this as-sprayed SAM2X5 coating was tested in the as-sprayed condition, a roughness factor (which is expected to range from a minimum of $\times 2$ to more than $\times 10$) must be applied to convert the ‘apparent’ current density into the ‘actual’ current density. While passivity at 315 mV vs. OCP is clear, current transients are observed at 415 mV on this as-sprayed surface that may be indicative of the onset of passive film breakdown. Such breakdown is clearly evident at a slightly higher potential of 515 mV vs. OCP. While this data shows very good corrosion resistance, more recent optimization has resulted in far better performance with this formulation. The coating represented by this figure is one of the first known thermal spray coatings with the SAM2X5 composition, and was produced by TNC and their subcontractor before fabrication of the new optimized UCD/Plasmatech coatings, which are represented by the preceding figures. The importance of supplier standardization and qualification is illustrated by the enhanced performance that has evolved as we have continued to work with these materials.

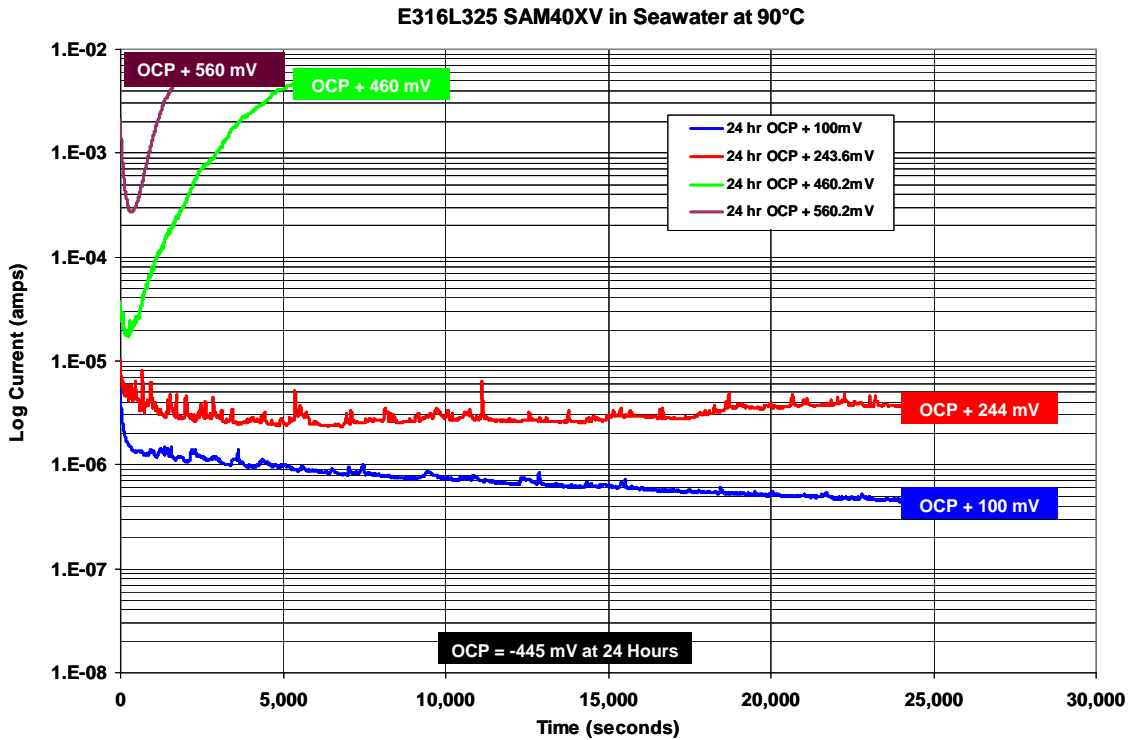


Figure 24. Transients in current density at various levels of constant applied potential ranging from 100 to 460 mV vs. OCP for an early unpolished (as sprayed) HVOF coating of SAM40XV on a Type 316L stainless steel substrate (S/N No. E316L325) in Half Moon Bay seawater at 90 °C are indicative of good passive film stability, comparable to that of wrought Alloy C-22. SAM40XV was an early version of SAM2X5 that TNC prepared for HPCRM with slightly less molybdenum added, and a corresponding lower critical potential. Since this as-sprayed SAMXV coating was tested in the as-sprayed condition, a roughness factor (which is expected to range from a minimum of $\times 2$ to more than $\times 10$) must be applied to convert the ‘apparent’ current density into the ‘actual’ current density. While passivity at 100 to 244 mV vs. OCP is clear, current transients observed at 460 and 560 mV are clearly indicative of passive film breakdown. Such high apparent current densities occur at higher potential in the case of SAM2X5. The coating represented by this figure is one of the first known thermal spray coatings with the SAM40XV composition, and was produced by TNC and their subcontractor before fabrication of the new optimized UCD/Plasmatech coatings, which are represented by the preceding figures. The importance of supplier standardization and qualification is illustrated by the enhanced performance that has evolved as we have continued to work with these materials.

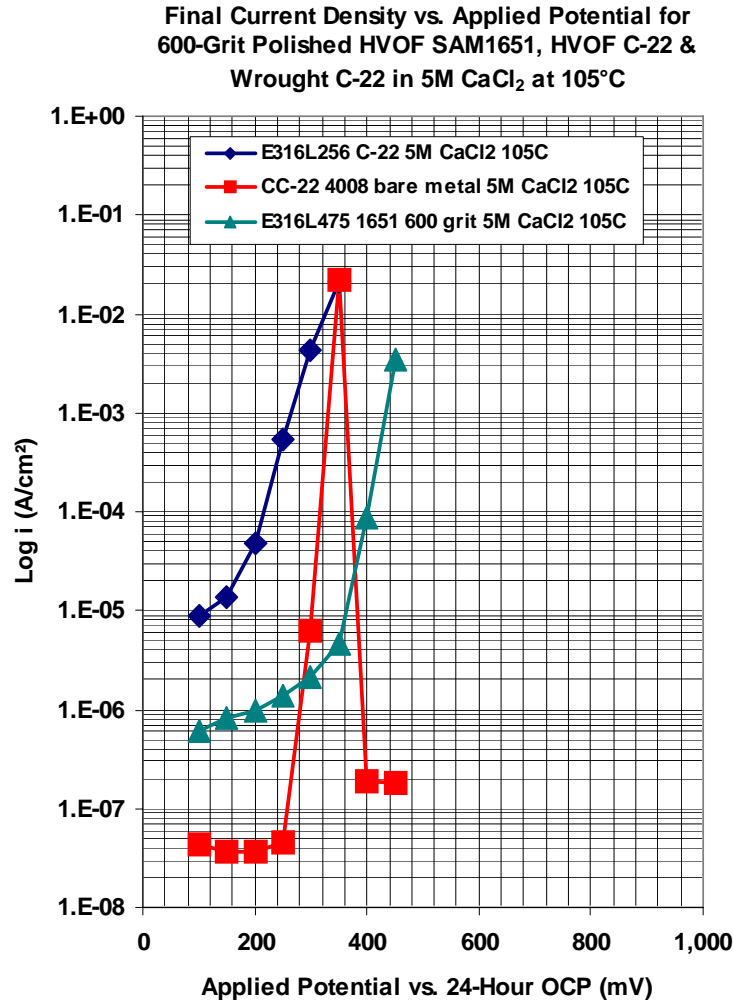


Figure 25. Potential-step testing has been performed on HVOF coatings of SAM1651 on a Type 316L stainless steel substrate (S/N No. E316L475) in extremely aggressive 5M CaCl₂ heated to 105°C. Tests were also performed on the reference material, Alloy C-22, in both wrought and thermally sprayed condition (S/N Nos. CC-22 4008 and E316L256, respectively). To eliminate the need for surface roughness corrections in the conversion of measured current and electrode area to current density, the SAM1651 coating was polished to a 600-grit finish prior to testing. The Alloy C-22 thermal spray coating was tested in the as-sprayed condition, so a roughness factor must be applied to convert the apparent current density into actual current density. The curves represent the asymptotic current density reached after 24 hours at the corresponding potential. In this series of experiments, the passive film on wrought Alloy C-22 also commences breakdown at a potential of only 240 mV above the open circuit corrosion potential, with evidence of repassivation at potentials above 400 mV. Even with the repassivation at higher potential, the window of vulnerability between 240 to 400 mV is problematic for the reference material (Alloy C-22). Passive film breakdown on the HVOF coating of SAM1651 occurred at a significantly higher applied potential, between 360 and 400 mV, where breakdown of the passive film on thermally sprayed Alloy C-22 was virtually spontaneous. The new SAM1651 coating provides clear advantages for operation in corrosive hot chloride brines with divalent cations, such as calcium.

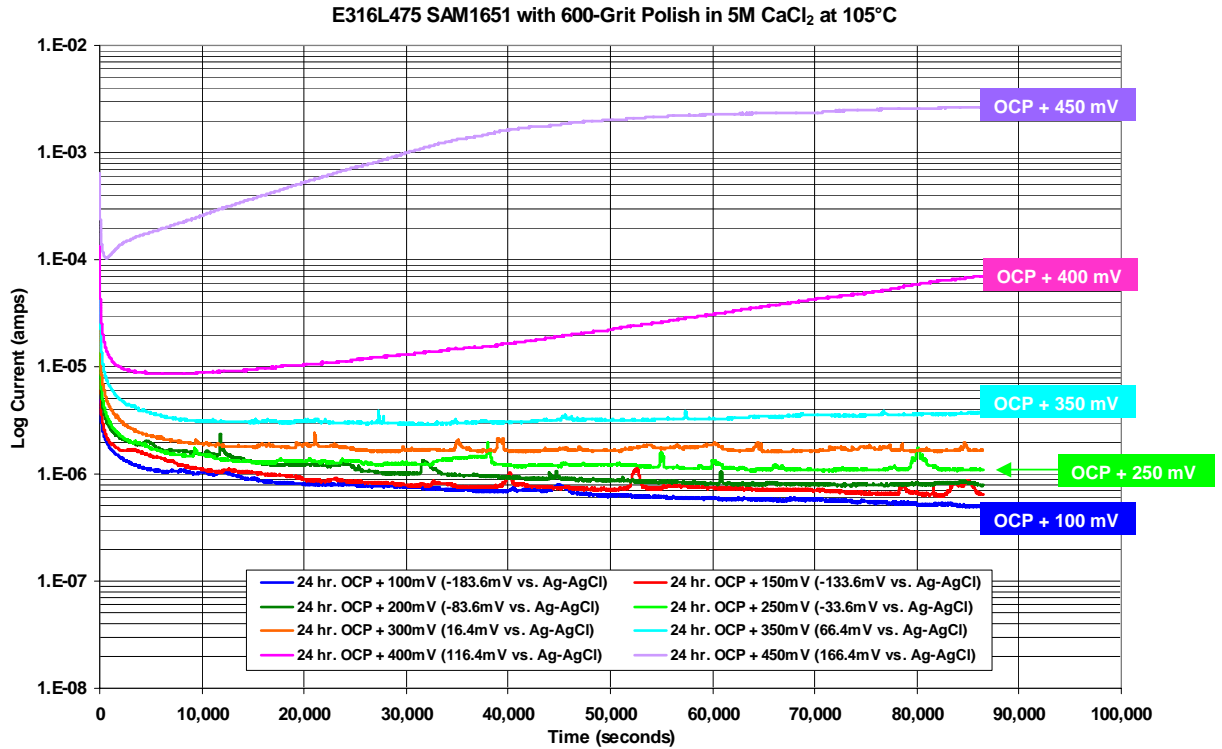


Figure 26. Transients in current density at various levels of constant applied potential ranging from 100 to 450 mV vs. OCP for a polished HVOF coating of SAM1651 on a Type 316L stainless steel substrate (S/N No. E316L475) in 5M CaCl₂ at 105 °C are indicative of good passive film stability, which is superior to that of wrought Alloy C-22 in this environment this very aggressive environment. To eliminate the need for surface roughness corrections in the conversion of measured current and electrode area to current density, the SAM1651 coating was polished to a 600-grit finish prior to testing. Passive film breakdown on the HVOF coating of SAM1651 occurred at an applied potential between 360 and 400 mV vs. OCP, with a clear loss of passivity at 450 mV. The coating represented by this figure is one of the first known thermal spray coatings with the SAM1651 composition, and was produced by TNC and their subcontractor before fabrication of the optimized UCD/Plasmatech coatings, which are represented by the preceding figures. The performance of this SAM1651 coating was very impressive.

*HPCRM FY05 Annual Report – UCRL-TR-234799
DOE-DARPA Co-Sponsored Advanced Materials Program*

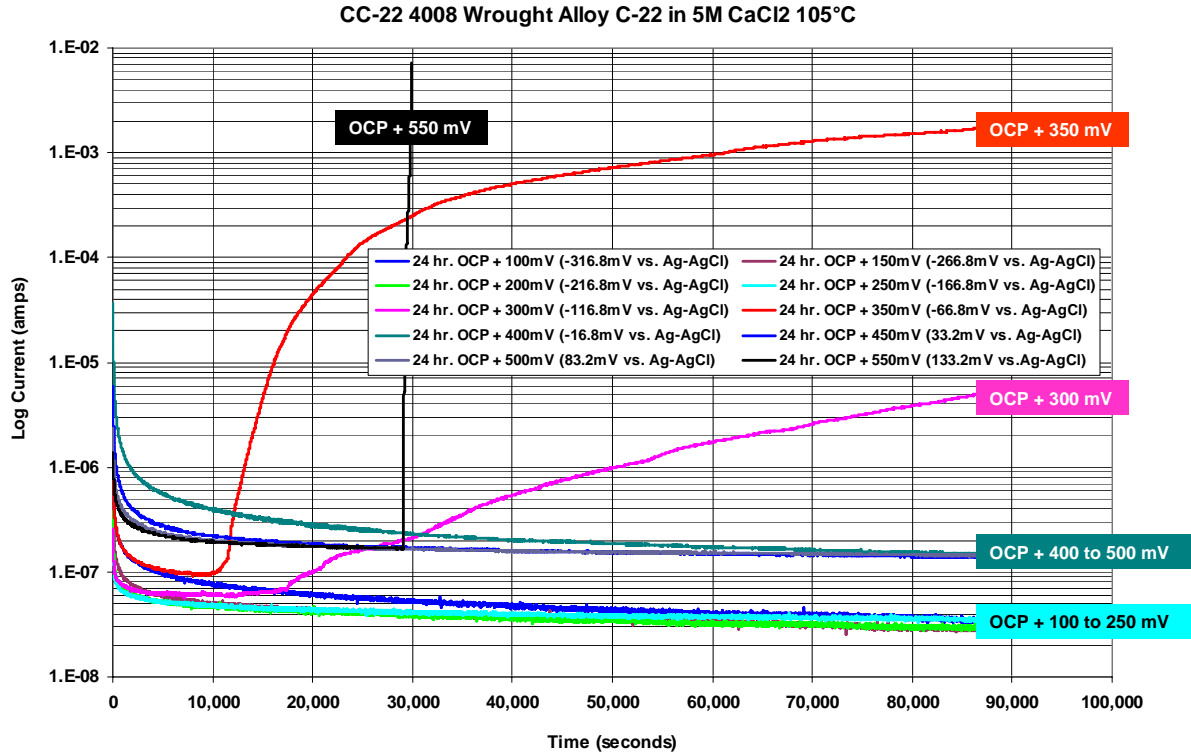


Figure 27. Transients in current density at various levels of constant applied potential ranging from 100 to 550 mV vs. OCP for wrought Alloy C-22 (S/N No. CC-22 4008) in 5M CaCl₂ at 105 °C, and shows complete breakdown of the passive film in two potential regimes, one regime located between 300-400 mV vs. OCP (350 mV), and the second located above 500 mV vs. OCP (550 mV). Like the polished SAM1651 coating, this reference was also polished to a 600-grit finish.

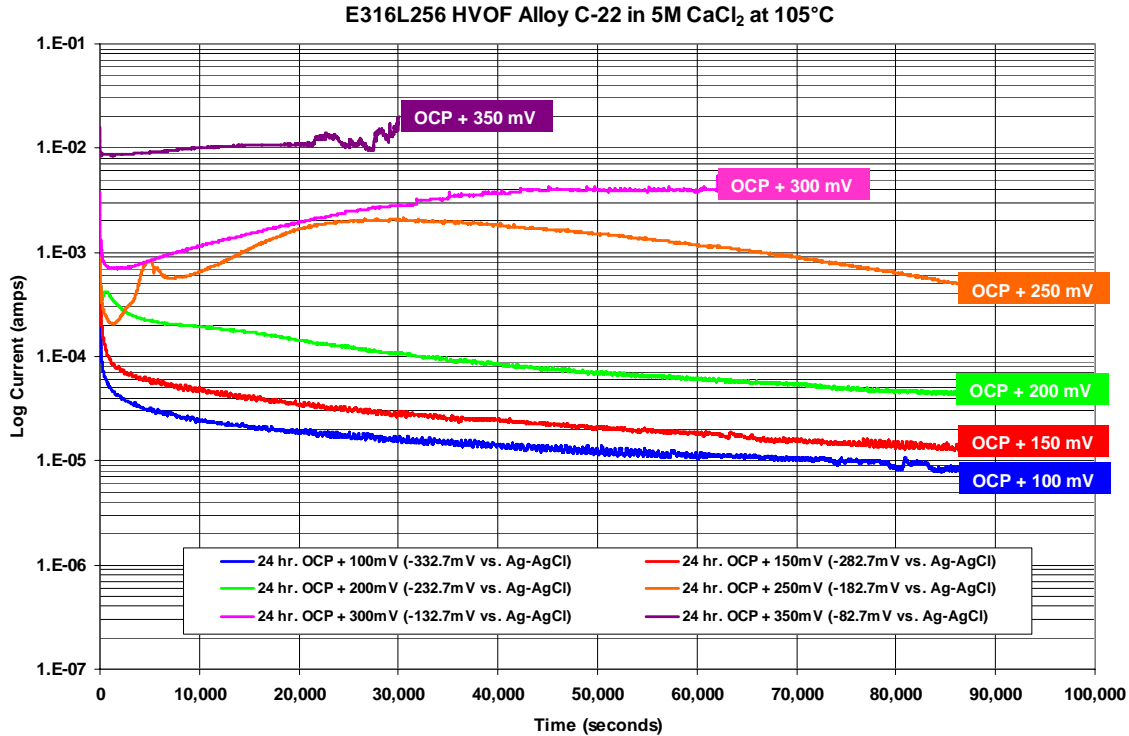


Figure 28. Transients in current density at various levels of constant applied potential ranging from 100 to 350 mV vs. OCP for an unpolished (as-sprayed) HVOF coating of Alloy C-22 on a Type 316L stainless steel substrate (S/N No. E316L256) in 5M CaCl₂ at 105 °C appears to be passive at 100-150 mV vs. OCP, but has a clear loss of passivity at potentials above 200 mV vs. OCP (250-350 mV). Since this as-sprayed Alloy C-22 coating was tested in the as-sprayed condition, a roughness factor (which is expected to range from a minimum of ×2 to more than ×10) must be applied to convert the ‘apparent’ current density into the ‘actual’ current density. The coating represented by this figure was produced by TNC and their subcontractor before fabrication of the optimized UCD/Plasmatech coatings, which are represented by preceding figures.

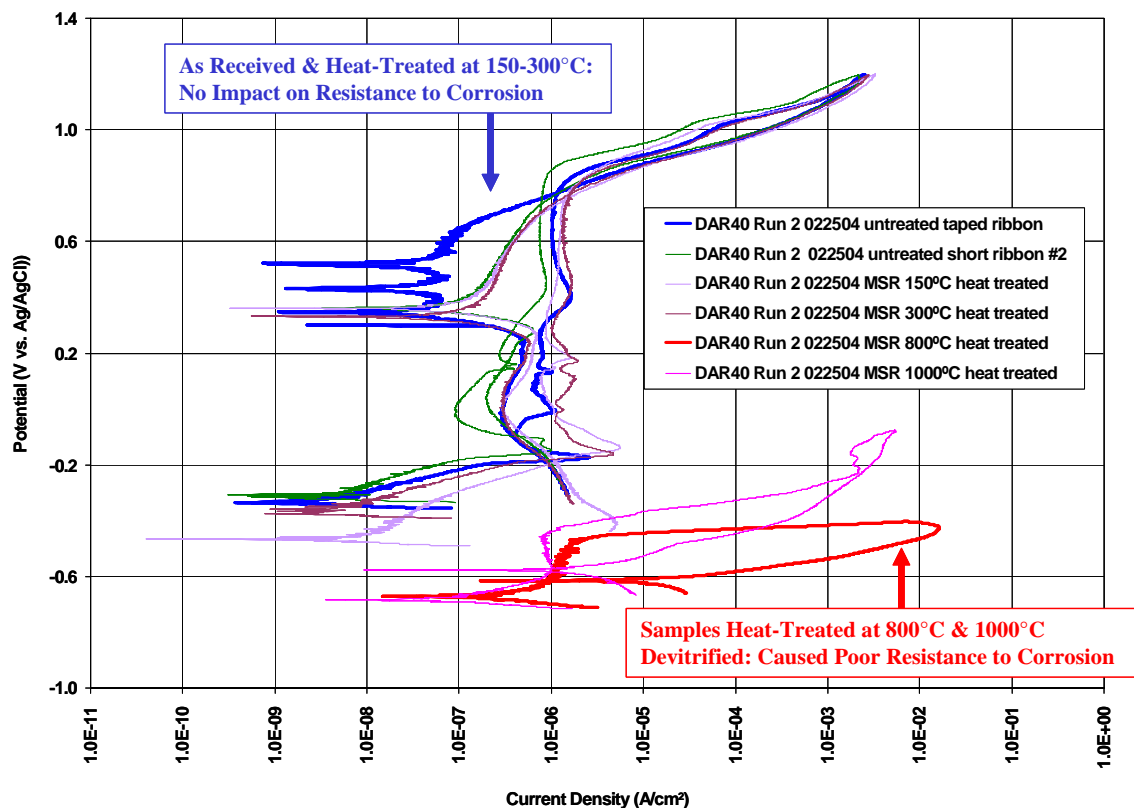


Figure 29. To assess the sensitivity of these iron-based amorphous metals to devitrification, which can occur at very elevated temperature, melt-spun ribbon of SAM40 (also referred to as DAR40) were intentionally devitrified by heat treating them at various temperatures for one hour. After heat treatment, the samples were evaluated in low temperature seawater (30 °C), to determine the impact of the heat treatment on passive film stability and corrosion resistance. The temperatures used for the heat treatment were: 150, 300, 800 and 1000 °C. Untreated (as received) ribbons were also tested, and provide insight into the baseline performance. These samples showed no significant hysteresis and change in repassivation potential at heat treatments of 150-300 °C, but showed a dramatic loss of corrosion resistance when heat treatments were performed at 800-1000 °C, which are above the known recrystallization temperature of approximately 600-650 °C (623 °C) given in Table 2 (Perepezko et al. 2004). Both ribbons treated at elevated temperature show large hysteresis loops, which are indicative of passive film breakdown, with a clearly defined repassivation potential near -600 mV vs. Ag/AgCl (about 100 mV above the OCP). The operational limit for these materials, when being used for corrosion resistance, appears to be bounded by the recrystallization temperature.

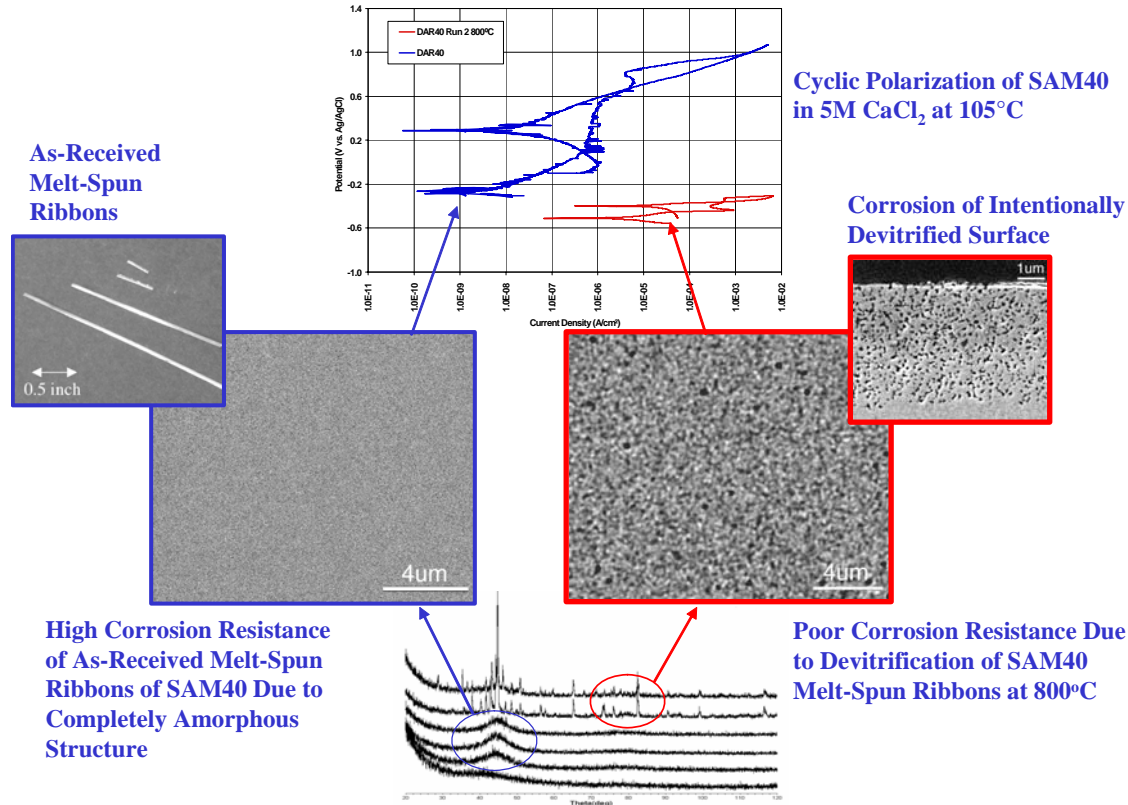


Figure 30. Melt spun ribbons of SAM40 (DAR40) were also intentionally devitrified by heat treating at 800 °C for one hour and then subjected to cyclic polarization in 5M CaCl₂ at 105 °C. In comparison to the as-received sample, the sample heat-treated at 800C showed a dramatic loss of corrosion resistance. As discussed in regard to the preceding figure, this heat-treatment temperature was known to be above the recrystallization temperature of approximately 600-650 °C (623 °C) given in Table 2 (Perepezko et al. 2004). The heat-treated ribbon showed a large hysteresis loop in the hot concentrated calcium chloride solution, which is indicative of passive film breakdown, with a clearly defined repassivation potential neat the OCP. The post heat-treatment microstructural characterization with electron microscopy and X-ray diffraction by Yang et al. verify the existence of a completely amorphous material below the recrystallization temperature, and the development of crystalline precipitates during heat treatment above this limit. These electron microscopy images may also indicate that the corrosive attack of the precipitated crystalline phases occur to a depth of approximately 10 microns. When being used for corrosion resistance in hot geothermal brines such as calcium chloride, the operational limit also appears to be bounded by the recrystallization temperature.

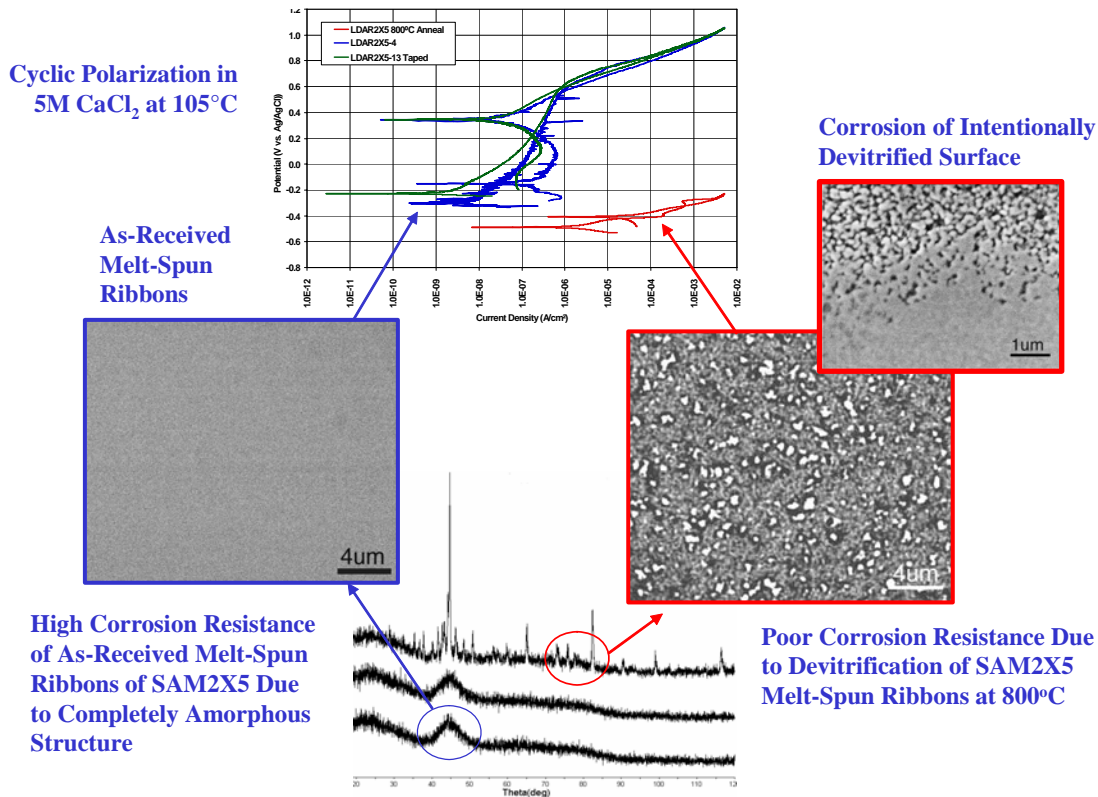


Figure 31. Melt spun ribbons of SAM2X5 were also intentionally devitrified by heat treating at 800 °C for one hour and then subjected to cyclic polarization in 5M CaCl₂ at 105 °C. In comparison to the as-received sample, the sample heat-treated at 800C showed a dramatic loss of corrosion resistance. As discussed in regard to the preceding figure, this heat-treatment temperature was known to be above the recrystallization temperature of approximately 600-650 °C (623 °C) given in Table 2 (Perepezko et al. 2004). The heat-treated ribbon showed a large hysteresis loop in the hot concentrated calcium chloride solution, which is indicative of passive film breakdown, with a clearly defined repassivation potential neat the OCP. The post heat-treatment microstructural characterization with electron microscopy and X-ray diffraction by Yang et al. verify the existence of a completely amorphous material below the recrystallization temperature, and the development of crystalline precipitates during heat treatment above this limit. These electron microscopy images may also indicate that the corrosive attack of the precipitated crystalline phases occur to a depth of approximately 10 microns. When being used for corrosion resistance in hot geothermal brines such as calcium chloride, the operational limit also appears to be bounded by the recrystallization temperature.



Figure 32. Temperature controlled baths for long-term corrosion testing of weight loss and crevice corrosion samples, with simultaneous monitoring of the open-circuit corrosion potential, corrosion rate via linear polarization, and passive film stability with electrochemical impedance spectroscopy (EIS). Water cooled condensers are used to prevent the loss of water and other volatiles from the baths, and a water-cooled reference electrode junction is used to enable the Ag/AgCl reference electrodes to be operated at standard temperature, thereby providing a sound thermodynamic reference. The upper photograph show LLNL technicians attending to the test equipment.

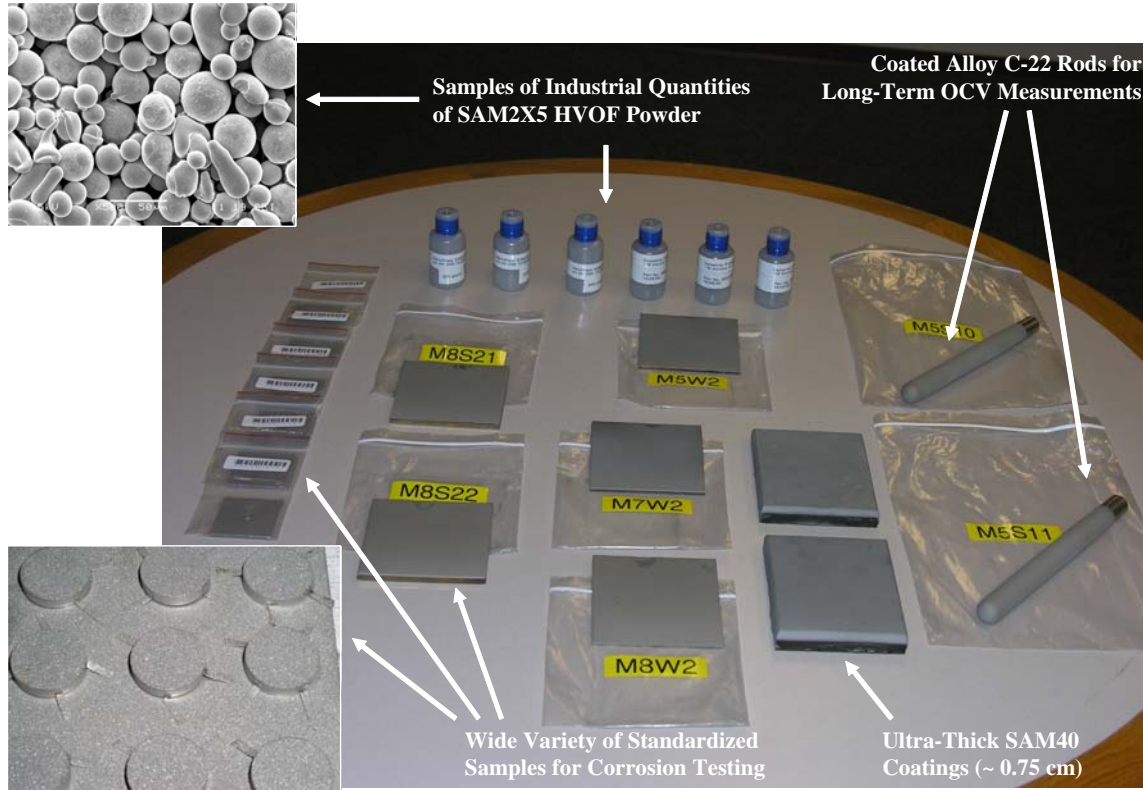


Figure 33. Weight loss and crevice samples for the long term test are 4-inch \times 4-inch \times 1/4-inch Alloy C-22 substrates with a 40-mil thermal spray coating of amorphous metal (SAM2X5, SAM1651, etc.). The crevice samples have a hole in the center to accommodate a crevice former, and are not shown. The long-term measurements of open-circuit corrosion potential, corrosion rate via linear polarization, and electrochemical impedance spectra are done with a 3/4-inch diameter Alloy C-22 rod with a hemispherical end, and with a 40-mil thermal spray coating of amorphous metal (SAM2X5, SAM1651, etc.). Small disks are used for quick screening tests with cyclic polarization, but are not considered truly representative coatings due to their small size and differences in cooling rate experienced by the disks and larger substrates with greater thermal mass and cooling capacity. The granularity of these disks is not representative can be easily seen. While small circular disk samples are relatively inexpensive and easy to produce, and can be employed in standard corrosion test cells with relative ease, they may not provide the best source of data.

*HPCRM FY05 Annual Report – UCRL-TR-234799
DOE-DARPA Co-Sponsored Advanced Materials Program*

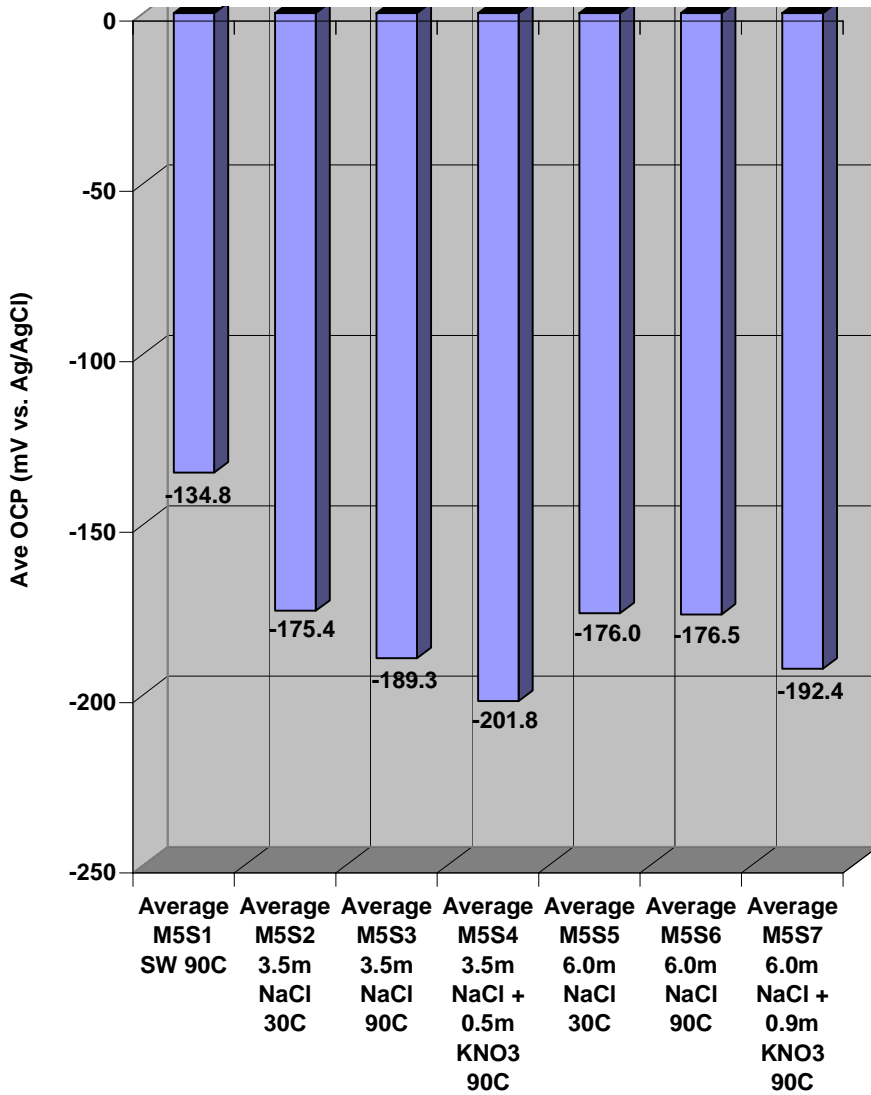


Figure 34. The long-term corrosion test for the SAM2X5 has been initiated, and the initial open circuit corrosion potentials for this material has been measured in several fully aerated environments, and will be monitored as a function of time for the next year. These environments include Half Moon Bay seawater, 3.5 m NaCl, 3.5 m NaCl with 0.5 m KNO₃, 6.0 m NaCl and 6.0 m NaCl with 0.9 m KNO₃. For each solution composition, tests are being done at two temperature levels, 30 and 90 °C.

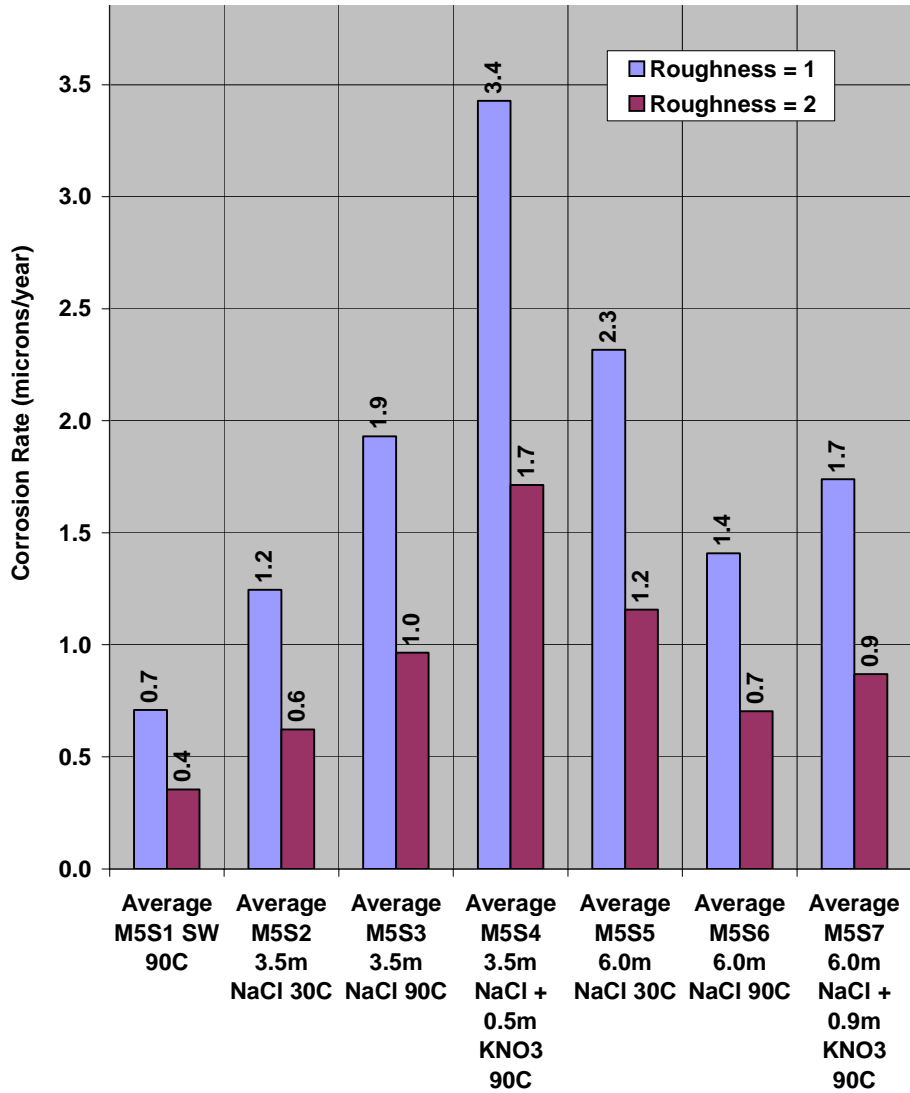


Figure 35. In addition to monitoring the open circuit corrosion potential in these fully aerated solutions, linear polarization is also being used periodically to measure the corrosion current, which is normalized by the apparent area of the electrode, and used to estimate the general corrosion rate. The roughness factor for these unpolished (as sprayed) SAM2X5 HVOF samples must be used to convert the apparent current density to the corrosion rate. In this figure, the first series of bars (blue) represent the estimated corrosion rate with no roughness correction, and the second series of bars (magenta) represent the estimated corrosion rate with the minimum estimated roughness factor of 2. The actual roughness may be significantly higher, and is in the process of being quantified. Even without the roughness factor correction, the measured corrosion rates are very low. It is somewhat surprising that in this case, the presence of nitrate appears to accelerate the general corrosion rate, both at 3.5 and 6.0 NaCl concentrations.

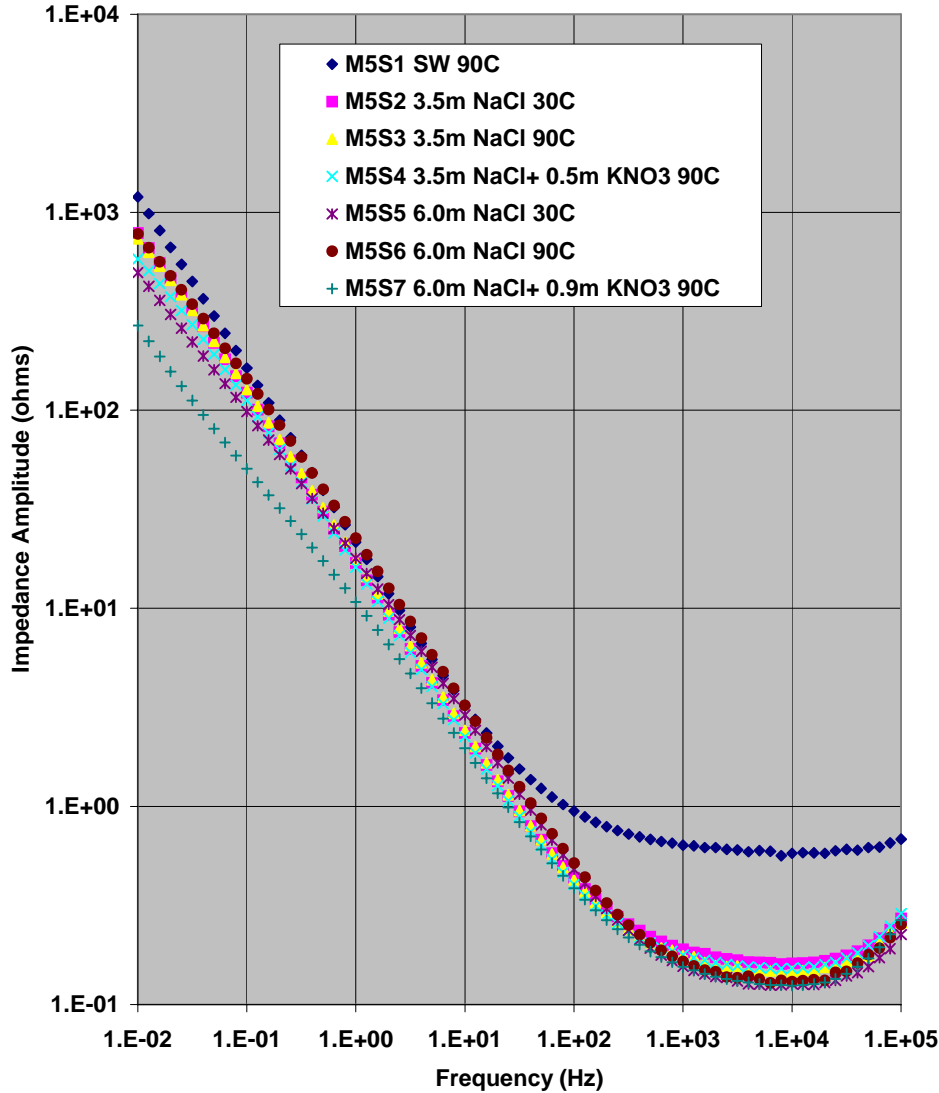


Figure 36. In addition to obtaining corrosion rates with linear polarization during the long term test, electrochemical impedance spectroscopy is used to periodically measure the complex impedance as a function of frequency. Such measurements are made for each environment. The data is presented in the form of a standard Bode plot, with the impedance amplitude as a function of frequency shown here. Interpretation of these data in terms of a simple linear circuit model is enabling the resistance and capacitance of the thermally sprayed samples, along with the electrolyte resistance to be determined as a function of time, temperature and environment. As the nature of the passive film changes, it will be detected through these impedance measurements. The corresponding phase angle of the complex impedance is given in the following figure.

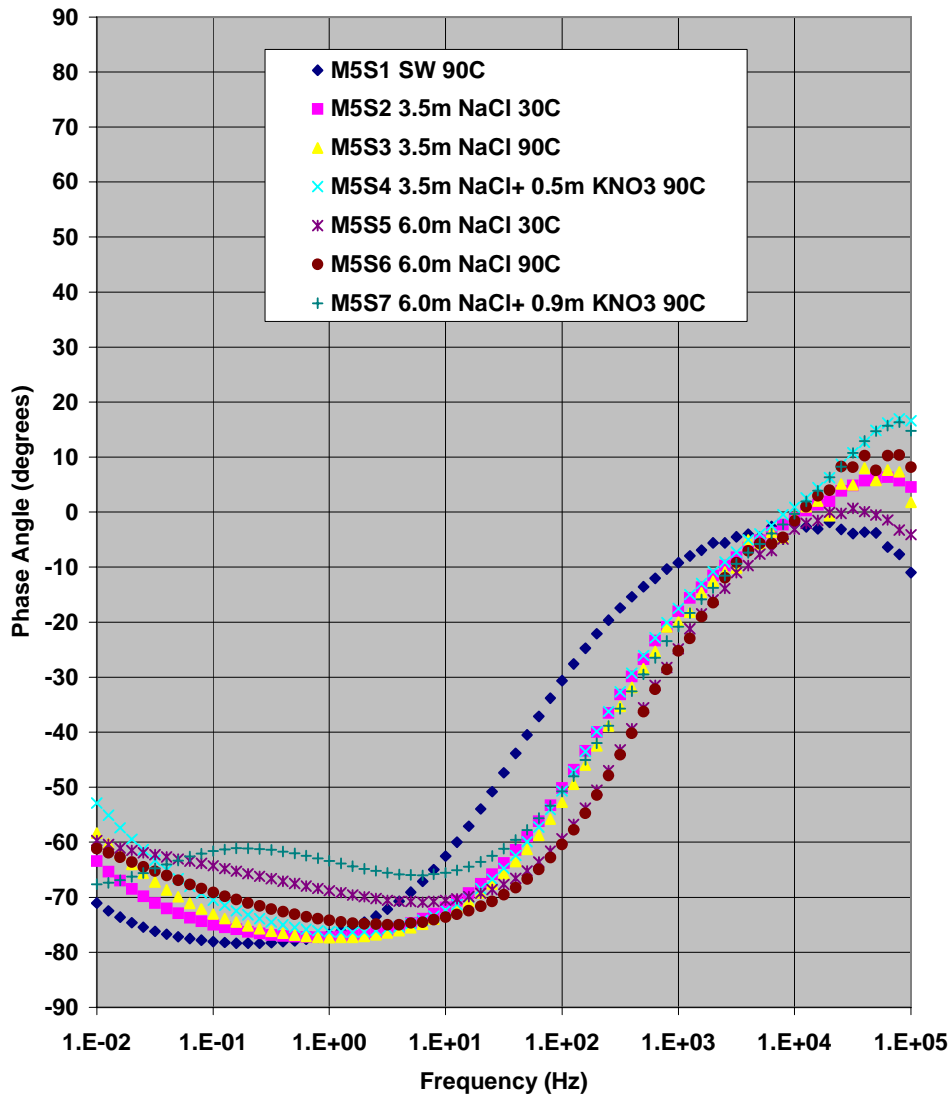


Figure 37. The phase angle as a function of frequency is shown here for the complex impedance data being gathered during the long-term test, and corresponds to the impedance amplitude in the previous figure.



Figure 38. This figure shows the gamma pit at LLNL. Actual spent fuel containers will be subjected to relatively high fluxes of gamma radiation, which will cause radiolytic reactions in the aqueous environment, including the production of hydrogen peroxide and other species. Work has begun on making electrochemical corrosion measurements inside the gamma pit, so that the impact of radiation on the amorphous metal coatings, and on the Alloy C-22 reference material can be assessed.